Title

Hyaluronidase Promotes Glucose Metabolism: Identification of the Extracellular Matrix as a Node of Cell-Extrinsic Metabolic Regulation

Author

Sullivan, William Juster

Publication Date

2017

Peer reviewed|Thesis/dissertation

UNIVERSITY OF CALIFORNIA

Los Angeles

Hyaluronidase Promotes Glucose Metabolism:

Identification of the Extracellular Matrix as a Node of Cell-Extrinsic Metabolic Regulation

A dissertation submitted in partial satisfaction of the

requirements for the degree Doctor of Philosophy

in Molecular & Medical Pharmacology

by

William Juster Sullivan

2017

ABSTRACT OF THE DISSERTATION

Hyaluronidase Promotes Glucose Metabolism:

Identification of the Extracellular Matrix as a Node of Cell-Extrinsic Metabolic Regulation

by

William Juster Sullivan

Doctor of Philosophy in Molecular & Medical Pharmacology

University of California, Los Angeles, 2017

Professor Heather R. Christofk, Chair

The metabolic state of a cell can be determined by cell-extrinsic factors, including nutrient availability and growth factor signaling. Here, we define extracellular matrix (ECM) remodeling as another fundamental node of cell-extrinsic metabolic regulation. Unbiased analysis of glycolytic drivers identified the hyaluronan-mediated motility receptor as among the most highly correlated with glycolysis in cancer. Confirming a mechanistic link between the ECM glycosaminoglycan hyaluronan and metabolism, treatment of cells with hyaluronidase (HAase) triggers a robust increase in glycolysis. This is largely achieved through rapid receptor tyrosine kinase-mediated induction of mRNA decay factor ZFP36, which targets *TXNIP* transcripts for degradation. Since TXNIP promotes internalization of the glucose transporter GLUT1, its acute decline liberates GLUT1 to the plasma membrane. In fibroblasts, the rapid induction of glycolysis induced by HAase is necessary for a concomitant increase in migration. Both tumor cross-sections and early mammalian

embryos exhibit a ZFP36- and TXNIP-mediated interconnection between extracellular matrix remodeling and metabolism *in vivo*.

In a subset of cells, HAase has sustained metabolic effects that track with changes in cell identity. HAase treatment of LiSa-2 liposarcoma cells led to the identification of GLUT1 as a target of sialylation—the addition of a sialic acid residue as the terminal monosaccharide of its N-glycan linkage. Increases in this modification coincide with the transcriptional upregulation of various sialyltransferases. Consistent with previous reports that sialylation is upregulated as part of the epithelial-to-mesenchymal transition (EMT), the gene expression profile of HAase-treated cells closely resembles that of both EMT in breast cancer cells and the dedifferentiated state in melanoma. This change in the transcriptional state of the cell is accompanied by stable metabolic and epigenetic reprogramming.

The dissertation of William Juster Sullivan is approved.

Thomas G. Graeber

Jing Huang

William E. Lowry

Peter J. Tontonoz

Heather R. Christofk, Chair

University of California, Los Angeles

2017

Dedicated to my family,

whose structure seems perpetually in flux, but whose support is unwavering.

TABLE OF CONTENTS

LIST OF FIGURES & TABLES

CHAPTER 1 | Unbiased expression analysis identifies involvement of extracellular matrix constituent hyaluronan in glycolytic metabolism.

CHAPTER 2 | Matrix digestion with hyaluronidase promotes plasma membrane GLUT1 through ZFP36-mediated targeting of *TXNIP*.

CHAPTER 4 | Sustained metabolic reprogramming by hyaluronidase in a subset of cells is accompanied by broad changes in the state of the cell.

EXPERIMENTAL PROCEDURES

ACKNOWLEDGEMENTS

Thank you

To Heather –

For giving me an undeservedly long leash. If it's true that you learn by making mistakes, I must be as erudite as you are patient. One can only aspire to your ability to revel in promising data and have amnesia take care of the rest.

To Club Christofk –

For an incredible ensemble cast performance. We really deserved some awards season buzz for our six-season spinoff of *The Office*. (Seriously, where are the cameramen hiding?) But if there's one lesson I've left you with, it's that you don't have to be an Emmy nominee to carry yourself like one.

To Shirley –

For your delight in discovery, which inspired this adventure.

To Abby –

For identifying and intervening on the early signs of addiction (to yodeling), for attempting (albeit with limited success) to mask your horror when I needed to unload about the *occasional* weekend indiscretion, and for making us all look bad by comparison. But hey – someone has to set the pace. While you're busy solving metabolism, do you think you can come up with a remedy for my problem areas?

To Daniel –

For always keeping it icy in our bay, even on the warmest of days. We will always be kindred curmudgeons.

To Margarita –

For your superhuman charm, and a smile that sparkles even brighter than our glassware.

To Shivani –

For your inquisitive mind and inquisitional spirit. You know they say you shouldn't try to rush fate because the best things in life are worth the wait – and the arc of our relationship is a good case in point. See ya, sari to leave ya!

To my family & friends -

For keeping me buoyed through the pummels of aborted projects, failed experiments, and miscellaneous dispiriting moments. But more importantly, for being the first to cheer even the most trivial of victories (though likely because, to the untrained eye, a tubulin blot is indistinguishable from a bona fide discovery). There's a lesson there: if you look hard enough, you'll always find a reason to pop a cork.

"When life gives you lemons, put nine in a bowl."

Thank you to all of the extraordinary collaborators who have lent their expertise, time, and tools to this project: Bill Lowry & Aimee Flores, for countless immunohistochemical stains of cutaneous tumors and wounds; Utpal Banerjee & Mark Sharpley, for bringing to our attention and following up on the punctuated regulation of hyaluronan in the early mammalian embryo; Tom Graeber & James Go, for their rank-rank hypergeometric overlap plots; Luisa Iruela-Arispe & Melanie Uebelhoer, for investigating the role of hyaluronan and hyaluronidase in retinal blood vessel sprouting and in aortic wound healing.

I would like to acknowledge funding from the UCLA Tumor Cell Biology Training Program (USHHS Ruth L. Kirschstein Institutional National Research Service Award # T32 CA009056), which supported most of this project.

The work for this dissertation was performed under the direction of Dr. Heather R. Christofk.

Chapters 1 & 2

These chapters are based upon work from the following manuscript:

Sullivan, WJ, Flores, AA, Sharpley, MS, Whiteley, AE, Maxwell, MB, Ayer, DE, Banerjee, U, de Aguiar Vallim, TQ, Lowry, WE, Braas, D, Christofk, HR. Extracellular matrix remodeling regulates glucose metabolism through TXNIP destabilization. (submitted)

VITA

Education

2011 AB, *cum laude*, Molecular Biology
Princeton University
Princeton, NJ

Academic Employment

2011-2017 Graduate Student Researcher

Chancellor's Prize Fellowship
Tumor Cell Biology Training Program

Department of Molecular & Medical Pharmacology
David Geffen School of Medicine
University of California, Los Angeles
Los Angeles, CA

Publications

Sullivan, WJ, Flores, AA, Sharpley, MS, Whiteley, AE, Maxwell, MB, Ayer, DE, Banerjee, U, de Aguiar Vallim, TQ, Lowry, WE, Braas, D, Christofk, HR. Extracellular matrix remodeling regulates glucose metabolism through TXNIP destabilization. (submitted)

Sullivan, WJ & Christofk, HR. The Metabolic Milieu of Metastases. *Cell* **160**, 363-364 (2015).

Ahler, E*, Sullivan, WJ*, *et al.* Doxycycline Alters Metabolism and Proliferation of Human Cell Lines. *PLOS ONE* **8**, e64561 (2013). *authors contributed equally to this work

Presentations

2017 UCLA Department of Biological Chemistry Seminar Series, Los Angeles, CA
2017 UCLA Metabolism Interest Group, Los Angeles, CA
2012-2017 UCLA Department of Molecular & Medical Pharmacology Seminar Series, Los Angeles CA
2016 Keystone Symposium: New Frontiers in Understanding Tumor Metabolism, Banff, Alberta, Canada

INTRODUCTION

•

The extracellular matrix as a node of cell-extrinsic metabolic regulation.

Cells have diverse circuitry to sense and respond to extrinsic metabolic signals, many of which have been extensively characterized. For instance, cells coordinate systemic and cellular metabolism by sensing nutrient availability through mTOR and shifting between anabolic and catabolic states accordingly; growth factors, hormones, and cytokines can relay metabolic cues to adjacent cells, as well as distal tissues, as part of a broader biological response. The unifying effect is to integrate the behavior and metabolism of the cell with the requirements of the tissue and organism of which it is a constituent.

Similarly fundamental to normal biology is reorganization of the extracellular matrix (ECM), which is central to both tissue expansion and regeneration—with embryogenesis and wound healing being hallmark cases, respectively (Adams and Watt, 1993; Martin, 1997; Raghow, 1994; Rozario and DeSimone, 2010; Singer and Clark, 1999; Toole, 2001). ECM remodeling is also a signature of pathological processes, such as tumorigenesis (Bissell and Radisky, 2001; Hanahan and Weinberg, 2011; Lu et al., 2012; Radisky et al., 2005). Another central feature of many of these processes is upregulation of glycolytic metabolism, which can provision the energetic currency and biosynthetic substrates required for rapid proliferation (DeBerardinis et al., 2008; Elson et al., 2000; Martin and Leese, 1995; Purcell and Moley, 2009). Although extracellular matrix remodeling and dependence on increased glycolysis co-occur in multiple biological contexts, mechanistic links between these processes are not well established.

Hyaluronan (HA; also called hyaluronic acid), a ubiquitous constituent of the ECM, is a megadalton glycosaminoglycan that is extruded directly into the extracellular space, where it ensheaths the cell in a voluminous pericellular matrix through tethering interactions with its plasma membrane receptors (Toole, 2001, 2004). HA is the canonical ligand for CD44—an established marker of cancer stem cells—and the hyaluronan-mediated motility receptor (HMMR), though interactions with a variety of other receptors have been described (Aruffo et al., 1990; Turley et al.,

2002). The exact signaling events orchestrated by HA are dependent not only on its abundance but also on its size—oligomers of HA have been reported to exert distinct effects on the behavior of the cell (Jiang et al., 2007; Stern et al., 2006). Therefore, the biological effects of HA are spatially patterned by the net activity of hyaluronan synthases (the class of enzymes that synthesize the polymer) and hyaluronidases (the enzymes that cleave it) in proximity of the cell.

Despite the simple structure of the HA polymer—disaccharide repeats of glucuronic acid and N-acetylglucosamine—its impact on both normal biology and pathology are diverse. Beyond regulation of cell behavior through CD44 and HMMR, it has been suggested that the state of HA in the matrix may have key role in establishing the permissiveness of the environment for cells to proliferate, migrate, and—specifically in the context of cancer—metastasize. Both HA *and* HAase, however, have been implicated in tumor progression, suggesting either a nonlinear role in disease progression or a high degree of subtype specificity (Evanko et al., 1999; Hayen et al., 1999; Itano et al., 2002; Simpson et al., 2002; Toole, 2004; Toole et al., 2002; Zhang et al., 1995). The importance of HA in development, however, is indisputable: deletion of the hyaluronan synthase gene *HAS2* has an embryonic lethal phenotype due, at least in part, to impairment of the endothelial cell migration required for cardiac development (Camenisch et al., 2000). In this study, we confirm that perturbation of HA in cultured cells dramatically impacts their proliferation and migration, and we report that these changes in cell behavior are accompanied by—if not dependent on—an increase in glycolytic metabolism. We therefore propose that ECM remodeling serves as an additional node of cell-extrinsic metabolic regulation, a form of metabolic regulation that can directly read out the structural state of the surrounding tissue and augment the behavior of the cell accordingly.

CHAPTER 1

•

Unbiased expression analysis identifies involvement of extracellular matrix constituent hyaluronan in glycolytic metabolism.

INTRODUCTION

Since the Warburg Effect was first described nearly a century ago, aerobic glycolysis has been an accepted metabolic feature of cancer cells. Although it was originally hypothesized to be a compensatory response to defective mitochondria, and later relegated as an 'epiphenomenon' that accompanies oncogene activation, glycolytic metabolism is now understood to have a fundamental role in supporting the anabolic and energetic demands of rapid proliferation (Koppenol et al., 2011). Glycolytic intermediates can be shunted into biosynthetic pathways to produce the nucleotides, amino acids, and lipids needed for daughter cells. Additionally, while aerobic glycolysis provides a considerably smaller yield of ATP than oxidative phosphorylation per molecule of glucose, it can provision this bioenergetic currency at a much faster rate (Lunt and Vander Heiden, 2011).

In normal cells, both proliferation and glycolytic metabolism are stimulated by growth factor signaling. In cancer, however, these signals are constitutively active, giving cells a more uniformly elevated rate of glycolysis, which couples with the rapid proliferation that is a hallmark of the disease (DeBerardinis et al., 2008). Indeed, metabolic alterations in cancer are downstream of oncogenes like Ras and PI3K, which upregulate glycolysis in tandem with transformation (Hsu and Sabatini, 2008). Cancer cells also develop further metabolic alterations that confer selective proliferative advantage, including isoform switching of pyruvate kinase to the embryonic M2 form (Christofk et al., 2008). Among the interesting features of this isoform switch is that it highlights the interconnections between hyperproliferative states—in this case, cancer and stem cells—as cancer cells coopt metabolic traits of embryonic tissue (Gu et al., 2016). In this way, cancer cells are simply a dramatic example of the inextricable link between glycolytic metabolism and the proliferative and migratory cell behaviors that it supports.

Coordinated transcriptional regulation of aerobic glycolysis has been well established, with HIF-1, Myc, and p53 among the best described mediators (Bensinger and Christofk, 2012). But here

we seek to use unbiased gene expression analysis to identify novel individual transcripts with a high degree of correlation with both glycolysis in breast cancer cell lines and ^{18}FDG uptake in breast cancer tumors. This approach is valuable because it reduces artefactual effects of cell culture systems, as well as clinical features that may track with glycolysis, such an angiogenesis. Although the analysis was performed on breast cancer cell lines and tumors to maximize signal to noise, the results may be generalizable beyond this disease state.

RESULTS

Unbiased analysis identifies ECM engagement as a regulator of glycolytic metabolism.

We have previously described an unbiased analysis to identify genes whose expression correlates with a glycolytic phenotype in both breast cancer cell lines and breast tumors (Hong et al., 2016). In 31 breast cancer cell lines, genes were ranked based on the correlation of their expression with glycolytic rate (nmol lactate produced/nmol oxygen consumed); and in 11 breast tumors, with uptake of the glucose analog PET tracer ^{18}F-fluorodeoxyglucose (FDG). *SLC16A1* emerged as the gene with highest average correlation between these conditions. It encodes monocarboxylate transporter 1 (MCT1), which has a critical role in mediating efflux of both lactate and pyruvate from the cell. In studies that validate the effectiveness of this approach—and its potential generalizability beyond breast cancer—we have recently described the key role that MCT1 plays not only in cancer cell metabolism and proliferation, but also in the maintenance of pluripotency in stem cells (Gu et al., 2016; Hong et al., 2016).

The second-most highly correlated gene is the HA receptor *HMMR*, whose protein product is also known as RHAMM and CD168 (Figure 1-1). The degree of correlation was initially surprising as the ECM has not been widely described as a direct regulator of glycolytic metabolism, nor are its impacts often considered in the context of standard cell culture. Many adherent cell types with active hyaluronan production assemble a pericellular matrix—often called a 'coat'—comprised largely of HA polymers anchored to the plasma membrane (Cohen et al., 2003). This coat can be visualized using biotinylated hyaluronan binding protein (HABP), a combination of the G1 domain of aggrecan and cartilage link protein, which together form a stable interaction with HA (Figure 1-2a) (Perkins et al., 1989; Toole, 1990). When cells are treated with bovine testicular hyaluronidase (HAase), the pericellular coat is digested away, but the effect is rescued when HAase is heat-inactivated (HI HAase).

Consistent with the results of our analysis suggesting a central role for HA in regulating the glycolytic phenotype, LiSa-2 liposarcoma cells treated with HAase for 24h show a significant and dose-dependent induction of glycolytic metabolism, as measured by glucose uptake and lactate production (Figures 1-2b and 1-3a). HI HAase does not show this effect, confirming that the effect is mediated by the enzymatic activity of the HAase preparation, and not by possible thermostable contaminants (Figures 1-2a,b). To confirm that the on-target effects of HAase are responsible for the induction of glycolysis, cells were co-treated with HAase and the flavonoid apigenin, which is an inhibitor of bovine testicular hyaluronidase activity (Kuppusamy et al., 1990). The combined treatment abolishes the effect of HAase on glucose uptake and lactate production (Figure 1-3b). Together, these data suggest that matrix digestion with HAase promotes increased glycolysis in cultured liposarcoma cells.

Matrix digestion with HAase acutely increases glycolytic metabolism in cultured cells.

In an attempt to stratify cells that have a glycolytic response to HAase from those that do not, we measured glucose uptake (Figure 1-4a) and lactate production (Figure 1-4b) in a panel of cell lines. This panel included primary, immortalized, and transformed cells; murine and human cells; as well as cancer cells that represent a diversity of genetic lesions. Interestingly, there is a unidirectional response to HAase: all treated cells show an increase in glycolytic metabolism. All but two cell lines (HFF-1 and Hs578T) show a significant increase in glucose uptake; all show a significant increase in lactate production. As a point of contrast, changes in glutamine uptake (Figure 1-5) are both bidirectional and of generally smaller magnitude. The contrasting results in glucose and glutamine consumption underscore the specificity of the glycolytic response to HAase.

To assess the temporality of the glycolytic response to HAase, both 24h and 5d treatments were performed on selected cell lines. LiSa-2 cells and mouse embryonic fibroblasts (MEFs) show a sustained response to HAase: glucose uptake is significantly higher after 5d than after 24h in LiSa-2

cells, and lactate production is higher after 5d than after 24h in both cell lines (Figure 1-6a). These sustained changes in glycolytic rate are evident even as observed in acidification of the media—a proxy for lactate production—and the corresponding yellowing of the pH-sensitive phenol red dye (Figure 1-6b). 293T cells, however, do not show a similarly sustained response to HAase, with glucose uptake reverting towards the baseline rate after five days of treatment (Figure 1-6c). Together, these data suggest that there may be an acute, universal response to HAase and a more specific, sustained response in certain cell types.

Because digested HA oligosaccharides (oligoHA) have been reported to initiate a variety of distinct signaling events and engage with a distinct set of receptors from the full-length HA polymer, we tested whether it is the production of oligoHA or the absence of the full-length polymer that triggers the glycolytic response to HAase. Cells were resuspended in media containing oligoHA (1 and 5mg/mL) to ensure access to receptors that might be masked or occupied by pericellular HA if the cells were adherent (Figure 1-7a). Their baseline metabolism was measured starting 24h thereafter. Neither concentration of oligoHA impacts the rate of glucose uptake or lactate production (Figure 1-7b), suggesting the effect of HAase is likely triggered by the absence of full-length HA from the cell surface.

Canonical HA receptors are likely not involved in the glycolytic response to HAase.

We then attempted to determine whether it is interaction of HA with its canonical receptors that mediates the glycolytic response to its depolymerization. Although HA has been reported to engage with a variety of receptors on the cell surface, HMMR and CD44 are the best described and both have a compelling connection to glycolytic metabolism. HMMR is among the top hits of our gene expression analysis and CD44 has been reported to promote glycolytic metabolism through direct interactions with PKM2 and monocarboxylate transporters 1 and 4 (Slomiany et al., 2009; Tamada et al., 2012). It is therefore surprising that there is a divergent change in levels of these receptors in

response to 24h of HAase treatment. HAase, in fact, lowers levels of HMMR (Figure 1-8a). Knockdown of HMMR exerts a dramatic impact on baseline glucose uptake, falling below the sensitivity of our measurements (Figure 1-8b). This is consistent with our unbiased gene expression analysis, which suggested a positive correlation with glycolysis. But it is inconsistent with involvement of HMMR in the glycolytic response to HAase, as knockdown shows the opposite of a HAase phenocopying effect.

While CD44 shows a promisingly dramatic upregulation in response to HAase, knockdown of the receptor does not abolish the glycolytic response to HAase (Figures 1-9a,b). While one of the CD44-targeted shRNAs does significantly blunt the increase in glucose uptake with 24h of HAase treatment, levels of CD44 are not proportional to glucose consumption rates. Additionally, although most cell lines tested show upregulation of CD44 after 24h and 5d of HAase treatment, one shows no change in levels (NCI-H1792) and another does not express CD44 (MDA-MB-453) (Figure 1-10). While these data strongly suggest that CD44 does not mediate the glycolytic response to HAase, it should be noted that the latter cell line, without detectable levels of CD44, also shows a relatively small induction of glycolysis in response to HAase (Figures 1-4a,b). It is therefore possible that *part* of the glycolytic response to HAase is due to binary signaling through CD44 that is irrespective of levels of the receptor.

HAase treatment increases levels of GLUT1 at the plasma membrane.

To probe for the regulatory node by which HAase upregulates glycolysis, we examined levels of glycolytic enzymes at both the transcript and protein level after 24h of HAase treatment and found neither significant upregulation of the KEGG-defined glycolytic gene set (Figure 1-11a) nor changes in glycolytic enzyme levels (Figure 1-11b). We therefore took a functional approach and measured enzymatic activity of hexokinase (HK), phosphofructokinase (PFK), and lactate dehydrogenase (LDH) after 24h of treatment (Figure 1-11c). The only significant change is a *decrease* in HK activity.

LDH activity was also assayed at earlier time points (30m, 1h, 5h) and no significant changes were detected (data not shown). Activity assays were also performed in SUM159PT cells with the same results (data not shown). Collectively, these data suggest that there is considerable spare glycolytic capacity at several steps in the pathway and that glucose entry into glycolysis may be rate-limiting.

Analysis of metabolite pool sizes by liquid chromatography-tandem mass spectrometry (LC/MS) has previously been used to identify altered nodes in the glycolytic pathway (Hu et al., 2016). Here, however, we find that HAase treatment increases levels of glycolytic intermediates by a similar magnitude at both 6h and 24h, consistent with a bottleneck at the level of glycolytic substrate availability (Figure 1-12a). Additionally, measurement of incorporation of a U-$^{13}C_6$-glucose tracer into glycolytic intermediates following 6h of HAase treatment (Figure 1-12b) shows an increase in the labeled fraction of metabolites at multiple steps in the pathway, further suggesting an increase in activity of the pathway rather than activation of a specific enzymatic node.

To identify whether HAase impacts glucose entry into the cell, we examined whether the subcellular distribution of the canonical facilitative glucose transporters, GLUT1-4, is altered by HAase treatment. Immunofluorescence staining of GLUT1 reveals that the transporter appears concentrated in punctae surrounding the nucleus in control cells, whereas it has considerably more diffuse staining after 24h of HAase treatment (Figure 1-13a). To confirm that this diffusion of signal represents increased trafficking of GLUT1 to the plasma membrane, we fractionated cytosolic and plasma membrane proteins and see markedly increased levels of both GLUT1 and GLUT3 in the plasma membrane fraction after treatment with HAase; no signal was observed for GLUT2 and GLUT4 (Figure 1-13b).

We then sought to determine whether changes in levels of glucose transporters at the plasma membrane correspond with changes in glycolytic metabolism. By comparing time courses of extracellular acidification (ECAR, a real-time proxy for lactate production) with membrane-bound

levels of GLUT1 and GLUT3, we observe overlapping temporality in response to HAase: both ECAR and plasma membrane transporter levels are increased by 6h (Figures 1-14a,b). To determine whether changes in GLUT1 and GLUT3 are regulated at the level of trafficking or upregulation, we examined transcript levels of all of the glucose transporters at 4h and 24h (Figure 1-15). While *SLC2A3* (GLUT3) is significantly upregulated at both time points, *SLC2A1* (GLUT1) transcript levels are actually decreased at 4h and then significantly upregulated at 24h. These data suggest that while the increases in plasma membrane GLUT3 may be due to transcriptional induction, increases in GLUT1 are largely due to increased mobilization to the membrane: transcript levels of GLUT1 are suppressed just before its plasma membrane levels approach their maximum. *SLC2A2* and *SLC2A4* do not show a transcriptional response to HAase, underscoring their lack of involvement in the induction of glycolysis in this context.

To determine whether increases in plasma-membrane GLUT1 and GLUT3 are universal features of the glycolytic response to HAase, we performed fractionations of 293T and MDA-686 cells after 24h of HAase treatment (Figure 1-16). Both cell lines show considerably increased levels of membrane-bound GLUT1 in response to HAase, but they do not show similar consistency in GLUT3: there is, in fact, a decrease in its plasma membrane levels in 293T cells, and it is barely detectable in MDA-686 cells. We therefore concluded that GLUT1 is the likely mediator of the universal glycolytic response to HAase, though trafficking of other glucose transporters might augment the response to HAase in some cells.

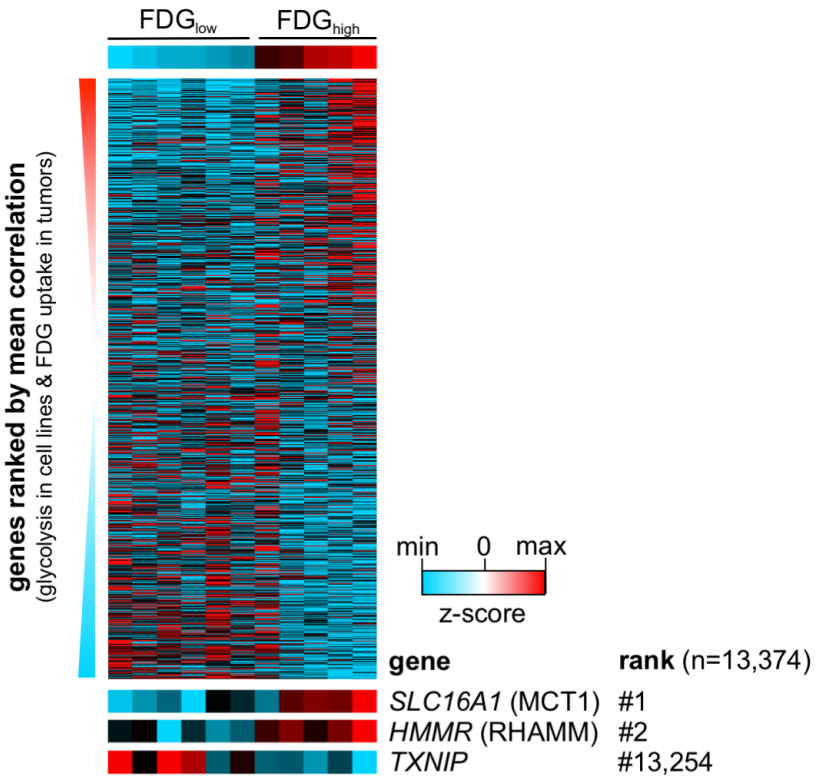

Figure 1-1. Unbiased analysis identifies correlation between expression of the *HMMR* and glycolytic metabolism. *(Adapted from Hong et al., 2016.)* Genes were ranked on the vertical axis by average correlation of expression with glycolysis in breast cancer cell lines (quantified as the following ratio: nmol lactate produced/nmol oxygen consumed) and with FDG maximum standardized uptake value (SUV_{max}) in breast tumors. Transcript levels are visualized here in 11 tumors presented in order of increasing SUV_{max} on the horizontal axis. Genes encoding *SLC16A1* and *HMMR* are ranked 1 and 2 of 13,374, respectively; *TXNIP* is ranked 13,254.

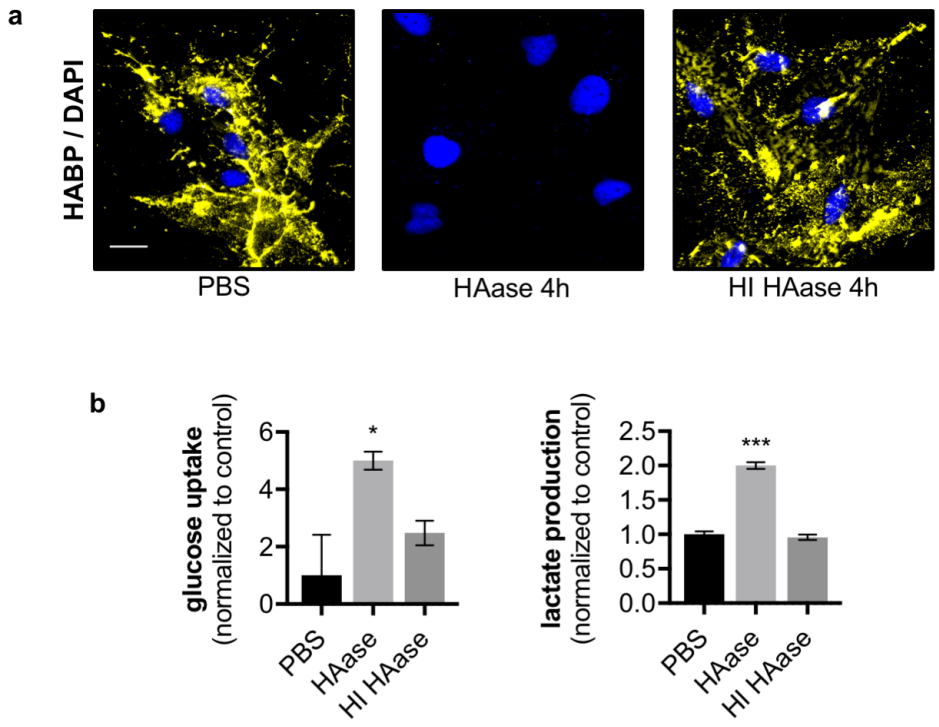

Figure 1-2. Digestion of the HA pericellular matrix increases both glucose uptake and lactate production in liposarcoma cells. (a) LiSa-2 cells were fixed without permeabilization after 4h treatment with PBS, 400μg/mL HAase, or 400μg/mL heat-inactivated (HI) HAase (concentrations used throughout study unless otherwise stated), then indirectly probed for pericellular HA using biotinylated hyaluronan binding protein (HABP, yellow) and fluorophore-conjugated streptavidin. Nuclei were stained with DAPI (blue). Scale bar, 25μm. **(b)** Glucose uptake and lactate production rates in LiSa-2 cells treated with PBS, HAase, or HI HAase for 24h. Rates were normalized to PBS control. Error bars denote SD (n=3). *$p<0.05$; ***$p< 0.001$.

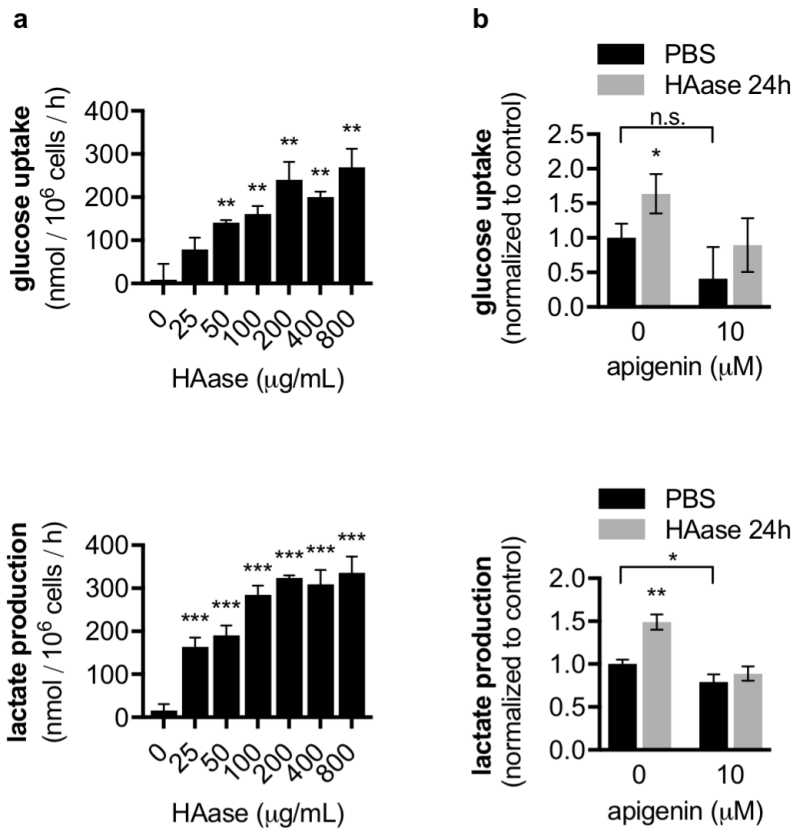

Figure 1-3. Glycolytic response to HAase is dose-dependent and can be abolished by an inhibitor of its hyaluronidase activity. (a) Dose-response relationship of HAase to glucose uptake and lactate production rates in LiSa-2 cells, which were treated for 24h with PBS or HAase at indicated doses (0, 25, 50, 100, 200, 400, and 800μg/mL). **(b)** Glucose uptake and lactate production rates in LiSa-2 cells treated with 10μM apigenin—a flavonoid inhibitor of bovine testicular hyaluronidase—or DMSO control, as well as with PBS or HAase for 24h. HAase and apigenin were incubated together in media for 1h before addition to cells. Rates were normalized to PBS+DMSO control. Error bars denote SD (n=3). *p<0.05; **p<0.01; ***p< 0.001; n.s. - not significant.

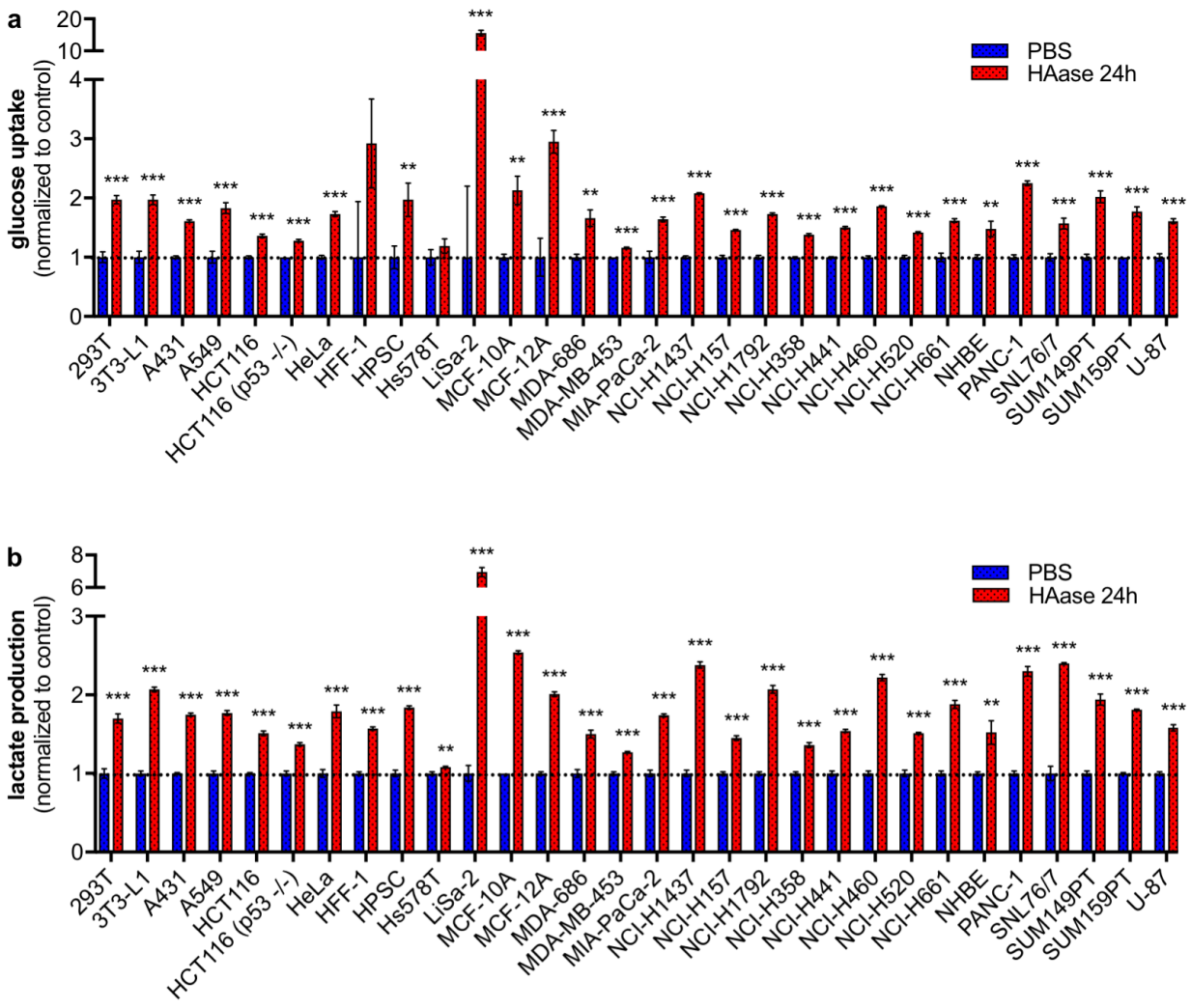

<u>Figure 1-4.</u> HAase treatment shows unidirectional effect on glycolysis in a panel of cultured cells and cell lines. (a) Glucose uptake and **(b)** lactate production rates in cultured cells treated with PBS or HAase for 24h. Rates were normalized to PBS control. Error bars denote SD (n=3). **p<0.01; ***p< 0.001.

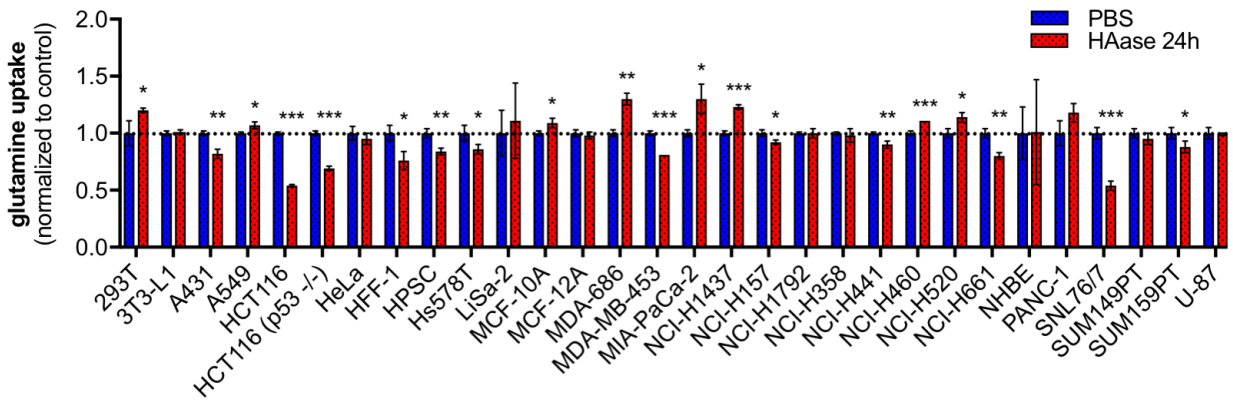

Figure 1-5. HAase treatment does not have uniform effect on glutamine uptake in a panel of cultured cells and cell lines. Glutamine uptake rates in cells treated with PBS or HAase for 24h. Rates were normalized to PBS control. Error bars denote SD (n=3). *p<0.05; **p<0.01; ***p< 0.001.

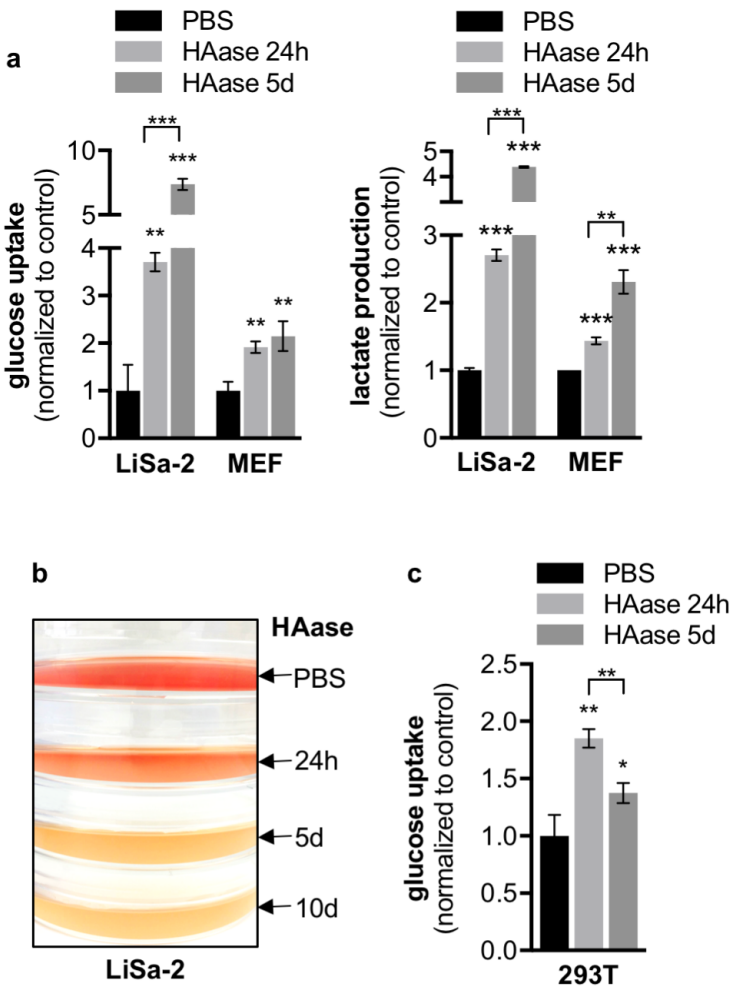

Figure 1-6. Cells differ in both magnitude and temporality of glycolytic response to HAase treatment. (a) Glucose uptake and lactate production rates in LiSa-2 and MEF cells treated with PBS or HAase (24h and 5d). Rates were normalized to PBS control. **(b)** Yellowing of pH-sensitive media constituent phenol red serves as a proxy for lactate production in cells of equal confluency that have been treated with PBS or HAase for times indicated and incubated in equal volumes of fresh media for 24h. **(c)** Glucose uptake rates in 293T cells treated with PBS or HAase (24h and 5d). Rates were normalized to PBS control. Error bars denote SD (n=3). *p<0.05; **p<0.01; ***p< 0.001.

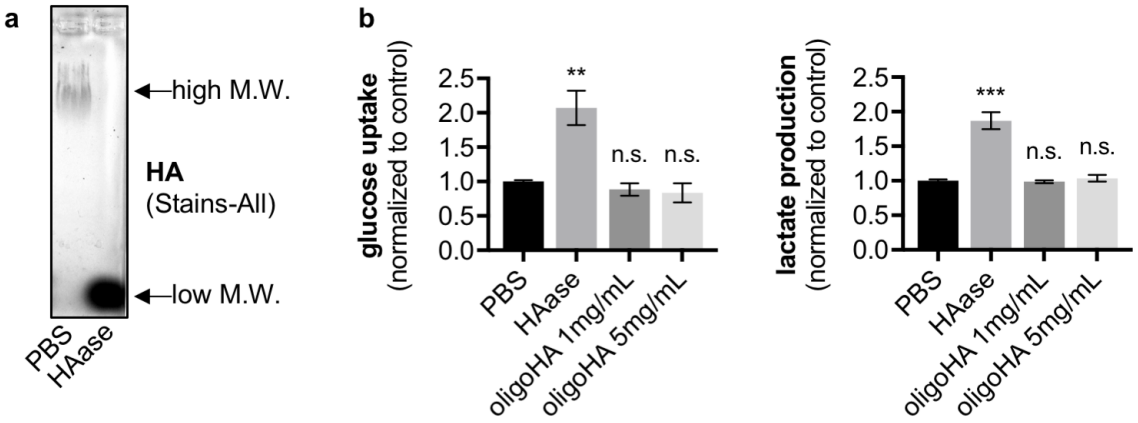

Figure 1-7. Exogenously digested HA does not phenocopy HAase treatment. (a) Agarose gel resolution of the full-length HA polymer (high M.W.) and the digestion products resulting from 72h incubation with HAase (oligoHA, low M.W.). Gel was incubated in Stains-All overnight. oligoHA shows more intense staining despite equal loading. **(b)** Glucose uptake and lactate production rates in LiSa-2 cells treated for 24h with PBS or HAase, and for 48h with exogenously digested oligoHA (1 and 5mg/mL). Rates were normalized to PBS control. Error bars denote SD (n=3). **p<0.01; ***p< 0.001; n.s. - not significant.

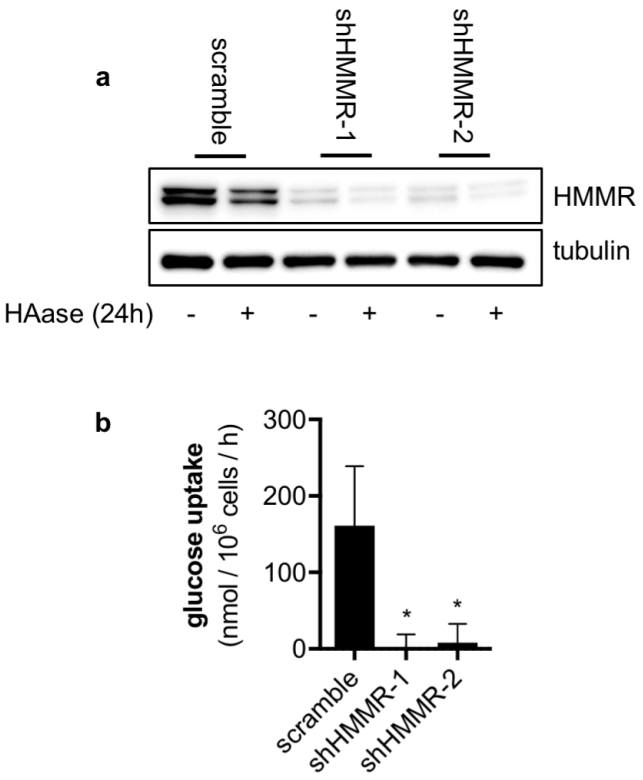

Figure 1-8. HAase treatment lowers levels of HMMR but knockdown of the receptor does not phenocopy the treatment. (a) Immunoblots showing levels of HMMR in LiSa-2 cells with stable shRNA knockdown of HMMR, or expression of a scrambled shRNA control. Cells were treated with PBS or HAase for 24h. **(b)** Baseline glucose uptake rates in LiSa-2 cells with stable shRNA-mediated HMMR knockdown or expression of scrambled shRNA control. Error bars denote SD (n=3). *$p<0.05$.

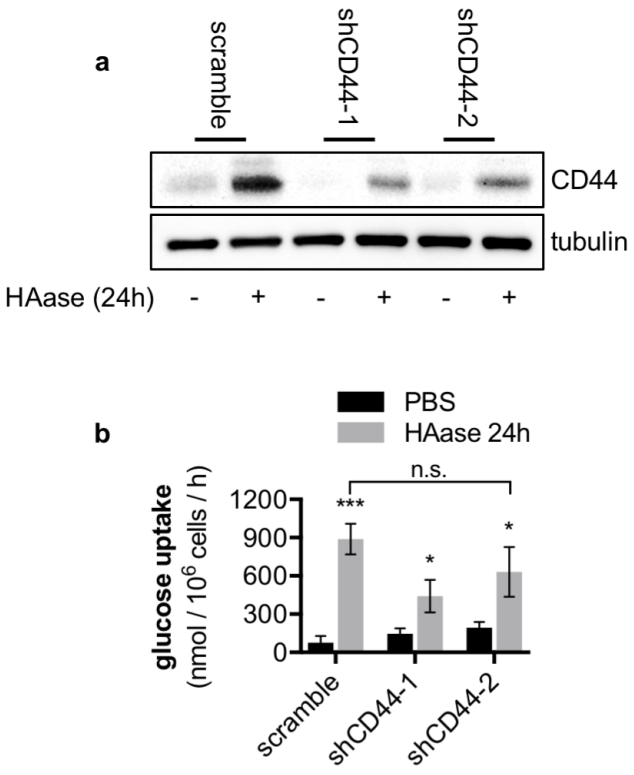

Figure 1-9. HAase treatment increases levels of CD44 but knockdown does not abolish the glycolytic response to HAase. (a) Immunoblots showing levels of CD44 in LiSa-2 cells with stable shRNA knockdown of CD44 or expression of scrambled control. Cells were treated with PBS or HAase for 24h. **(b)** Glucose uptake rates in LiSa-2 cells with stable knockdown of CD44 or expression of scrambled shRNA control. Cells were treated with PBS or HAase for 24h. Error bars denote SD (n=3). *$p<0.05$; ***$p< 0.001$.

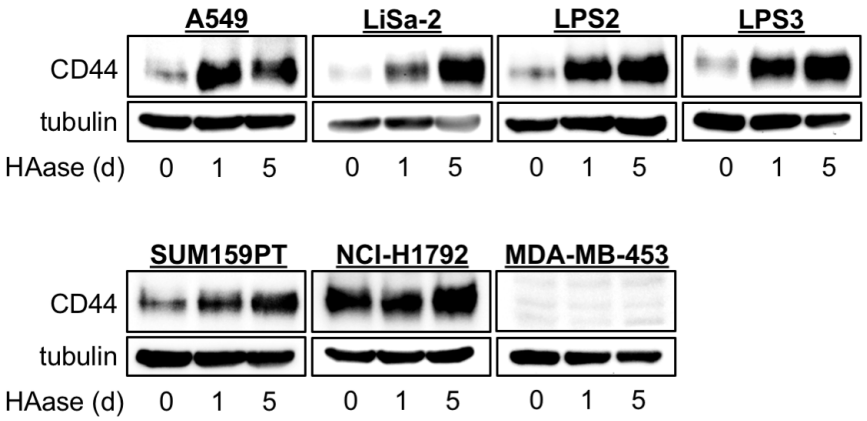

Figure 1-10. Not all cell lines that show a glycolytic response to HAase also express CD44.

Immunoblots showing CD44 levels in various cell lines treated with PBS or HAase (24h, 5d).

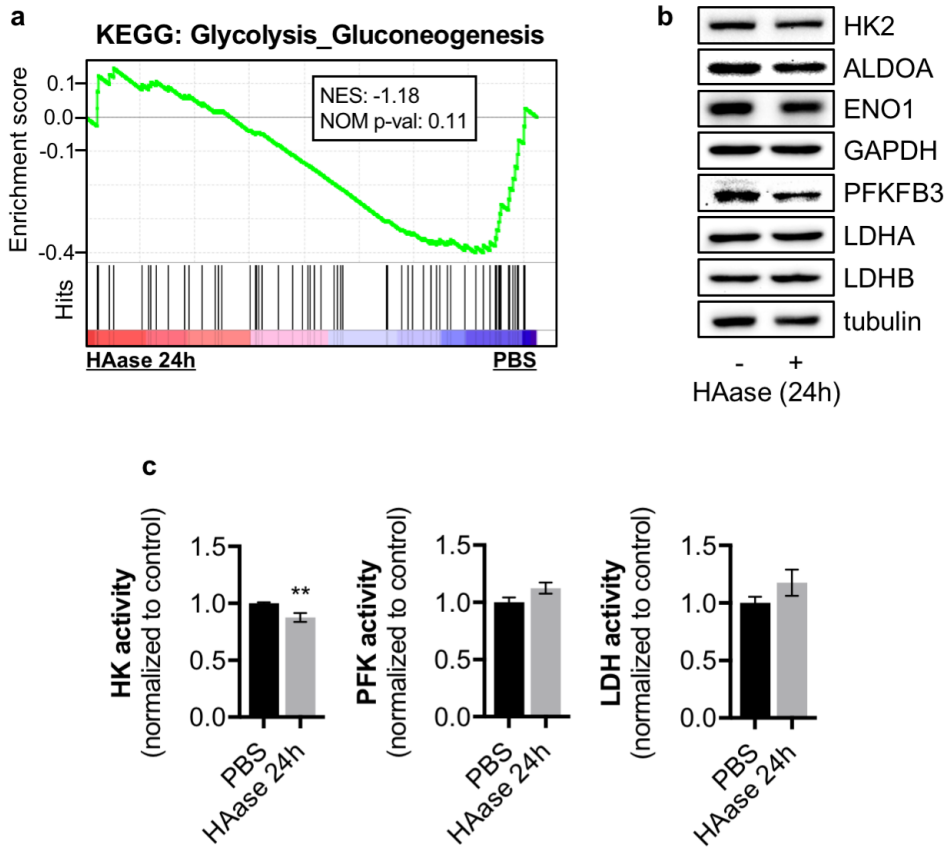

Figure 1-11. HAase treatment promotes coordinated upregulation of glycolytic machinery on neither the transcriptional nor the protein level—nor does it increase activity of key enzymatic nodes. (a) Gene set enrichment analysis (GSEA) mountain plot showing enrichment of the KEGG-defined pathway Glycolysis/Gluconeogenesis (hsa00010) in LiSa-2 cells treated for 24h with either PBS or HAase. Input expression data from U133 Plus 2.0 microarray. **(b)** Immunoblots showing levels of glycolytic enzymes in LiSa-2 cells treated with either PBS or HAase for 24h. **(c)** Enzymatic activity of hexokinase (HK), phosphofructokinase (PFK), and lactate dehydrogenase (LDH) were measured in LiSa-2 cells following 24h treatment with either PBS or HAase. Rates were normalized to PBS control. Error bars denote SD (n=3). **p<0.01.

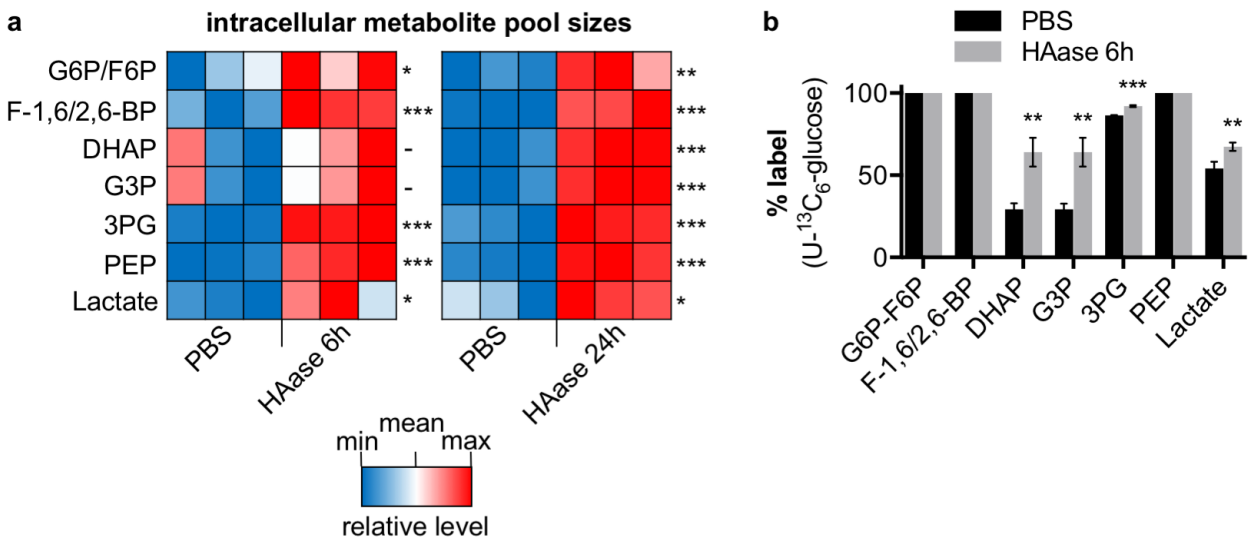

Figure 1-12. HAase treatment increases both pool sizes of and glucose incorporation into glycolytic intermediates throughout the glycolytic pathway. (a) Heatmaps showing relative intracellular levels of glycolytic intermediates in LiSa-2 cells 6h and 24h following treatment with PBS or HAase. Levels were assessed by LC/MS. **(b)** Incorporation of U-$^{13}C_6$-glucose into glycolytic intermediates after 6h of labeling with PBS or HAase in LiSa-2 cells, as measured by LC/MS. Error bars denote SD (n=3). **p<0.01; ***p< 0.001.

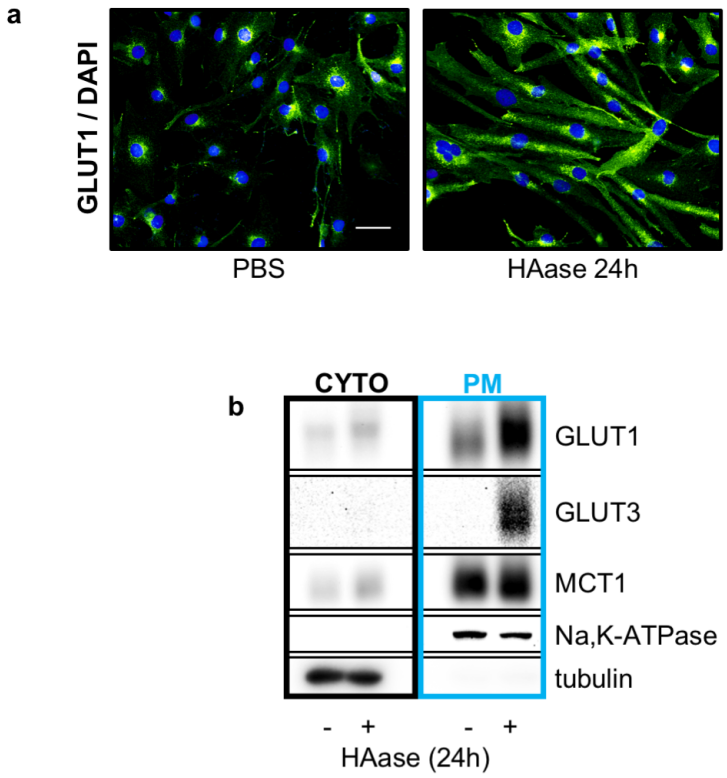

Figure 1-13. HAase treatment increases levels of glucose transporters at the plasma membrane. (a) Immunofluorescence staining of GLUT1 (green) in LiSa-2 cells following 24h treatment with either PBS or HAase. Nuclei were stained with DAPI (blue). Scale bar, 50μm. **(b)** Immunoblots showing levels of GLUT1, GLUT3, and MCT1 in both the cytoplasmic (CYTO) and plasma membrane (PM) fractions of LiSa-2 cells treated with PBS or HAase for 24h. Na,K-ATPase serves as a loading control for plasma membrane proteins, and tubulin for cytoplasmic proteins.

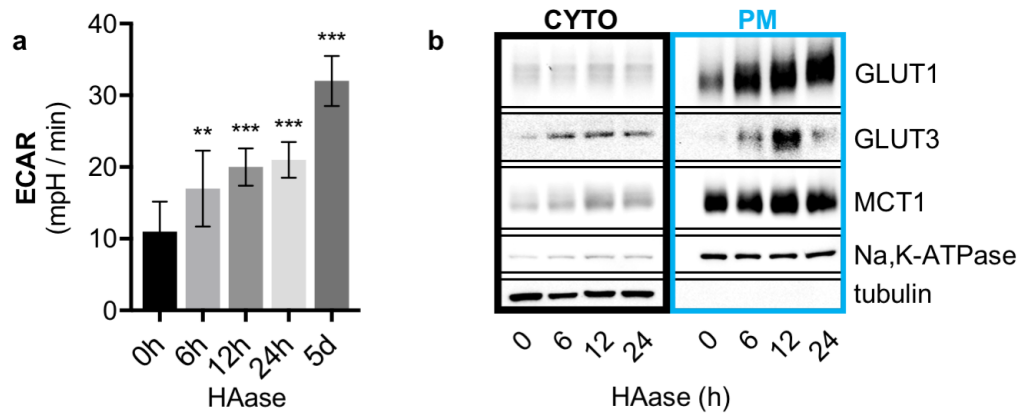

Figure 1-14. There is temporal overlap in the elevation of glycolytic metabolism and in the increased levels of GLUT1 at the plasma membrane. (a) Extracellular acidification rate (ECAR) of LiSa-2 cells treated with PBS or HAase for the indicated times. **(b)** Immunoblots showing levels of GLUT1, GLUT3, and MCT1 in both the cytoplasmic (CYTO) and plasma membrane (PM) fractions of LiSa-2 cells treated with PBS or HAase for the indicated times. Error bars denote SD (n=12). **p<0.01; ***p< 0.001.

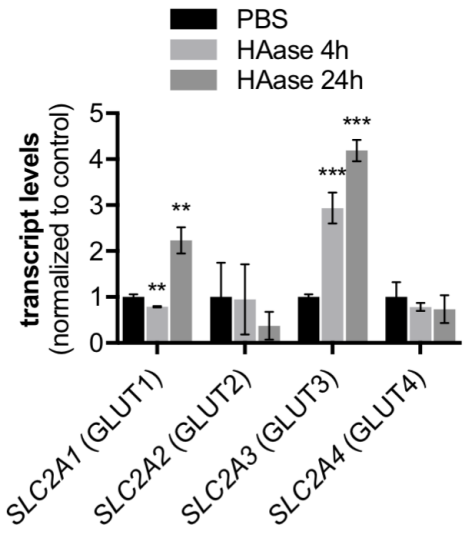

Figure 1-15. Changes in plasma membrane levels of the glucose transporters do not uniformly correspond with changes in their transcript levels. Transcript levels of *SLC2A1-4* in LiSa-2 cells following treatment with PBS or HAase (4h and 24h). Values for each gene were normalized to PBS control. Error bars denote SD (n=3). **p<0.01; ***p< 0.001.

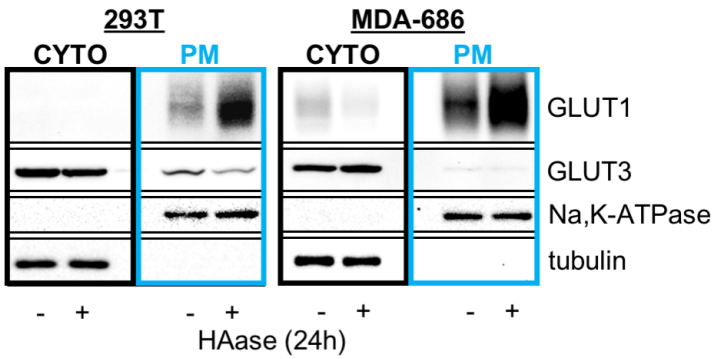

Figure 1-16. Elevated plasma membrane GLUT1—but not GLUT3—is a consistent feature of HAase treatment. Immunoblots showing levels of GLUT1 and GLUT3 in both the cytoplasmic (CYTO) and plasma membrane (PM) fractions of 293T and MDA-686 cells treated with PBS or HAase for 24h.

DISCUSSION

In summary, unbiased expression analysis identified the possibility that the ECM can exert a potent regulatory effect on glycolytic metabolism, of which there have been few notable reports despite the co-occurrence of changes in ECM and metabolism in many normal and disease processes. Confirming this possibility, treatment of a broad range of cells with HAase significantly upregulates glycolysis in a manner that is specific to its on-target enzymatic activity. A unidirectional response to HAase is not seen in glutamine uptake, underscoring the specificity of the metabolic response and ruling out the possibility that it represents an indiscriminate increase in metabolic activity across all pathways involved in anabolic metabolism.

Increases in glycolytic rate track with increases in GLUT1 at the plasma membrane in all cell lines tested. However, transcription or trafficking of GLUT3—or other unmeasured metabolic events downstream of HAase—may be involved in further augmenting the glycolytic response in some cells. Interestingly, some cell lines show a sustained glycolytic response to HAase whereas others show only an acute response. Identification of the variables that determine this metabolic segmentation could inform how different cell types respond to signals from the ECM, and elucidate the possible biological impacts of the glycolytic response to HAase in different tissues and contexts.

CHAPTER 2

•

Matrix digestion with hyaluronidase promotes plasma membrane GLUT1 through ZFP36-mediated targeting of *TXNIP*.

INTRODUCTION

Among the facilitative glucose transporters, GLUT1 is the most widely expressed and is thought to provide the cell with its basal glucose requirements (Mueckler, 1994). It is expressed most highly in tissues with high constitutive glycolytic activity—namely, brain and fetal tissue (Pessin and Bell, 1992). Consistently, it has been reported to be broadly upregulated in cancer (Younes et al., 1996). Levels of GLUT1 track with both proliferation and grade in breast carcinoma (Younes et al., 1995) and predict poor prognosis in both this disease and colorectal carcinoma (Haber et al., 1998; Kang et al., 2002). In some contexts, such as non-small cell lung cancer, GLUT1 and GLUT3 are co-expressed and are both associated with a poor prognosis (Younes et al., 1997). GLUT1 is transcriptionally upregulated by a HIF-1, a transcription factor important in tumorigenesis, and by effectors downstream of the mitogenic kinase Akt1 (Barthel et al., 1999; Semenza, 2010); it is repressed by the tumor suppressor p53 (Schwartzenberg-Bar-Yoseph et al., 2004).

Although GLUT1 is not as dynamically regulated as the insulin-responsive GLUT4, there are mechanisms known regulate its levels at the plasma membrane. PI3K signaling has been well established as a regulator of GLUT1 plasma membrane levels, suggesting localization of GLUT1 is an aspect of the glycolytic response to cell-extrinsic mitogenic signals—although the exact mechanism governing the subcellular distribution of the transporter is not clear. PI3K inhibitor wortmannin can block trafficking of GLUT1 to the plasma membrane in response to insulin stimulation (Clarke et al., 1994). Mimicking growth factor stimulation, activated Akt can increase plasma membrane trafficking and prevent internalization of GLUT1 (Wieman et al., 2007). Suggesting that mitogenic signaling pathways converge on GLUT1 localization, Ser226 on GLUT1 has recently been described as a target of protein kinase C (PKC), with phosphorylation of this site required for the increase in plasma membrane levels of GLUT1 in response to PKC activator TPA

(Lee et al., 2015). Together, these data show that GLUT1 can be dynamically trafficked in response to cell-extrinsic stimuli.

In the previous chapter, we showed that matrix digestion with HAase promotes a dramatic increase in glycolytic metabolism in cultured cells with a corresponding increase in plasma membrane GLUT1. Here, we show that this change in localization of GLUT1 is mediated largely by a preceding drop in TXNIP, which has been shown to negatively regulate GLUT1 transcription and promote its internalization from the plasma membrane in clathrin-coated pits (Wu et al., 2013). We also define a novel node of TXNIP regulation: HAase treatment triggers rapid induction of mRNA decay factor ZFP36, which targets the *TXNIP* transcript pool for degradation. We see evidence of ZFP36- and TXNIP-mediated interconnections between ECM remodeling and metabolism *in vivo*, both in cross-sections of an early cutaneous neoplasm and in transcriptional profiling of early murine embryos.

RESULTS

Reduced TXNIP expression can mediate the acute glycolytic response to HAase.

We then sought to determine how HAase mediates its effects on GLUT1 trafficking to the plasma membrane. While GLUT1 is thought to provide basal levels of glucose to the cell—and is therefore not as dynamically regulated as the insulin-responsive GLUT4—there are well established mechanisms that influence its distribution between intracellular compartments and the surface of the cell. While both PI3K and PKC are known to promote trafficking of GLUT1 to the membrane, we do not see induction of either pathway in response to HAase (data not shown) (Lee et al., 2015; Wieman et al., 2007). We therefore investigated whether HAase can induce rapid changes in levels of TXNIP, the thioredoxin-interacting protein whose effects on glucose metabolism are independent of its eponymous interaction (Patwari et al., 2009). TXNIP is known to regulate both the transcription and trafficking of GLUT1—the latter by binding the transporter at the plasma membrane and promoting its internalization in clathrin-coated pits (Wu et al., 2013). *TXNIP* levels also show strong anti-correlation with the glycolytic phenotype in our initial unbiased gene expression analysis (Figure 1-1). Indeed, TXNIP levels drop acutely in response to HAase treatment in 293T, LiSa-2, and MDA-686 cells (Figure 2-1). All show considerably reduced levels after 2h treatment, which is sufficiently rapid to possibly explain the increased levels of GLUT1 at the plasma membrane after 6h of treatment.

We therefore employed Txnip knockout (KO) MEFs to test whether the glycolytic response to HAase could be attributed to its negative regulation of Glut1. As previously described, Txnip KO cells have higher baseline rates of both glucose uptake and lactate production than their WT counterparts (Figure 2-2a), and, expectedly, have higher baseline levels of plasma membrane Glut1 (Figure 2-2b) (Elgort et al., 2010). After confirming that Txnip levels drop in response to HAase treatment in the WT MEFs (Figure 2-2c), we performed plasma membrane fractionations on both

the WT and KO MEFs after 6h and 24h of HAase treatment (Figure 2-3). While WT MEFs show a dramatic induction of membrane-bound Glut1, the KO cells show only a modest response. These differences are highlighted in the heatmap in Figure 2-3, which represents the ratio of band intensities between Glut1 and its respective loading control (Na,K-ATPase). Consistent with the hypothesis that trafficking of Glut1 is largely responsible for mediating the glycolytic response to HAase, Txnip KO MEFs show a dramatically smaller magnitude increase in both glucose uptake and lactate production in response to HAase (Figure 2-4).

ZFP36 is rapidly induced by HAase and targets *TXNIP* transcripts for degradation.

We next asked what upstream events might culminate in the acute decrease in TXNIP following HAase treatment. TXNIP is known to be regulated at both the transcriptional and post-translational level; given the acute nature of the change in TXNIP protein, we first probed the latter possibility. AMPK has been reported to phosphorylate TXNIP and accelerate its proteasomal degradation (Wu et al., 2013). While we confirmed this effect with an AMPK activator, A-769662, we do not see activation of AMPK—using phosphorylation of its target ACC as a readout—in response to HAase treatment (Figure 2-5).

We then investigated whether the JNK pathway might be responsible for TXNIP degradation, as it is activated in response to HAase in all cell lines tested (data not shown). The E3 ubiquitin ligase ITCH, which targets the two PPxY motifs on TXNIP, is activated by JNK phosphorylation—and also by HAase in cell lines tested (data not shown) (Chang et al., 2006; Gallagher et al., 2006; Wu et al., 2013; Zhang et al., 2010). Treatment of LiSa-2 cells with JNK inhibitor (JNKi) SP600125 prevents the activating phosphorylation of ITCH upon HAase treatment, but this robust inhibition has only a very modest rescue effect on TXNIP (Figure 2-6a). ITCH-mediated degradation of TXNIP may have some role in the glycolytic response to HAase, but the rescue effect of JNKi is below the sensitivity of our measurements, if so, as we did not see a

significantly decreased induction of glucose uptake with HAase in JNKi-treated cells (Figure 2-6b). Additionally, JNKi shows no rescue effect in GLUT1 plasma membrane trafficking in response to HAase (Figure 2-6c).

To examine whether the acute drop in TXNIP levels resulting from HAase treatment is due to TXNIP protein degradation, we expressed 3xFLAG-tagged TXNIP in LiSa-2 cells and then treated the cells with HAase for 4h. As shown in Figure 2-7a, we see a clear decrease in the endogenous TXNIP band with HAase treatment but no detectable decrease in the ectopically expressed band. These results suggest that the HAase-mediated drop in TXNIP levels is unlikely due to proteasomal degradation of TXNIP protein, and is more likely due to *TXNIP* transcriptional repression or mRNA processing. Indeed, *TXNIP* transcript levels drop by over 50% after 1h of HAase treatment in 293T, MDA-686, and LiSa-2 cells (Figure 2-7b).

Because of the rapidness with which *TXNIP* transcript levels drop in response to HAase, and because there is an AU-rich element (ARE) in its 3' untranslated region (UTR), we explored the possibility that mRNA processing might be involved. We constructed a reporter with a luciferase gene fused to the human *TXNIP* 3' UTR and transfected it into HEK293 cells. We then treated the transfected cells with HAase and measured the change in luciferase activity with different lengths of treatment (Figure 2-8a). The reduction in luciferase activity with HAase indicates that the treatment activates mRNA processing factors or targets them towards the 3' UTR sequence of the *TXNIP* transcript, which leads to subsequent degradation of the reporter. These results are consistent with matrix digestion by HAase acutely stimulating *TXNIP* mRNA degradation.

We identified an mRNA processing factor whose expression is induced by HAase in all cell lines tested: zinc finger protein 36 (ZFP36, also known as tristetraprolin/TTP). There is over a 2-fold transcriptional induction of *ZFP36* after just 1h of HAase treatment in 293T, MDA-686, and LiSa-2 cells (Figure 2-8b). Although originally cloned and identified as an insulin-responsive gene,

ZFP36 has also been shown to be rapidly and transiently induced by a variety of mitogens, including growth factors, serum, and 12-O-tetradecanoylphorbol-13-acetate (an activator of protein kinase C) (Blackshear, 2002; DuBois et al., 1990; Lai et al., 1990; Lim et al., 1989). ZFP36 engages with the AREs of its short-lived target transcripts and promotes their destabilization through recruitment of the CCR4-NOT deadenylase complex (Lykke-Andersen and Wagner, 2005; Sandler et al., 2011). A transcriptome-wide atlas of ZFP36 binding using crosslinking immunoprecipitation (CLIP) has shown binding of ZFP36 to the 3' UTR of the *Txnip* transcript (Sedlyarov et al., 2016), suggesting a potential role for ZFP36 in *TXNIP* regulation. Demonstrating that ZFP36 is at least *among* the processing factors that target the *TXNIP* 3' UTR, we see a dose-dependent decrease in luciferase activity when a ZFP36 expression vector is co-transfected with the *TXNIP* 3' UTR luciferase reporter, with dose defined as the amount of ZFP36 expression vector DNA co-transfected with a fixed amount of the reporter construct (Figure 2-8c).

To examine whether ZFP36 degrades *TXNIP* mRNA in response to matrix digestion with HAase, we first compared the temporality of changes in ZFP36 and TXNIP protein levels by performing a HAase treatment time course to capture changes between 5min and 24h (Figure 2-9). We observe synchronized divergence of these two proteins, with ZFP36 induction preceding the drop in TXNIP in 293T, LiSa-2, and MDA-686 cells. To assess the extent to which ZFP36 is responsible for the reduction in TXNIP levels, ZFP36 expression was knocked down by shRNA in LiSa-2 cells and these cells were then treated with HAase (Figure 2-10a). Both shRNA sequences reduce ZFP36 induction upon HAase treatment, and that with the stronger knockdown (shZFP36-2) also shows stronger rescue of TXNIP levels. Importantly, ZFP36 knockdown in LiSa-2 cells also blocks the increase in glucose uptake upon HAase treatment (Figure 2-10b). Together these data suggest that ZFP36-mediated degradation of *TXNIP* mRNA plays a critical role in the HAase-induced increase in glycolysis in LiSa-2 cells.

To examine whether ZFP36-mediated TXNIP reduction is a general response to HAase treatment across cells, we knocked down ZFP36 in a second cell line, MDA-686, using the same shRNA sequences as used in Figures 2-10a,b. Strong ZFP36 knockdown in MDA-686 cells, accomplished with shZFP36-1 expression, rescues the HAase-mediated drop in TXNIP levels, consistent with that seen in LiSa-2 cells (Figure 2-11a). However, shZFP36-2 expression results in a weaker knockdown of ZFP36 and shows no rescue of TXNIP protein levels upon HAase treatment. These data suggest that MDA-686 cells may be particularly sensitive to levels of ZFP36. Alternatively, other ZFP36 family members may play a more important role in the HAase-mediated TXNIP reduction in MDA-686 cells since these cells show significant upregulation of both of the other members of the *ZFP36* family (*ZFP36L1* and *ZFP36L2*) in response to HAase, whereas 293T and LiSa-2 cells do not (Figures 2-11b,c). These ZFP36 family members may collectively target the *TXNIP* transcript for degradation.

Since *TXNIP* mRNA can be regulated at the transcriptional and post-transcriptional levels, coordination of these TXNIP regulatory processes may happen in response to HAase, with the importance of either branch weighted differently in each cell line. Consistent with its role in transcriptionally programming glycolytic metabolism, Myc has been reported to suppress transcription of *TXNIP* (Shen et al., 2015). Interestingly, we detect elevated levels of Myc in response to HAase in some cell lines. LiSa-2 and MDA-686 cells show a robust increase in Myc that coincides with the reduction in TXNIP, similar to the pattern of ZFP36 induction and consistent with the possibility that Myc participates in the repression of TXNIP (Figure 2-9). Though the expression of ZFP36 and Myc is somewhat synchronous, their effects are likely staggered: the former acutely targets the existing transcript pool, whereas the latter tunes transcription in a more protracted way. The speed with which *TXNIP* transcript levels plummet after HAase treatment—

coupled with the rescue effect of ZFP36 knockdown—suggests a disproportionate role for ZFF36 in the *acute* regulation of TXNIP.

Expression of ZFP36 in response to HAase is transient (Figure 2-9), therefore Myc may be responsible for determining which cells have a sustained glycolytic response to HAase—and which do not. LiSa-2 cells, which have stably elevated levels of Myc following HAase treatment, show significantly higher rates of glucose uptake and lactate production at 5d of HAase treatment compared to 24h (Figure 1-6a). By contrast, while induction of Myc in response to HAase is much subtler in 293T cells, there is a decrease in Myc at later time points (12h, 24h) that corresponds with the return of TXNIP levels to baseline after 24h of HAase treatment (Figure 2-9). Consistent with the notion that Myc may be involved in the protracted glycolytic response to HAase, glucose uptake in 293T cells reverts towards baseline after 5d of treatment (Figure 1-6c). Levels of Myc, however, do not necessarily imply activity: gene set enrichment analysis of LiSa-2 cells treated with HAase for 24h does not reveal consistently significant upregulation of Myc targets (example plots highlighted in Figure 2-12).

To determine whether HAase treatment elicits canonical induction of *ZFP36* through growth factor signaling, we used an antibody array to assess phosphorylation of receptor tyrosine kinases. Indeed, after 30min of HAase treatment, activation of PDGFR-β is apparent in LiSa-2 cells (Figure 2-13a) and EGFR in MDA-686 cells (Figure 2-13b). In addition, we see phosphorylation of Ephrin A4 in LiSa-2 cells, as well as ALK and Ephrin B3 in MEFs (Figure 2-13a,c). To confirm that growth factor signaling is upstream of ZFP36 induction in this context, we used MDA-686 cells because they show striking activation of EGFR without activation of any other RTKs in the array, reducing the possibility of redundant signaling events triggered by HAase in these cells. We treated the cells with the EGFR inhibitor erlotinib and show that this suppresses induction of ZFP36—as

well as suppressing its baseline levels—and causes a striking increase in baseline TXNIP levels, which do not seem to decrease when additionally treated with HAase (Figure 2-14).

Degradation of the ECM reduces contact inhibition and increases migration.

After mechanistically determining how HAase treatment impacts glycolytic metabolism, we wanted to examine the biological contexts in which increased glycolysis in response to matrix remodeling might be important, and the impact this increased glycolysis may have on cell proliferation and migration. An elevated glycolytic rate is a hallmark metabolic characteristic of highly proliferative cells as it can support the energetic and biosynthetic demands of rapid proliferation (Vander Heiden et al., 2009). And proliferation, we reasoned, should require remodeling of the ECM to accommodate the increase in biomass and reorganization of cells within the tissue. As such, we hypothesized that the glycolytic response to HAase treatment may suggest a causal relationship between ECM remodeling and proliferation.

To examine a potential relationship between proliferation rate and levels of matrix deposition in tissue, we performed immunohistochemical staining of a murine model of cutaneous squamous cell carcinoma development. As shown in Figure 2-15, hyperplastic epidermis adjacent to the tumor shows discrete regions of proliferation—indicated by positive staining for Ki-67—that strongly anti-correlate with regions of strong staining for core ECM constituents collagen IV (Figure 2-15a) and HA (probed with HABP) (Figure 2-15b). This seemingly mutually exclusive staining pattern leaves open two distinct possibilities: that digestion of the matrix is a secondary effect of proliferation—that once cells respond to proliferative stimuli, they secrete matrix-digesting enzymes to accommodate their expansion; or, that matrix-digesting enzymes can be secreted by neighboring cells, with the changes in surrounding matrix serving as paracrine proliferative signals.

To test whether HAase has a direct effect on proliferation of cultured cells, we measured proliferation rates of cells grown from medium density (some cell-cell contacts) to high density

(Figure 2-16). In HFF-1, LiSa-2, and MEF cells, treatment with HAase has minimal impact on proliferative rate during the exponential growth phase (within the first 1-2 days of treatment), despite having a dramatic impact on cell morphology (illustrated in phase-contrast images of LiSa-2 cells in Figure 2-16). When cell-cell contacts begin to increase, however, HAase confers a significant proliferative advantage, suggesting that HAase allows the cell to overcome contact inhibition. While control-treated HFF-1 and MEF cells form classic monolayers at high density, their HAase-treated counterparts appear to grow on top of each other, forming lattices of cell projections (as seen in representative images of both cell lines in Figure 2-16). To examine whether the acute drop in TXNIP levels in response to HAase treatment is involved in the HAase-mediated increase in proliferation, we measured the proliferation rates of HAase-treated WT versus Txnip KO MEFs. Interestingly, despite their considerably blunted glycolytic response to HAase, Txnip KO MEFs do not show an altered proliferative response to HAase treatment relative to WT MEFs (Figure 2-16). These results suggest that matrix remodeling with HAase promotes cell proliferation by reducing contact inhibition, but acute reduction of TXNIP is not involved in this response to HAase in MEFs.

What, then, is the reason for the cell to upregulate glycolysis in response to HAase if metabolism is not limiting for proliferation? One explanation would be that the metabolic response that we observe is advantageous *in vivo*, where nutrients are found in much lower abundance than in standard cell culture and may indeed be limiting for proliferation. Another explanation would be that the disruption of monolayer architecture that we observe with HAase treatment represents not only insensitivity to contact inhibition but also increased migration. It is possible that proliferation and migration both occur in response to perturbations in the matrix, and that the increase in glycolysis supports the former by provisioning biosynthetic intermediates and the latter by generating a rapid

pool of ATP. Indeed, HA has been widely described to exert both mitogenic and migratory effects on cells (Toole, 2001).

To assess the possibility that HAase treatment increases migration—and that the glycolytic response to HAase *in vitro* at least in part supports the energetic requirements of this migration—we performed a scratch assay on monolayers of both WT and Txnip KO MEFs (Figure 2-17). In this simplistic approximation of wound healing, a consistently sized scratch is made in the monolayer and movement of cells into the discontinuity is measured. To rule out the possibility that differences in proliferative rate could confound the analysis, the monolayers were pre-treated with mitomycin C prior to the scratch assay, which renders them able to migrate but unable to divide. Consistent with our hypothesis, WT MEFs show a significant increase in their rate of "wound" closure with HAase treatment. Interestingly, though, there is no difference in migratory rate between the PBS- and HAase-treated Txnip KO MEFs, and their absolute rates of migration are not statistically different from the HAase-treated WT MEFs. Together, these data suggest that the rate of cell migration tracks with rate of glycolytic metabolism. The glycolytic response to matrix digestion with HAase, therefore, may serve to rapidly generate ATP and fuel a broader migratory response to changes in the ECM.

ECM correlates and Zfp36 anti-correlates with Txnip in neoplastic tissue.

Proliferation and the glycolytic metabolism that accompanies it are hallmarks of cancer. Also fundamental to tumorigenesis is disruption of tissue architecture (implicitly, profound remodeling of the matrix). Tumors, however, present with tremendous internal heterogeneity in both proliferation and metabolism (Hensley et al., 2016). Could our model help explain spatial variations in cell behavior within the tumor?

To probe the relationships between ECM constituents, Txnip, Zfp36, and glucose transporters *in vivo*, we performed immunohistochemical staining of a neoplasia driven by

KrasG12D and loss of p53 in the hair follicle stem cells (Figure 2-18). We reasoned this was an ideal context to examine as there are high levels of proliferation and considerable tissue disorganization, which produces helpful architectural reference points. Comparable regions within the tissue are highlighted with boxes of uniform color and magnified for ease of comparison (Figures 2-19 & 2-20). As expected, we see strong correlation in staining between ECM constituents—particularly collagen IV—and Txnip (Figure 2-18). Because the collagen protein is much smaller than the HA polymer and because its cellular interactions are more discrete, it is unsurprising that its staining pattern shows clearer boundaries of expression than HABP. Also, since HABP can bind with partially digested HA fragments, faint signal would still be expected in areas where the ECM is being actively digested.

Consistent with our findings and previous reports, Txnip and Glut1 show a striking anti-correlation in this neoplasm (Figure 2-19). The regions of highest intensity HABP staining—marking speckles of HA deposition—also appear to anti-correlate with both *cytoplasmic* Zfp36 and proliferation marker Ki-67, as well as Glut3, reinforcing the possibility of a coordinated metabolic and proliferative response to digestion of the ECM (Figure 2-20). Importantly, cytoplasmic Zfp36 represents the compartment actively engaged in mRNA processing. Some of the mitogenic signals known to rapidly induce ZFP36 transcription can also lead to its phosphorylation and subsequent trafficking from the nucleus to the cytosol, where it is active (Blackshear, 2002). As shown in Figures 7C-D, there is some baseline nuclear Zfp36 signal that overlaps with Txnip and the ECM, however the cytoplasmic Zfp36 primarily overlaps with the Ki-67 and Glut3 signals.

HA digestion may influence glucose metabolism in the early mammalian embryo.

Mammalian oocytes are surrounded by a network of cumulus cells—the cumulus oophorus—that are held together by a dense matrix of HA (Matzuk et al., 2002). These cells support the maturation of the oocyte by shuttling pyruvate and other metabolites into it through channels in the gap

junctions (Kidder and Mhawi, 2002). Sperm cells have GPI-anchored HAase that allow the sperm to penetrate the cumulus of HA and fertilize the oocyte (Lin et al., 1994). Shortly after fertilization, the cumulus is dispersed by the residual seminal HAase activity (Figure 2-21a). The digestion of HA, then, coincides with the genesis of a metabolically independent zygote.

Though pre-implantation embryos continue to rely predominantly on pyruvate and can be cultured in the absence of glucose without severe consequence until the 8-cell stage, there is consistent expression of GLUT1 coupled with non-negligible rates of glucose consumption through these early divisions (Leese and Barton, 1984; Purcell and Moley, 2009). It is thought, however, that glucose in the pre-blastocyst stage is used not for glycolysis per se, but rather used as a substrate for glycogen synthesis or shunted into the pentose phosphate pathway and used for biosynthesis (Gardner et al., 2000; Martin and Leese, 1995). It has even been reported that, despite the support of the cumulus cells, oocytes consume glucose at a rate that is governed, at least in part, by Txnip. A group has knocked down *Txnip* in oocytes via microinjection and found that its suppression increases both its glucose uptake and lactate production (Lee et al., 2013). This finding, albeit in an artificial system, suggests the possibility that dispersal of the HA-rich cumulus may impact glucose metabolism in the early embryo by regulating Txnip.

To assess the impact of HAase-mediated cumulus dispersal on glucose metabolism in early pre-implantation embryos, we performed RNA-Seq at sequential stages of cell division. Consistent with our previous findings, *Zfp36* transcript levels increase as *Txnip* levels decrease after dispersal of the HA-rich matrix (Figure 2-21b). Furthermore, glucose transporters do not appear to undergo meaningful transcriptional upregulation at these stages of development, as the absolute reads per kilobase mapped (RPKM) remain low for these transcripts (Figure 2-21c). This suggests that their trafficking might be a more important regulatory node for glucose metabolism in the early embryo.

These results are consistent with a possible stimulation of glucose metabolism in early mammalian embryos by HAase-mediated regulation of ZFP36 and TXNIP.

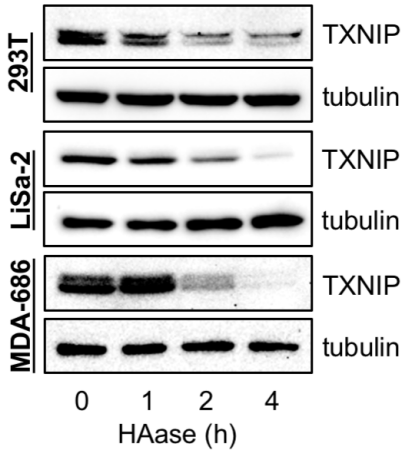

Figure 2-1. TXNIP levels drop acutely in response to HAase treatment in all cells tested.

Immunoblots showing TXNIP levels in 293T, LiSa-2, and MDA-686 cells treated with PBS or HAase (1h, 2h, and 4h).

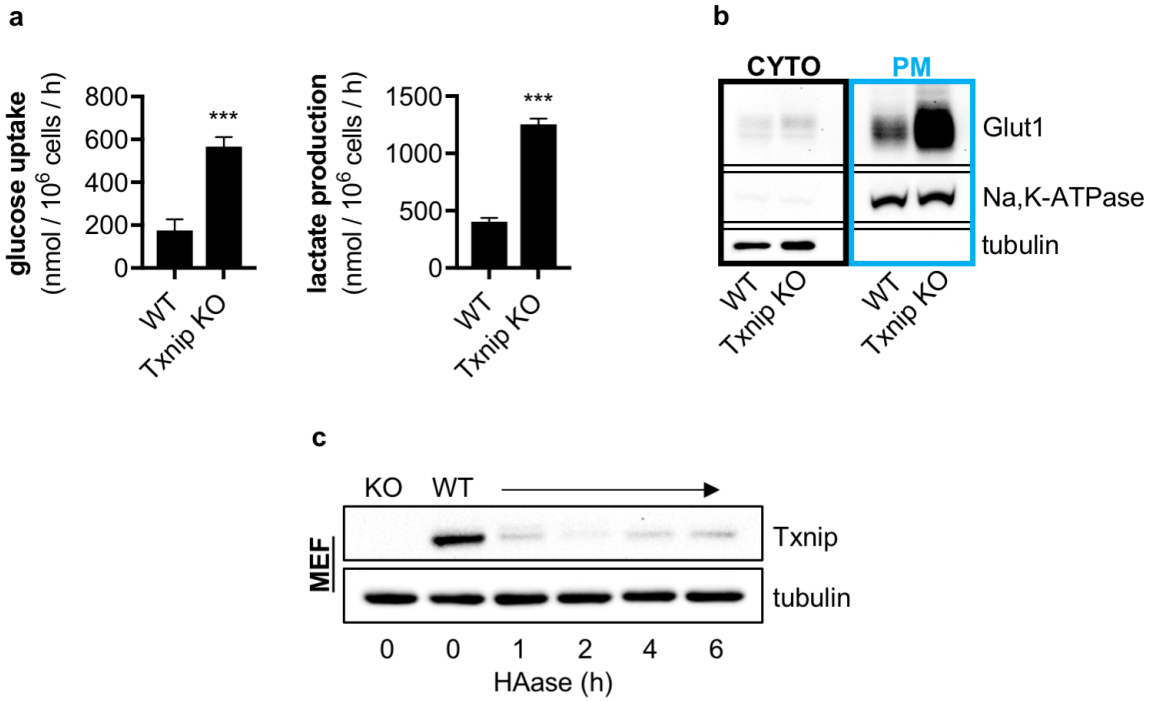

Figure 2-2. Txnip KO MEFs have a higher baseline glycolytic rate, as well as higher levels of plasma membrane GLUT1. (a) Baseline glucose uptake and lactate production rates in wild-type (WT) and Txnip knockout (KO) MEFs. **(b)** Immunoblots showing GLUT1 levels in both the cytoplasmic (CYTO) and plasma membrane (PM) fractions of WT and Txnip KO MEFs at baseline. **(c)** Immunoblots showing Txnip levels in KO MEFs at baseline and in WT MEFs treated with PBS or HAase for the indicated times. Error bars denote SD (n=3). ***p< 0.001.

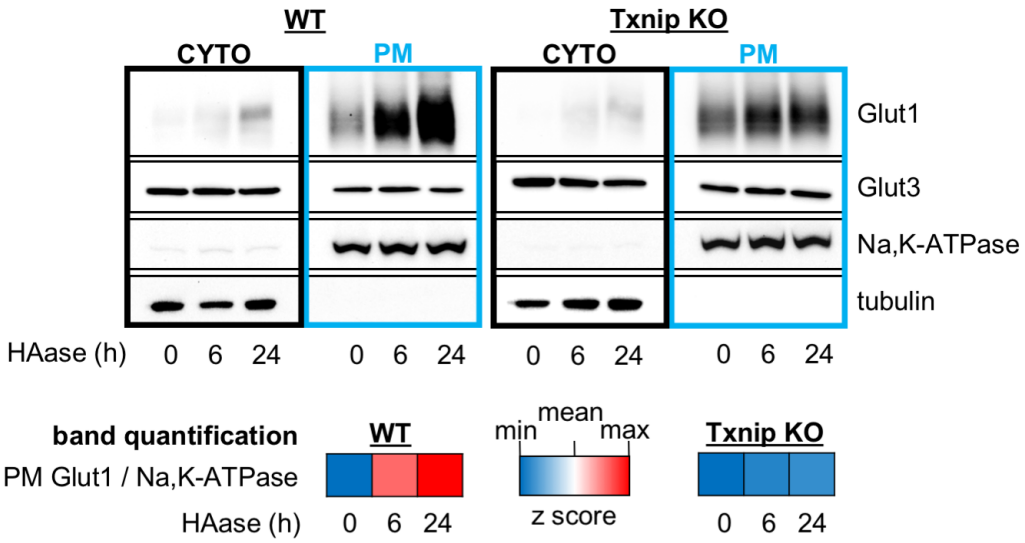

Figure 2-3. Txnip KO MEFs show considerably less enrichment of plasma membrane GLUT1 in response to HAase treatment. Immunoblots showing levels of Glut1 and Glut3 in both the cytoplasmic (CYTO) and plasma membrane (PM) fractions of WT and Txnip KO MEFs treated with PBS or HAase for the indicated times. Bands intensities were quantified for plasma membrane Glut1 and normalized to Na,K-ATPase. Heatmaps represent the z scores from the resulting ratios.

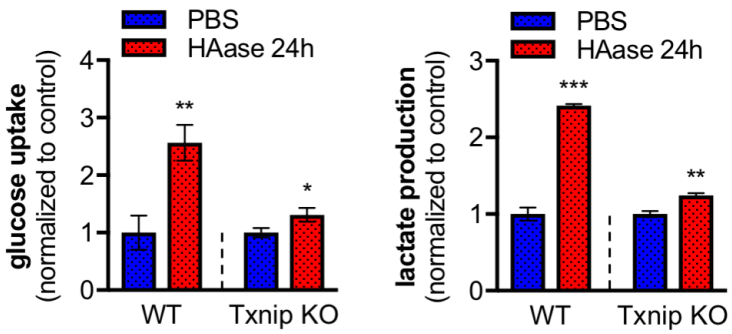

Figure 2-4. Txnip KO MEFs show considerably smaller magnitude glycolytic response to HAase treatment. Glucose uptake and lactate production rates in WT and Txnip KO MEFs treated with PBS or HAase for 24h. Rates for each cell line were normalized to PBS control. Error bars denote SD (n=3). *p<0.05; **p<0.01; ***p< 0.001.

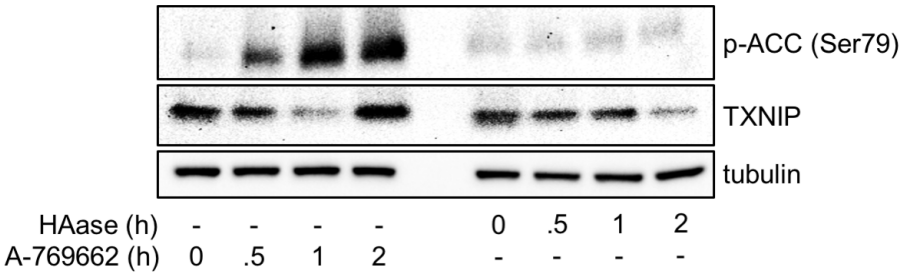

Figure 2-5. HAase treatment does not activate AMPK. Immunoblots showing levels of phosphorylated AMPK target acetyl-CoA carboxylase (ACC, Ser79) and TXNIP in LiSa-2 cells treated with 1mM AMPK activator A-769662 or HAase for indicated times, and with DMSO and PBS controls, respectively. Cells were serum starved overnight before experiment.

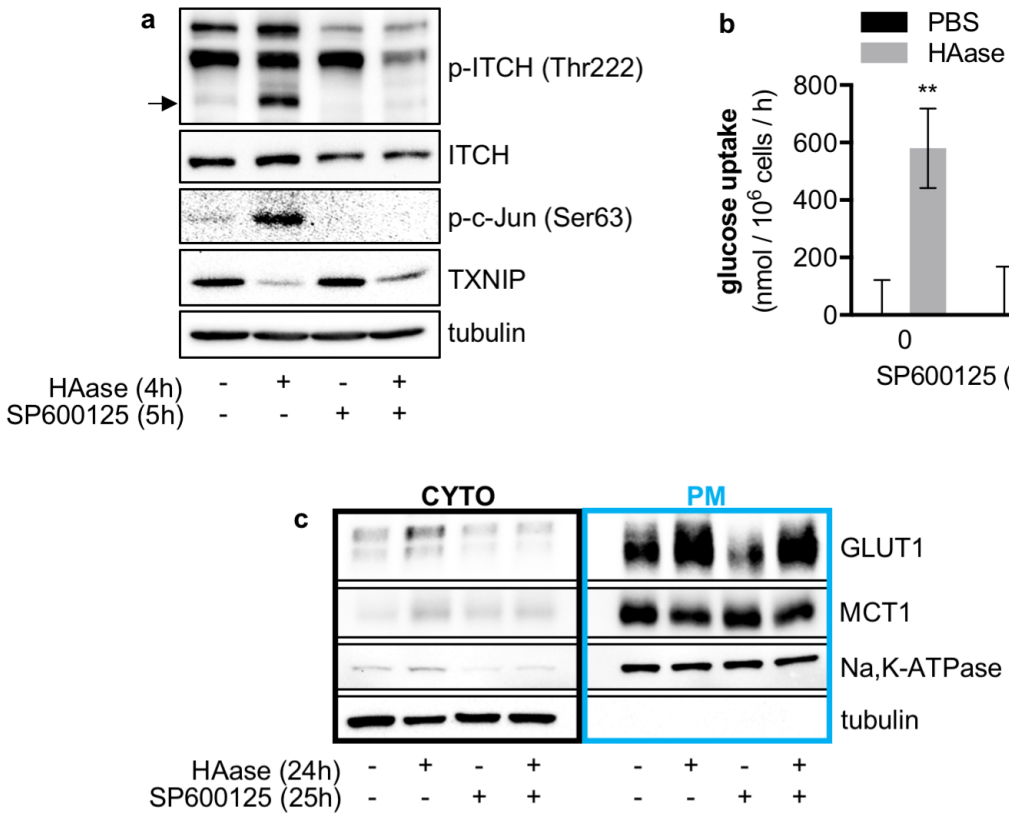

Figure 2-6. HAase treatment activates JNK signaling, but this pathway is not upstream of the drop in TXNIP. (a) Immunoblots showing levels of phosphorylated JNK targets—E3 ligase ITCH (Thr222) and c-Jun (Ser63)—as well as TXNIP in LiSa-2 cells. Pretreatment for 1h with either 20μM JNK inhibitor SP600125 or DMSO control was followed by an additional 4h treatment with PBS or HAase. Cells were serum starved overnight before experiment. Arrow indicates specific p-ITCH band. **(b)** Glucose uptake rates in LiSa-2 cells pretreated for 1h with 20μM SP600125 or DMSO and then treated with additional PBS or HAase for 24h hours. Cells were serum starved starting the night before the assay, and continuously through its completion. **(c)** Immunoblots showing levels of GLUT1 and MCT1 in both the cytoplasmic (CYTO) and plasma membrane (PM) fractions of LiSa-2 cells pretreated for 1h with 20μM SP600125 or DMSO and then treated with additional PBS or HAase for 24h hours. Error bars denote SD (n=3). *p<0.05; **p<0.01.

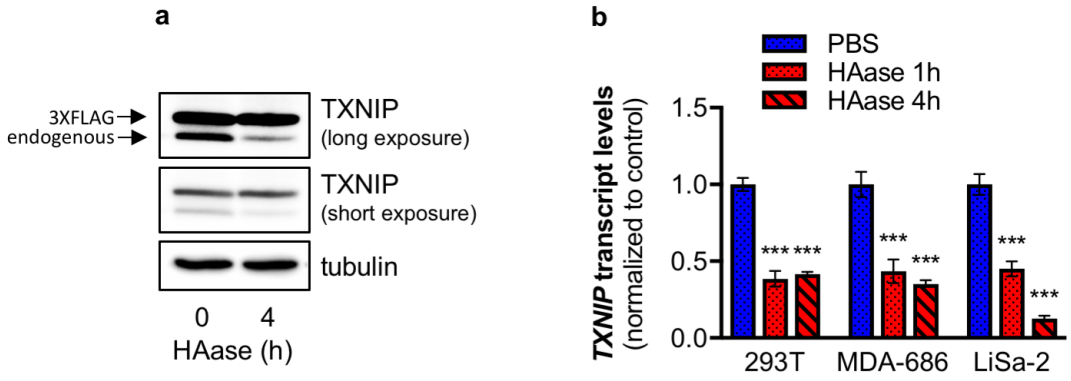

Figure 2-7. ***TXNIP*** **transcript levels drop acutely in response to HAase treatment. (a)** Immunoblots showing TXNIP levels in LiSa-2 cells stably expressing a 3xFLAG-tagged version of the protein. Cells were treated with PBS or HAase for 4h. **(b)** *TXNIP* transcript levels in 293T, MDA-686, and LiSa-2 cells treated with PBS or HAase (1h, 4h). Transcript levels were normalized to PBS control. Error bars denote SD (n=3). ***p< 0.001.

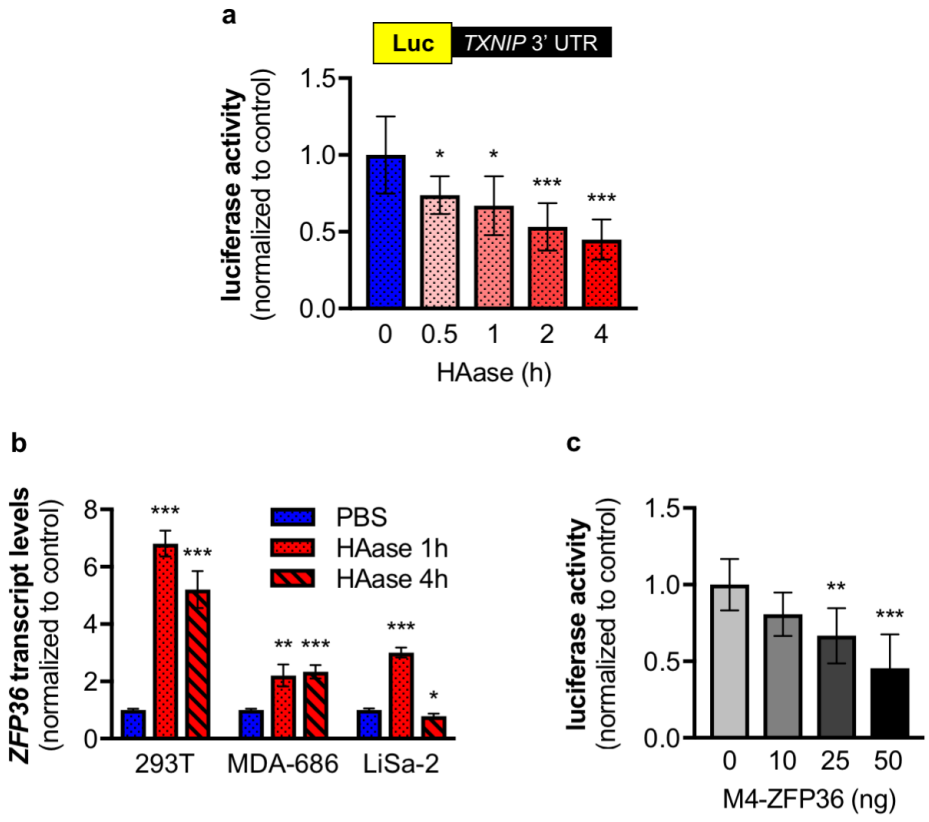

Figure 2-8. ZFP36 is rapidly induced by HAase treatment & targets the *TXNIP* transcript.

(a) Luciferase activity measured in lysates of HEK293 cells transfected with a *TXNIP* 3' UTR luciferase reporter, as well as a β-gal control plasmid, and treated with HAase for times indicated. Luciferase activity was normalized to β-gal activity to account for differences in transfection efficiency. Luciferase activity is presented relative to vehicle control. **(b)** *ZFP36* transcript levels in 293T, MDA-686, and LiSa-2 cells treated with PBS or HAase (1h, 4h). Transcript levels were normalized to PBS control. **(c)** Luciferase activity measured in lysates of HEK293 cells co-transfected with a fixed amount of the *TXNIP* 3'UTR luciferase reporter and increasing amounts of a ZFP36 expression vector (M4-ZFP36)—or the expression vector backbone without the insert as a control. Cells were also transfected with a β-gal control plasmid. Luciferase activity was normalized to β-gal activity to account for differences in transfection efficiency. Luciferase activity is presented

relative to empty vector control. Error bars denote SD (n=6 for **(a)** and **(c)**; n=3 for **(b)**). *p<0.05; **p<0.01; ***p< 0.001.

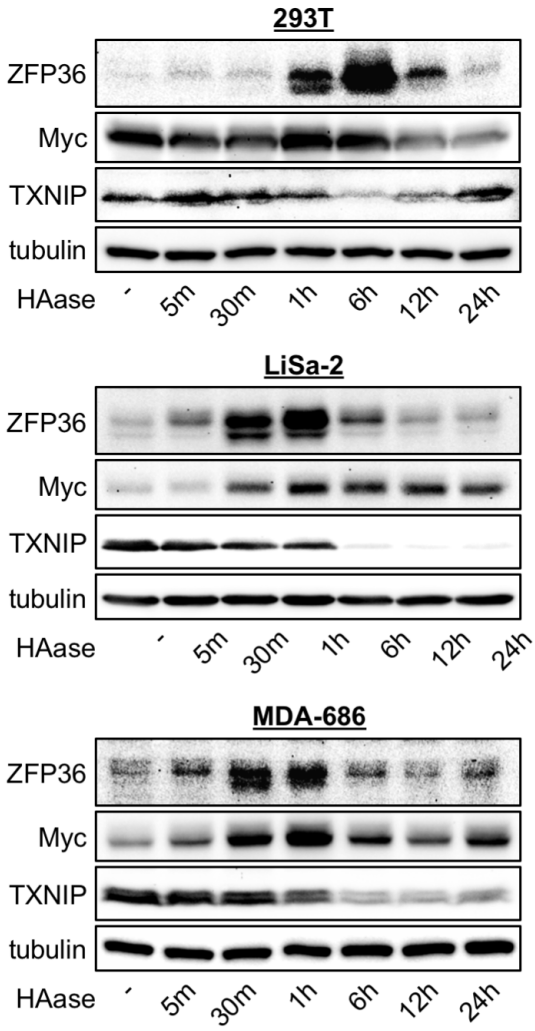

Figure 2-9. Induction of both ZFP36 and Myc precedes the drop in TXNIP following HAase treatment. Immunoblots showing levels of ZFP36, Myc, and TXNIP in 293T, MDA-686, and LiSa-2 cells treated with a time course of HAase (5min, 30min, 1h, 6h, 12h, 24h), or with PBS.

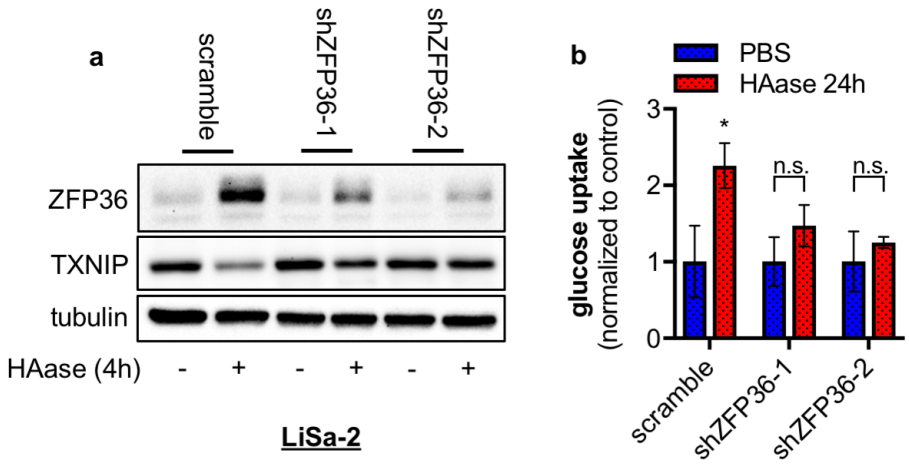

Figure 2-10. ZFP36 knockdown rescues drop in TXNIP following HAase treatment in LiSa-2 cells. (a) Immunoblots showing levels of ZFP36 and TXNIP in LiSa-2 with stable shRNA knockdown of ZFP36 or expression of a scrambled shRNA control. Cells were treated with PBS or HAase for 4h. **(b)** Glucose uptake rates in LiSa-2 cells with stable shRNA knockdown of ZFP36 or expression of a scrambled control. Cells were treated with PBS or HAase for 24h. Rates for each cell line were normalized to PBS control. Error bars denote SD (n=3). *$p<0.05$; n.s. - not significant.

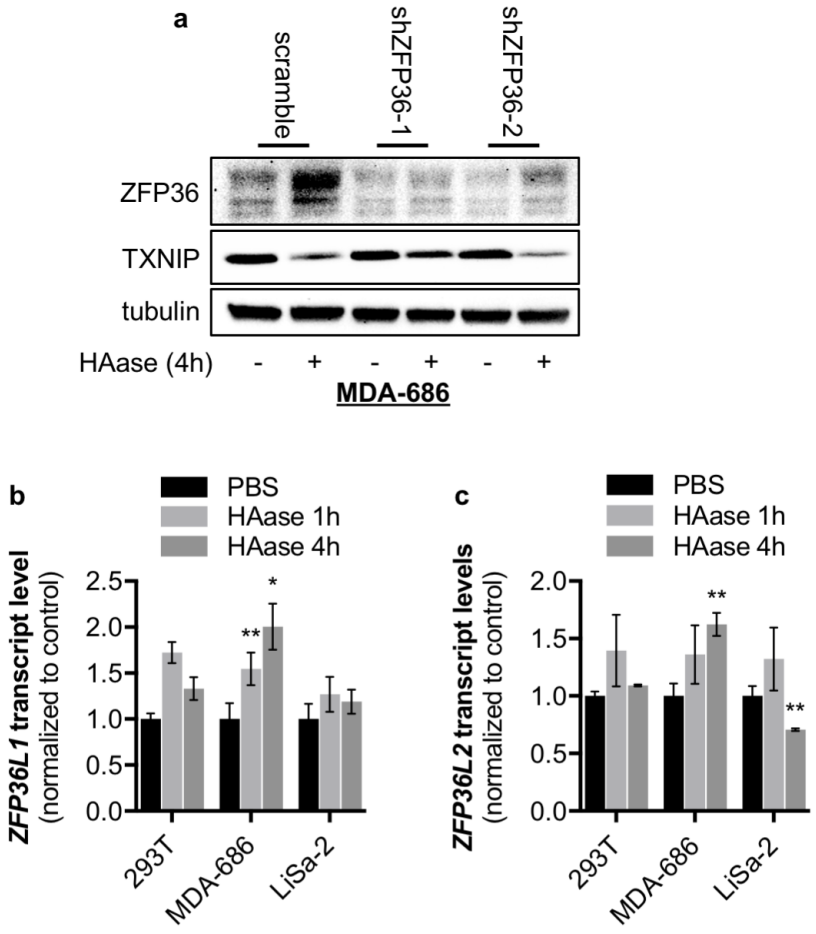

Figure 2-11. ZFP36 knockdown shows weak rescue of TXNIP in MDA-686 cells, possibly due to parallel upregulation of *ZFP36L1* and *ZFP36L2*. **(a)** Immunoblots showing levels of ZFP36 and TXNIP in MDA-686 cells with stable shRNA knockdown of ZFP36 or expression of a scrambled shRNA control. Cells were treated with PBS or HAase for 4h. **(b)** *ZFP36L1* and **(c)** *ZFP36L2* transcript levels in 293T, MDA-686, and LiSa-2 cells treated with PBS or HAase (1h, 4h). Transcript levels were normalized to PBS control. Error bars denote SD (n=3). *p<0.05; **p<0.01.

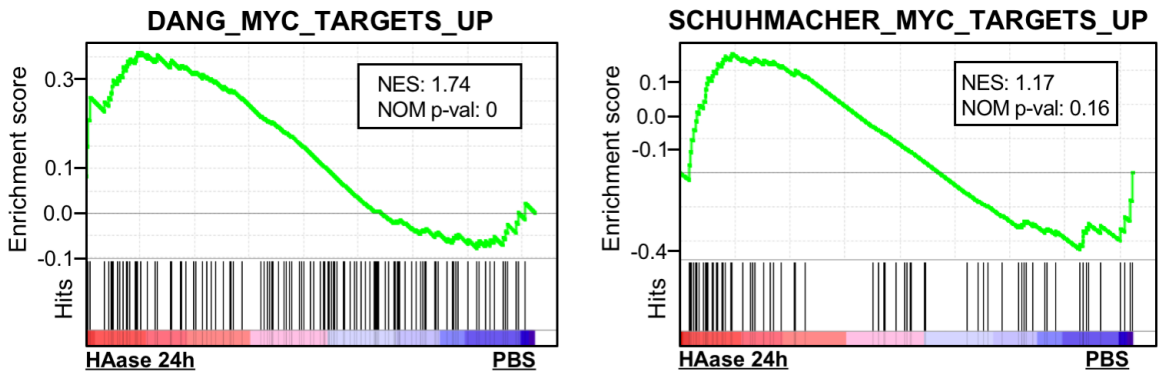

Figure 2-12. Myc targets do not show robust enrichment following HAase treatment. GSEA mountain plots showing enrichment of gene sets defined as Myc targets (Schuhmacher et al., 2001; Zeller et al., 2003) in LiSa-2 cells treated for 24h with HAase.

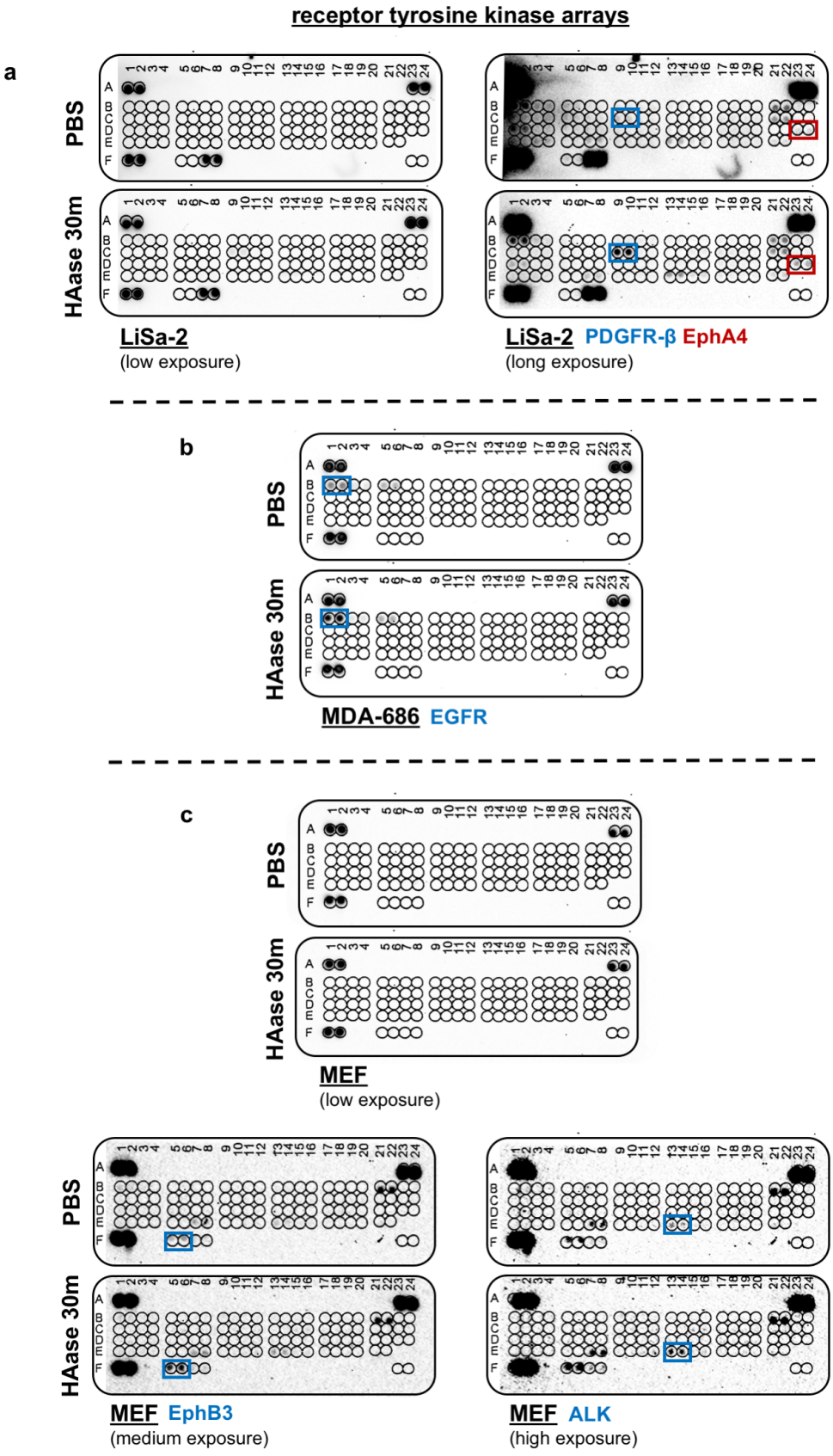
receptor tyrosine kinase arrays
a
PBS
HAase 30m
LiSa-2
(low exposure)
LiSa-2 PDGFR-β EphA4
(long exposure)
b
PBS
HAase 30m
MDA-686 EGFR
c
PBS
HAase 30m
MEF
(low exposure)
PBS
HAase 30m
MEF EphB3
(medium exposure)
MEF ALK
(high exposure)

(previous page)

Figure 2-13. Antibody arrays show activation of receptor tyrosine kinases in response to HAase treatment. Arrays with immobilized antibody spots (in duplicate) representing a variety of receptor tyrosine kinases (RTKs). Membranes were incubated with lysates from **(a)** LiSa-2 cells, **(b)** MDA-686 cells, and **(c)** MEFs treated for 30min with PBS or HAase then probed for phosphorylated tyrosine residues. Cells were serum starved overnight before treatment. RTK spots showing increased levels of phosphorylation upon HAase treatment are indicated.

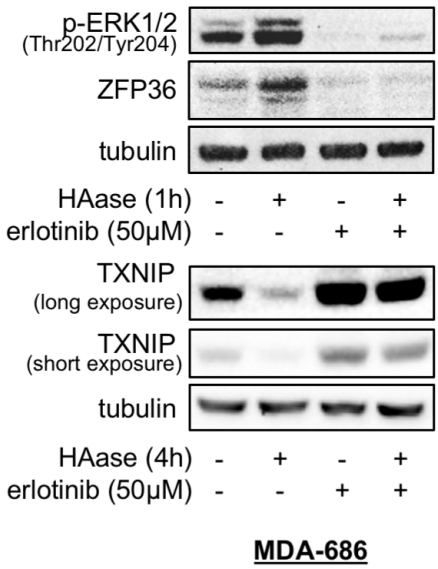

Figure 2-14. EGFR inhibition in MDA-686 cells blocks both the induction of ZFP36 and the drop in TXNIP following HAase treatment. Immunoblots showing levels of ZFP36, TXNIP, and p-ERK1/2 in MDA-686 cells pretreated for 1h with 50μM erlotinib or DMSO control, then with PBS or HAase (1h or 4h).

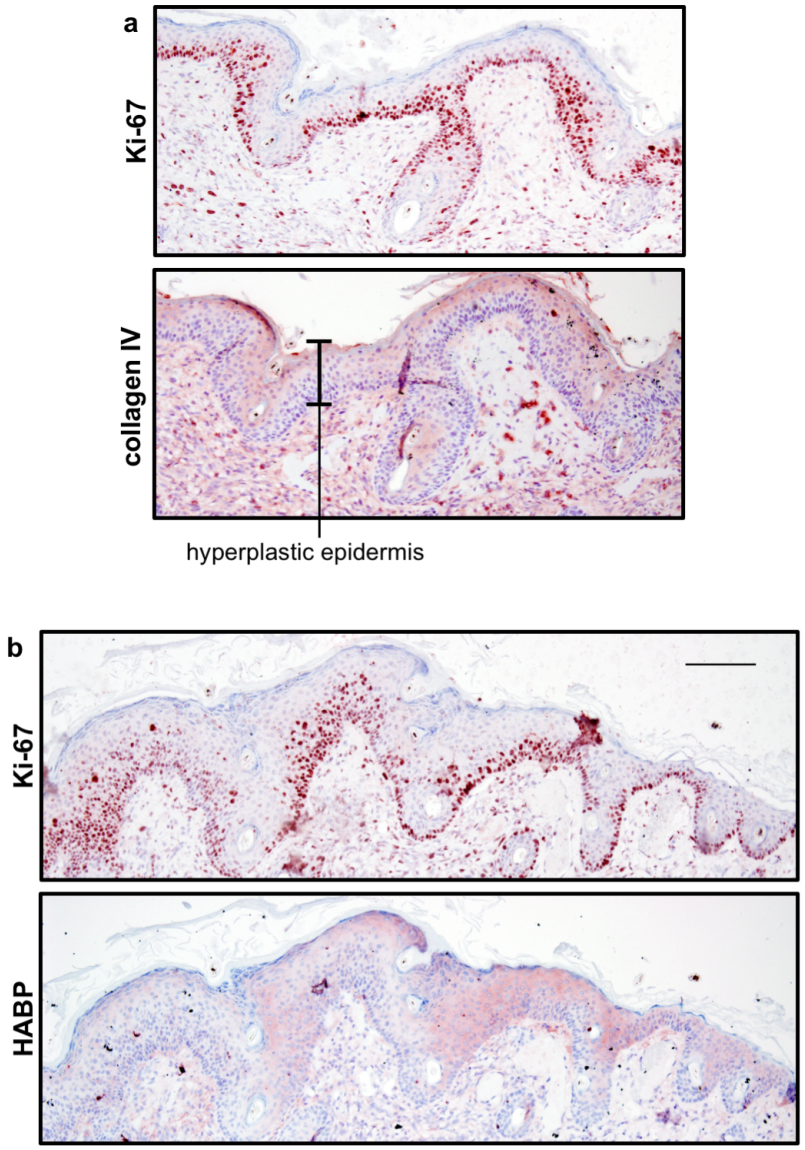

<u>Figure 2-15.</u> ECM anti-correlates with regions of active proliferation in tissue.

Immunohistochemical staining of hyperplastic epidermis (marked by brackets in collagen IV panel; adjacent to late-stage cutaneous squamous cell carcinoma). **(a)** One pair of serial sections was probed for collagen IV and Ki-67, a well-established marker of active proliferation. **(b)** Another was probed for HA (with hyaluronan binding protein, HABP) and Ki-67. Scale bar, 100μM.

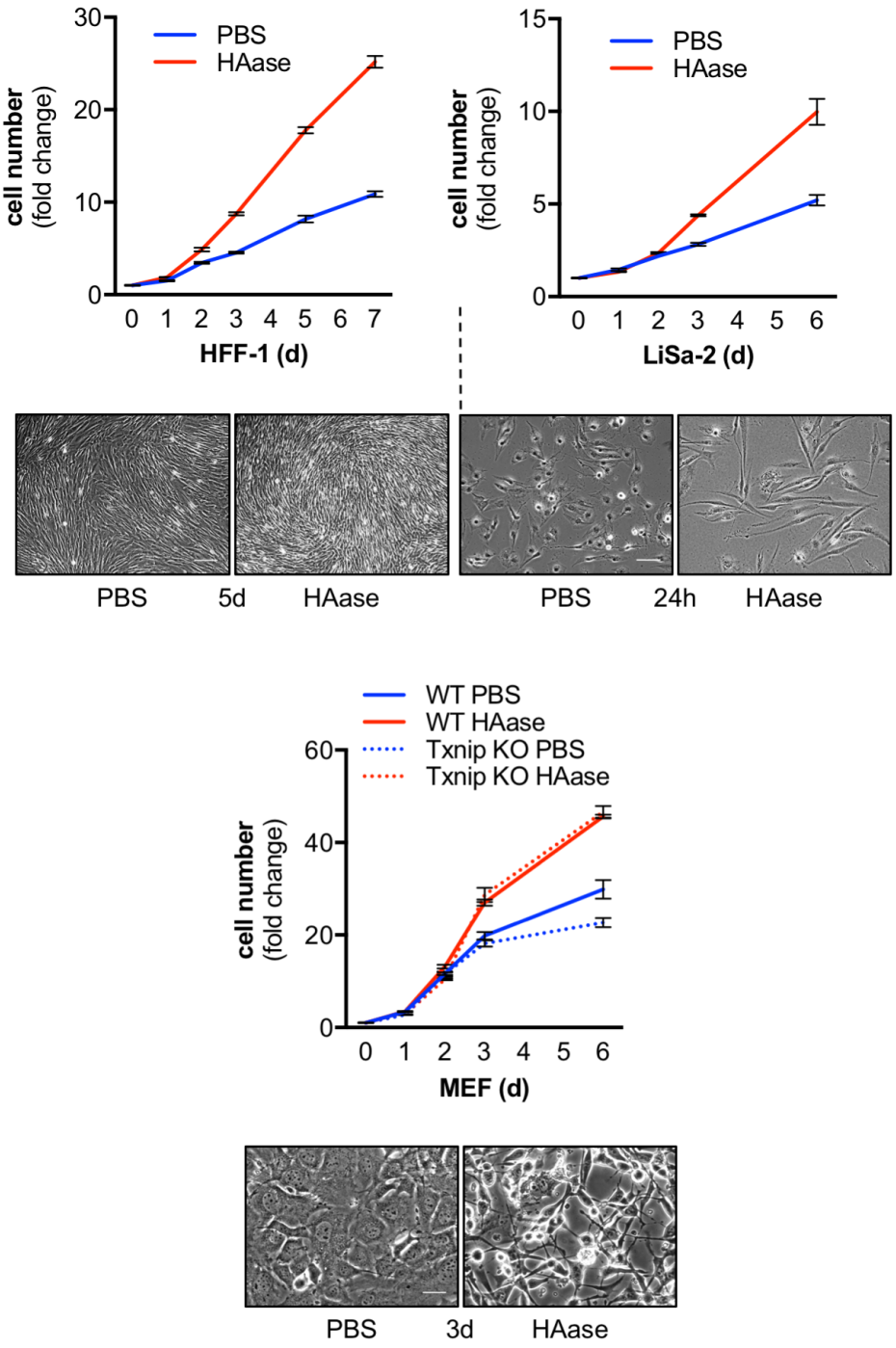

Figure 2-16. HAase treatment increases proliferation at high density, possibly through reduction of contact inhibition. Proliferation curves of HFF-1, LiSa-2, and MEF cells treated with PBS or HAase and counted at days indicated. Cells were seeded such that a one-week window would

capture both subconfluent and contact-inhibited phases of growth. Representative images of cell morphology and density are displayed below growth curves for each cell line. Scale bars, 250μM (HFF-1), 100μM (LiSa-2), 50μM (MEF).

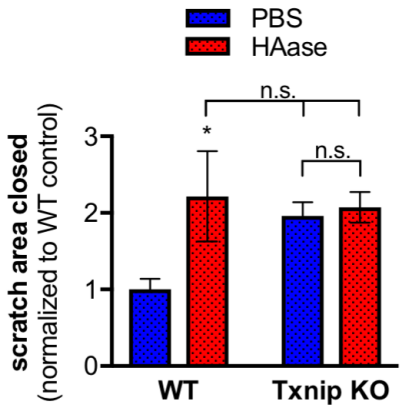

Figure 2-17. MEFs show increased rate of migration in response to HAase treatment, and this effect is dependent on Txnip. Scratch assay showing area of 'wound' closed by WT and Txnip KO MEFs pre-treated with mitomycin C (10μg/mL, 2h) followed by PBS or HAase for 12h before disruption of the monolayer. Absolute closure was measured between 6h and 12h after scratches were made, and these values were normalized to the WT PBS control. Error bars denote SD (n=3). *$p<0.05$; n.s. - not significant.

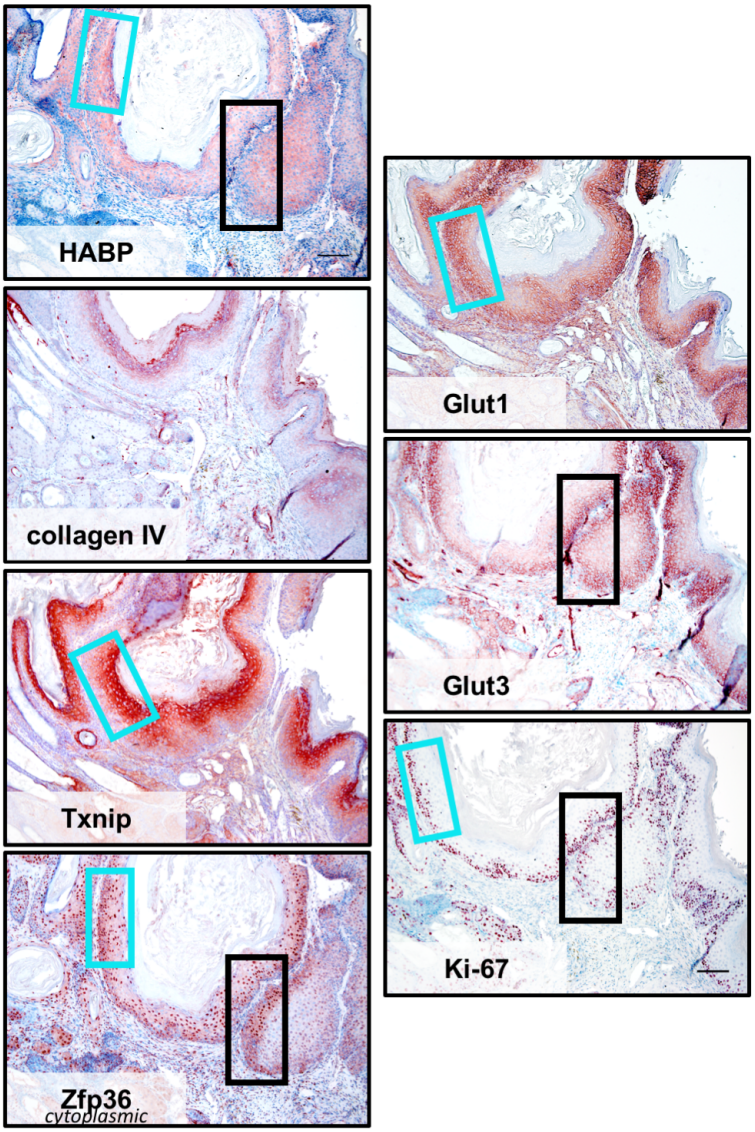

Figure 2-18. Interconnections between ECM and glycolytic metabolism are evident in early cutaneous neoplasm. Immunohistochemical staining of an early-stage cutaneous neoplasm driven by KrasG12D and loss of p53 in the hair follicle stem cells. Serial sections were probed for matrix constituents collagen IV and HA (indirectly, with hyaluronan binding protein, HABP), Txnip, Zfp36, Glut1 and Glut3, and well as Ki-67. Boxes highlight comparable architectural reference points with informative staining patterns; they are expanded in a color-coordinated fashion in subsequent figures**.** Scale bar, 100μm.

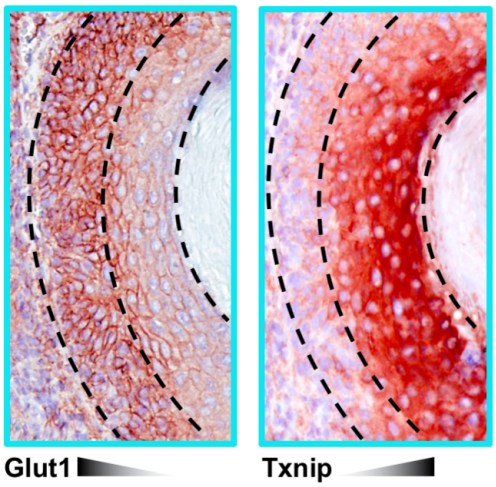

Figure 2-19. Txnip and Glut1 strongly anti-correlate in early neoplasm. Immunohistochemical staining of an early-stage cutaneous neoplasm driven by KrasG12D and loss of p53 in the hair follicle stem cells. Shown here is a region highlighting strong anti-correlation between Txnip and Glut1. Panels are annotated to demarcate boundaries of tissue structures and to highlight illustrative gradients of signal.

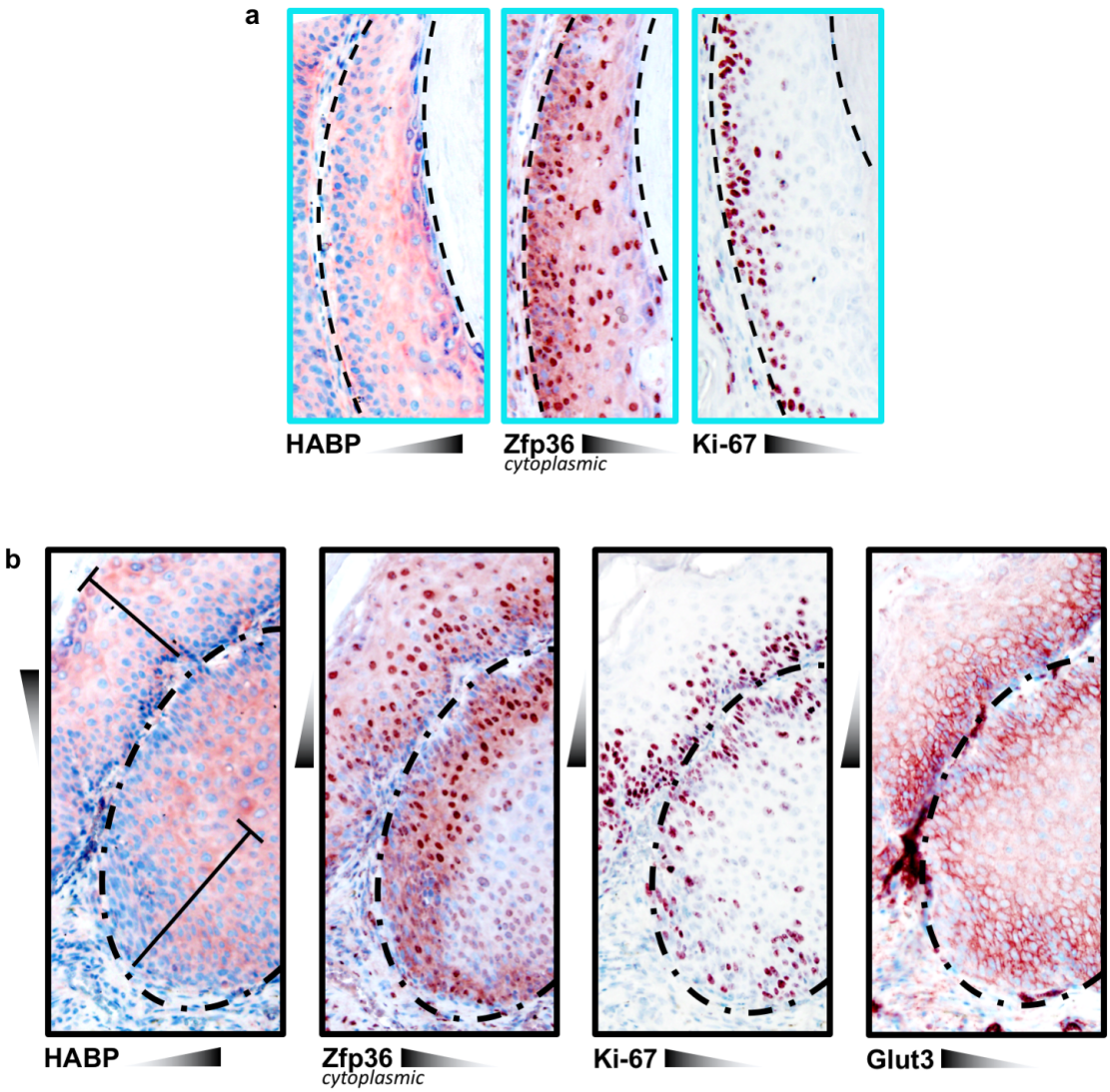

Figure 2-20. HA anti-correlates with both proliferation and glycolytic metabolism, as well with cytoplasmic Zfp36, in early neoplasm. Immunohistochemical staining of an early-stage cutaneous neoplasm driven by KrasG12D and loss of p53 in the hair follicle stem cells. **(a,b)** Shown here are regions of HA (probed with HABP) anti-correlation with cytoplasmic Zfp36, as well at Ki-67 and Glut3. Although there is some diffuse signal for HABP throughout the tissue section, the most concentrated depositions of HA seem to be more strongly localized. There are two illustrative gradients in **(b)** that are identified by brackets in the HABP panel.

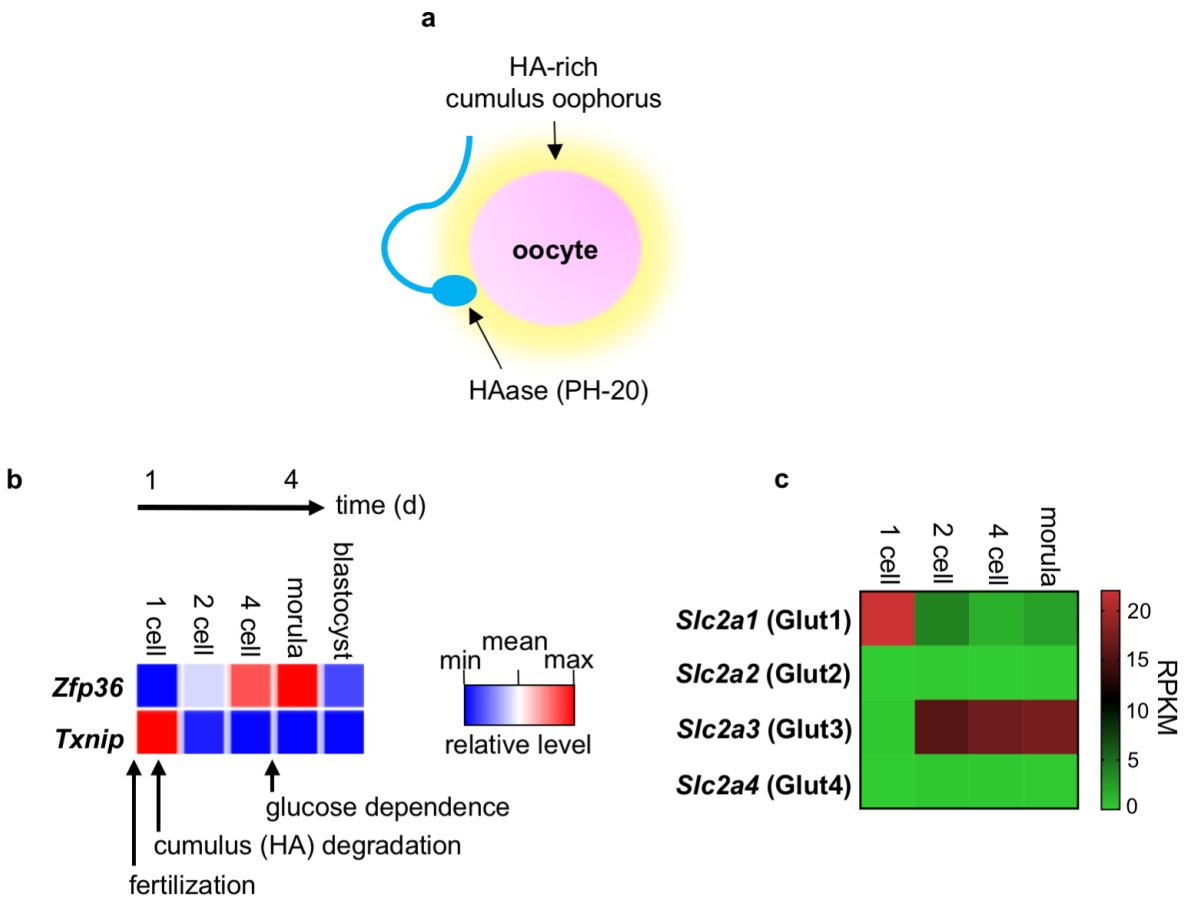

Figure 2-21. HA digestion may influence glucose metabolism in the early mammalian embryo. (a) Schematic illustrating the key role that HA digestion plays in fertilization: HA tightly binds together the cumulus oophorus-oocyte complex, and must be penetrated by the acrosomal HAase of the sperm. Shortly after fertilization, the HA-rich cumulus is dispersed. **(b)** Transcript levels (RPKM) of *Zfp36* and *Txnip* in early murine embryos, with important developmental milestones marked, including dispersal of the HA-rich cumulus and dependence on glucose for survival. Minimum and maximum values were normalized by row. **(c)** Absolute RPKM values for the canonical facilitative glucose transporters at indicated stages of cell division in early murine embryos.

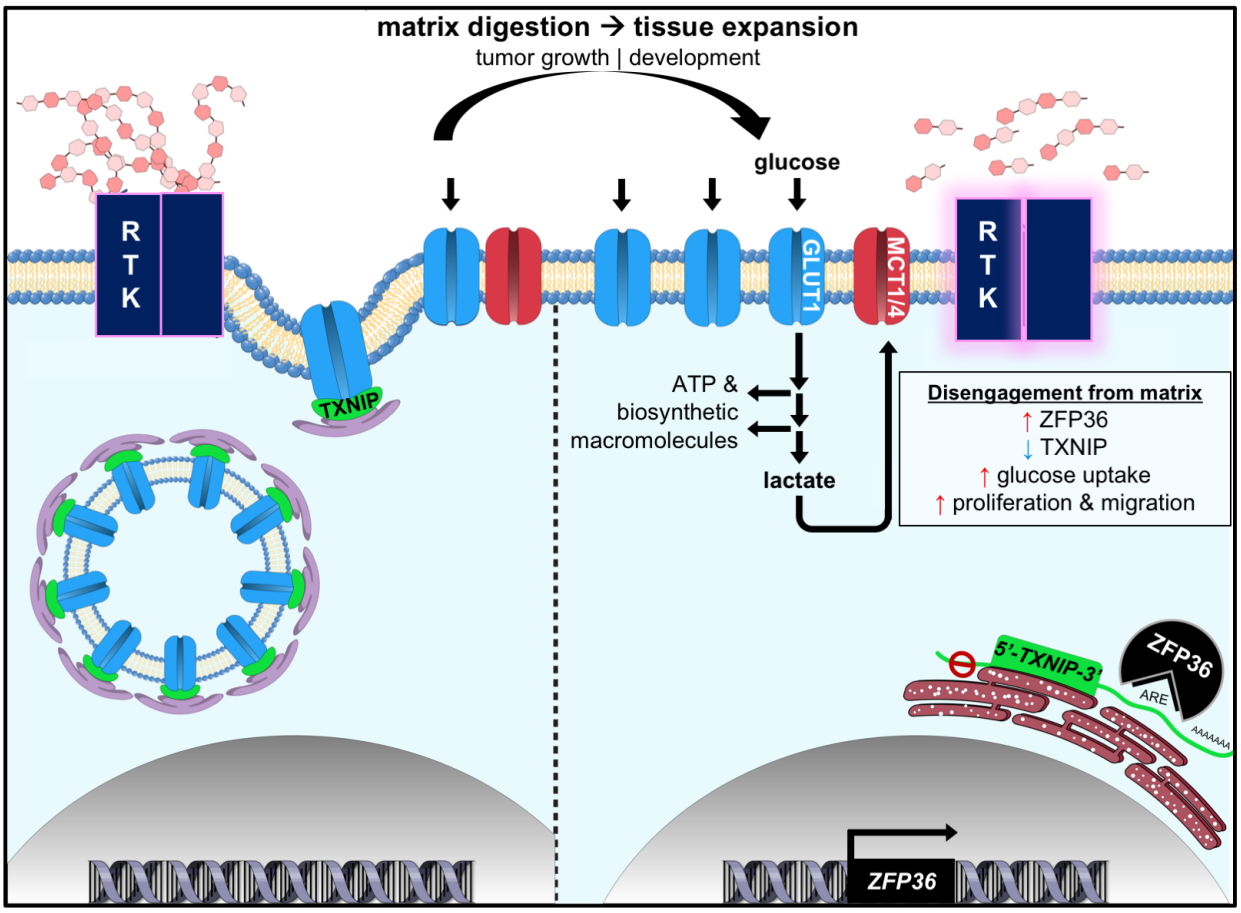

Figure 2-22. Model depicting how extracellular matrix remodeling acutely promotes increased glycolysis. Treatment with hyaluronidase activates receptor tyrosine kinases that rapidly induce ZFP36-mediated destabilization of TXNIP mRNA. The resulting drop in TXNIP protein reduces internalization of GLUT1, and therefore promotes increased GLUT1 plasma membrane localization, leading to increased glucose uptake and glycolytic rate. These acute changes in glucose metabolism occur in parallel with increased migration and proliferation, both *in vitro* and *in vivo*. Because migration and proliferation have high energetic and biosynthetic demands, respectively, we propose that their co-occurrence with changes in glucose metabolism may represent a coordinated response to ECM signals.

DISCUSSION

In this study, we report the surprising finding that ECM digestion with HAase acutely promotes cellular glucose metabolism. We describe a novel molecular pathway by which HAase stimulates glucose metabolism involving induction of ZFP36 downstream of receptor tyrosine kinase signaling, which rapidly targets the *TXNIP* transcript for degradation, and lifts its negative regulation of plasma-membrane GLUT1 (Figure 2-22). We also show that HAase treatment increases both cellular proliferation and migration, the energetic demands of which glycolysis may be induced to support. Correlational evidence in cutaneous neoplasia and in early embryos suggests possible contexts in which these relationships among matrix, metabolism, and proliferation may be important. In this way, we posit that matrix remodeling might serve—in addition to its other multivariate effects on the biology of the cell—as a potent node of cell-extrinsic metabolic regulation.

That TXNIP serves as a key node in integrating matrix signals with metabolism only adds to its broad cellular repertoire, which includes both acute and protracted regulation of glucose uptake. The MondoA:Mlx transcription factor complex can sense and respond to elevated glucose levels by translocating to the nucleus, binding to the carbohydrate response element in the *TXNIP* promoter, and upregulating its transcription as part of a negative feedback loop (Havula and Hietakangas, 2012; Stoltzman et al., 2008). Conversely, their transcriptional activity is repressed when the cell enters G_1 and requires biosynthetic glucose metabolites for anabolism (Elgort et al., 2010). As previously described, *TXNIP* can also be the target of stable downregulation, as Myc has been shown to bind to the E-box-containing region of its promoter and repress transcription—part of its broad transcriptional upregulation of glycolysis—possibly through competition with the MondoA:Mlx complex (Shen et al., 2015). Although TXNIP levels have been shown to be indirectly regulated through modulation of a destabilizing microRNA in the context of programmed cell death in

pancreatic beta cells, regulation of *TXNIP* transcript stability has not been shown in the context of metabolism (Lerner et al., 2012). We provide evidence for acute targeting of the *TXNIP* transcript pool by the mRNA decay factor ZFP36. Targeting *TXNIP* transcript stability endows the cell with an exquisitely nimble way to regulate its glycolytic rate in response to external stimuli, and to coordinate it with punctuated cellular behaviors like migration.

ZFP36 regulation of glucose metabolism has not been previously described, but may not be limited to the cellular responses to changes in the ECM. Because ZFP36 is known to be induced by both growth factors and cytokines, it may be an additional facet of their otherwise well described impact on glycolytic metabolism. Like ECM signals, growth factors and cytokines often elicit acute cellular responses, and ZFP36-mediated destabilization of *TXNIP* mRNA may provide a rapid way to upregulate glycolysis without having to augment or reprogram baseline glycolytic machinery: this is a rapid and reversible way to toggle the glycolytic valve.

The mechanistic link we describe between ECM remodeling and glucose metabolism might provide another layer of explanatory value in understanding the heterogeneity of cells in tissues: how cells sense and integrate environmental signals is imperfectly understood. Changes in the state of the matrix could elicit spatially and temporally circumscribed cellular responses. Hanahan & Weinberg have lamented the difficulty of experimentally assessing proliferative regulation in normal tissue due to the heterogeneous nature of paracrine signaling—as opposed to cancer cells, they argue, which are easier to understand due to constitutive activity of these signals (Hanahan and Weinberg, 2011). But in tumors, too, there is well documented spatial heterogeneity in mutational status but also in metabolism and proliferation (Hensley et al., 2016; Meacham and Morrison, 2013). Our data suggest the possibility that within such asynchronous tissue, local modulation of the matrix may be a way to elicit acute coordination of these interdependent processes.

CHAPTER 3

•

Hyaluronidase treatment identifies GLUT1 as a target of sialylation.

INTRODUCTION

Glycosylation of GLUT1—on Asn45, its only *N*-glycosylation site—affects its function, trafficking, and stability. In addition to dramatically altering migration of the protein on an SDS/PAGE gel, mutation of this site has been reported to reduce affinity of the transporter for glucose and subsequently reduce glucose flux into the cell (Ahmed and Berridge, 1999; Asano et al., 1991). Glycosylation-defective mutants also show disproportionate sequestration in intracellular compartments, and a decreased half-life (Asano et al., 1993). Consistent with these findings, chemical inhibition of glycosylation with tunicamycin substantially decreases levels of glycosylated plasma membrane GLUT1 and represses glucose metabolism (Samih et al., 2000).

Glycosylation of GLUT1 has been associated with tumorigenicity and the epithelial-to-mesenchymal transition (EMT). Comparisons of tumorigenic and non-tumorigenic HeLa x fibroblast cell hybrids show that an increase in GLUT1 glycosylation correlates with transformation, and that transformed hybrids have twofold higher uptake of 2-deoxyglucose (Kitagawa et al., 1995). Ras-transformed fibroblasts show an increase in glycosylation of GLUT1, as well as the increase in glucose metabolism characteristic of tumorigenesis (Onetti et al., 1997). Tunicamycin treatment of these transformed cells rescues the shift in gel migration of GLUT1 and the increase in glucose metabolism, suggesting a causal link between these co-occurring cellular events. Additionally, treatment of 3T3 fibroblasts with TGF-β1 causes both an increase in transcription and glycosylation of GLUT1 that accompany its mitogenic effect (Masumi et al., 1993).

N-acetylneuraminic acid (sialic acid, Neu5Ac) can be conjugated to the terminal ends of glycan linkages to form sialoglycans. This additional modification is enzymatically catalyzed in the Golgi by families of sialyltransferases (STs) named for both the carbon position onto which they transfer a sialic acid and the acceptor carbohydrate (Harduin-Lepers et al., 2005). While addition of sialic acid sugars to membrane glycoproteins and glycolipids occurs in most vertebrate cells, tumor

cells exhibit a marked hypersialylation, which is negatively correlated with patient prognosis (Büll et al., 2014). Sialylation enhances the invasive and migratory behavior of cells, and it can affect both cell-cell and cell-matrix interactions. Interestingly, cancer cells specifically upregulate sialylation of proteins involved in these processes, rather than that of all proteins (Almaraz et al., 2012).

Transcriptional upregulation of STs has been widely reported as part of the expression prolife associated with EMT in many cancer subtypes (Büll et al., 2014; Maupin et al., 2010). In addition to its role in GLUT1 glycosylation, Ras activation can increase sialylation of integrin β1 and increase its affinity for collagen (Seales et al., 2003). Myc—which we have found to be upregulated in response to HAase treatment in the previous chapter—has also been implicated in upregulation of ST3GAL family members and increased expression of sialyl Lewis x and sialyl Lewis a antigens during EMT, which increase extravasation and accelerate metastasis (Julien et al., 2011; Sakuma et al., 2012).

To our knowledge, however, the GLUT1 *N*-glycan has not been reported to be a target of sialylation. Here, we show that treatment of LiSa-2 cells with HAase induces an increase in apparent molecular weight of GLUT1 on an SDS/PAGE gel that can be rescued by cleavage of sialic acid from glycan linkages with sialidase. The functional consequences of this specific sialylation event, however, remain unclear—though it may be involved in the protracted glycolytic response to HAase observed in these cells.

RESULTS

HAase treatment identifies GLUT1 as a target of sialylation.

In our previous work, we have shown that HAase treatment causes increased plasma membrane trafficking of GLUT1 in all cells tested—despite no acute changes in total levels of the transporter. In LiSa-2 cells, however, we see a mobility shift in GLUT1 at later time points (24h, 5d) when resolved via SDS/PAGE (Figure 3-1a). The temporality of this shift suggests it might be involved in promoting the durable glycolytic response to HAase that we observe in these cells.

To identify the posttranslational modification responsible for this mobility shift, we digested lysates from LiSa-2 cells treated for 24h with PBS or HAase using calf intestinal phosphatase (to remove phosphate groups), PNGase F (to cleave glycan linkages), and sialidase (to remove sialic acid from glycan linkages) (Figure 3-1b). Both PNGase F and sialidase rescue the mobility shift associated with HAase, so we identified the responsible modification as sialylation, as it is more specific (schematic in Figure 3-1c). That is to say, only sialic acids are cleaved by sialidase, whereas entire glycan linkages including sialic acids are cleaved by PNGase F.

To determine whether GLUT1 sialylation is the result of increased ST expression—as opposed to increased sialic acid biosynthesis or selective targeting of GLUT1— we examined changes in expression of the four well established ST families in LiSa-2 cells treated with HAase for 24h or 5d (Figure 3-2). 5 of the 6 members of the ST3GAL family are upregulated in at least one time point, as is *ST8SIA6*. We then attempted to identify the responsible ST(s) by individually knocking down those that were upregulated by HAase using shRNA constructs. We found, however, that the selection marker, puromycin, alone abolished GLUT1 sialylation in response to HAase, even in the cells expressing the scrambled control construct (data not shown). We faced similar difficulty trying to knock down GNE, which encodes a bifunctional enzyme that regulates sialic acid biosynthesis, UDP-GlcNAc 2-epimerase/N-acetylmannosamine kinase.

Cleavage of exofacial sialic acid with sialidase substantially alters neither levels of plasma membrane GLUT1 nor the acute glycolytic response to HAase.

If sialylation were to exert a similar effect on GLUT1 as glycosylation, we reasoned it could affect the following parameters: trafficking, kinetics, or stability (both at the plasma membrane and with respect to the protein half-life). To address stability at the plasma membrane, we co-treated LiSa-2 cells with HAase and sialidase and examined levels of GLUT1 in this fraction (Figure 3-3). Sialidase in the media can cleave sialic acid from exofacial glycans, once the transporter has already been trafficked to the membrane. Although we see rescue of the mobility shift in plasma membrane GLUT1 co-treated with sialidase—as opposed to HAase alone—there is at most a very modest reduction in plasma membrane levels.

To address the possibility that the affinity of GLUT1 for glucose is augmented by sialylation, we measured glucose uptake and lactate production in LiSa-2 cells co-treated with HAase and increasing doses of sialidase (Figure 3-4). Because most of the sialylated GLUT1 is trafficked to the membrane, we see nearly complete rescue of this modification in whole-cell lysates of cells treated with sialidase at a concentration of 250U/mL or higher—little is sequestered in intracellular compartments inaccessible to the extracellular sialidase (Figure 3-4a). We do not, however, see a rescue effect in the induction of glycolysis in response to HAase when cells are co-treated with sialidase. It is possible, however, that the mobilization of GLUT1 to the plasma membrane in response to HAase is a saturated effect and therefore not rate-limiting. Changes in GLUT1 affinity for glucose, in that case, would be imperceptible when measuring the glycolytic response.

To determine whether sialylation of GLUT1 is involved in its increased plasma membrane trafficking in response to HAase, we attempted a variety of strategies to block the sialylation event itself rather that remove the modification once presented outside the cell. The most direct approach was use of a fluorinated sialic acid analog to chemically inhibit GLUT1 sialylation. $3F_{ax}$-Neu5Ac has

been described to be taken up through monosaccharide salvage pathways and converted to its nucleotide sugar conjugate, CMP-3F_{ax}-Neu5Ac, which not only competes with sialic acid but also can be sensed by the cell and lead to a decrease in endogenous biosynthesis of sialic acid (Rillahan et al., 2012). Treatment of serum-starved LiSa-2 cells with 3F_{ax}-Neu5Ac at published concentrations, however, did not rescue the mobility shift in GLUT1 (data not shown). One explanation for this could be relative insensitivity of the sialic acid biosynthesis pathway in these cells to feedback inhibition from high intracellular levels of the sialic acid analog.

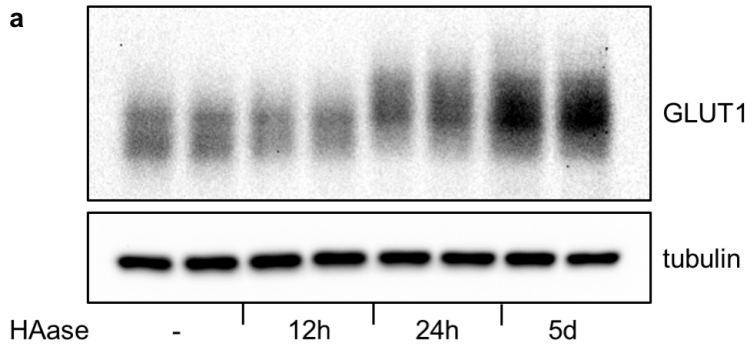
a
GLUT1
tubulin
HAase
-
12h
24h
5d

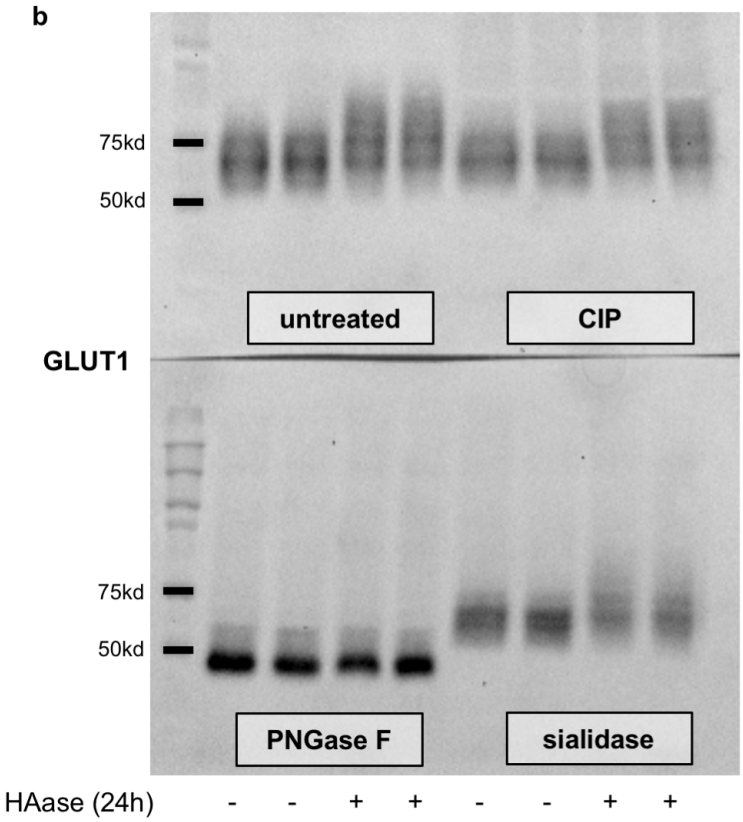
b
75kd
50kd
untreated
CIP
GLUT1
75kd
50kd
PNGase F
sialidase
HAase (24h)
- - + + - - + +

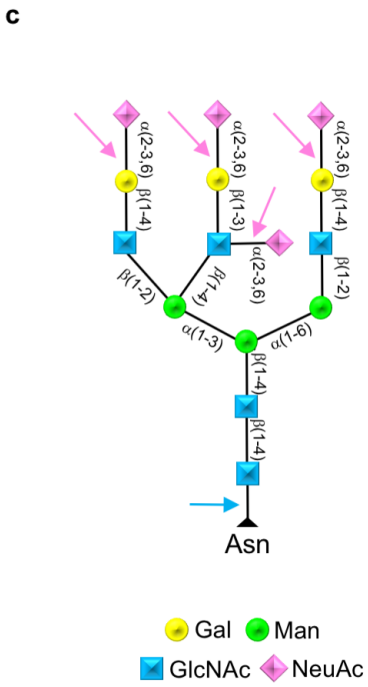
c
α(2-3,6)
β(1-4)
β(1-3)
α(2-3,6)
β(1-2)
β(1-4)
α(2-3,6)
β(1-4)
β(1-2)
α(1-3)
α(1-6)
β(1-4)
β(1-4)
Asn
Gal
Man
GlcNAc
NeuAc

(previous page)

Figure 3-1. Treatment of lysates with PNGase F and sialidase rescues the mobility shift in GLUT1 following HAase treatment. (a) Immunoblots showing GLUT1 levels in LiSa-2 cells treated in duplicate with PBS or HAase for times indicated (12h, 24h, 5d). **(b)** Immunoblots showing differential mobility of GLUT1 in lysates treated to remove posttranslational modifications. Lysates were prepared in duplicate from LiSa-2 cells treated with PBS or HAase for 24h. 15μg of lysate were then incubated at 37°C with water for 3h; calf intestinal alkaline phosphatase (CIP) for 1h; Peptide:N-glycosidase F (PNGase F) for 1h; or α2-3,6,8 neuraminidase (sialidase) for 3h. **(c)** Schematic shows the glycan linkage cleavage sites for the latter two enzymes; PNGase F is represented in blue & sialidase in pink (adapted from New England Biolabs).

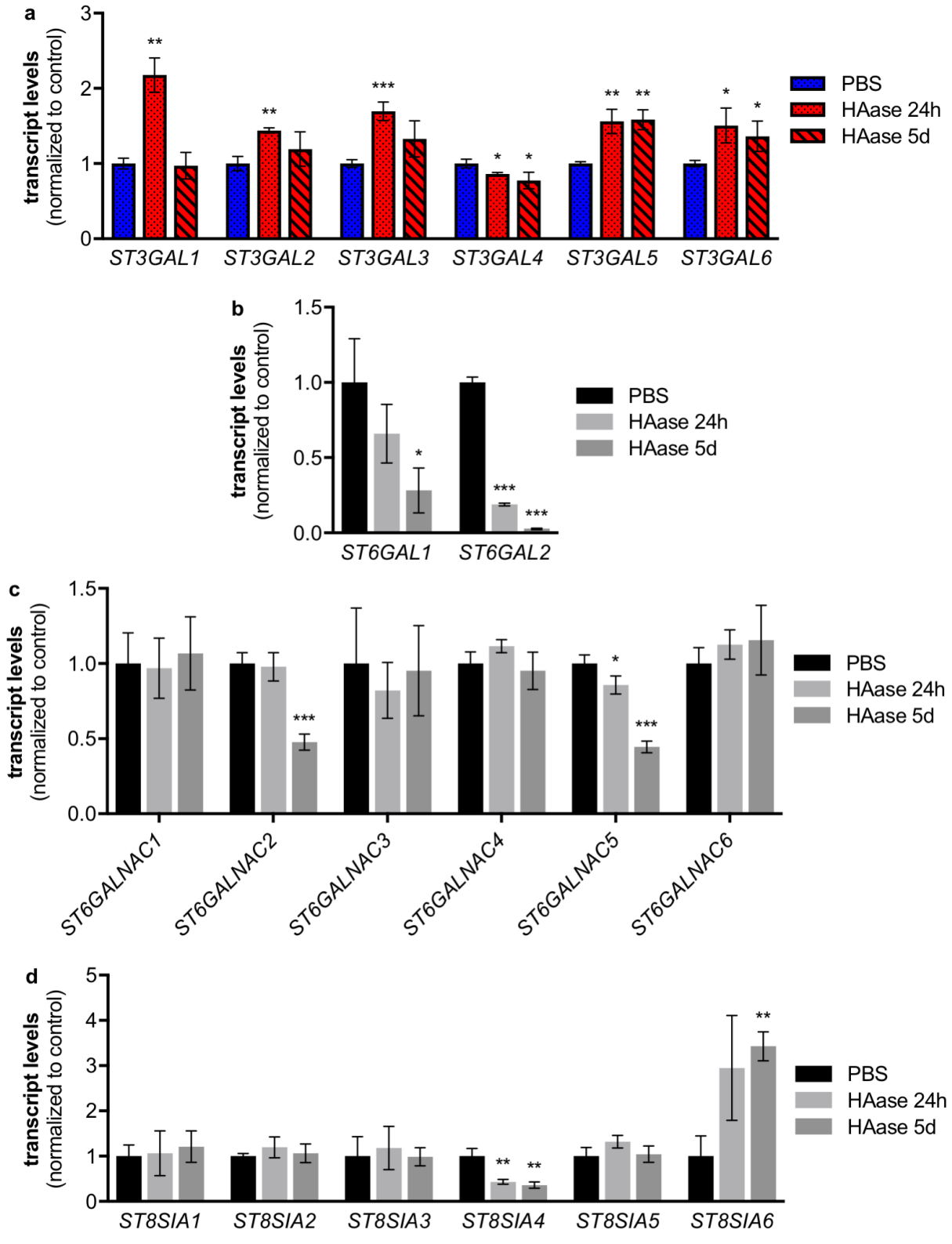
a
transcript levels
(normalized to control)
PBS
HAase 24h
HAase 5d
ST3GAL1
ST3GAL2
ST3GAL3
ST3GAL4
ST3GAL5
ST3GAL6
b
transcript levels
(normalized to control)
PBS
HAase 24h
HAase 5d
ST6GAL1
ST6GAL2
c
transcript levels
(normalized to control)
PBS
HAase 24h
HAase 5d
ST6GALNAC1
ST6GALNAC2
ST6GALNAC3
ST6GALNAC4
ST6GALNAC5
ST6GALNAC6
d
transcript levels
(normalized to control)
PBS
HAase 24h
HAase 5d
ST8SIA1
ST8SIA2
ST8SIA3
ST8SIA4
ST8SIA5
ST8SIA6

(previous page)

Figure 3-2. Expression of most ST3GAL family sialyltransferases is upregulated in response to HAase treatment. Transcript levels of canonical sialyltransferases in LiSa-2 cells treated with PBS or HAase (24h and 5d). Genes are organized by family, which are established based on the position of the transferred sialic acid on the recipient monosaccharide (ST3GAL family in **(a)**, ST6GAL in **(b)**, ST6GALNAC in **(c)**, and ST8SIA in **(d)**; see Figure 3-1c). Error bars denote SD (n=3). *p<0.05; **p<0.01; ***p< 0.001.

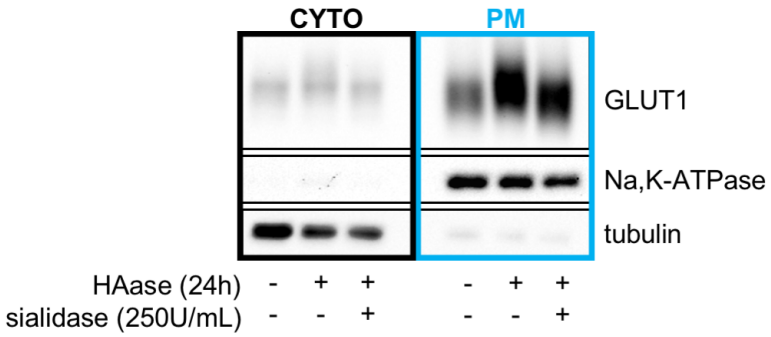

Figure 3-3. Cleavage of sialic acid from exofacial glycans does not substantially destabilize plasma membrane GLUT1. Immunoblots showing GLUT1 levels in both the cytoplasmic (CYTO) and plasma membrane (PM) fractions of LiSa-2 cells treated for 24h with PBS, HAase, or both HAase and α2-3,6,8 neuraminidase (sialidase, 250U/mL), the latter of which can cleave sialic acid from extracellular glycan linkages. The readout of sialidase activity is the rescue of the mobility shift in GLUT1.

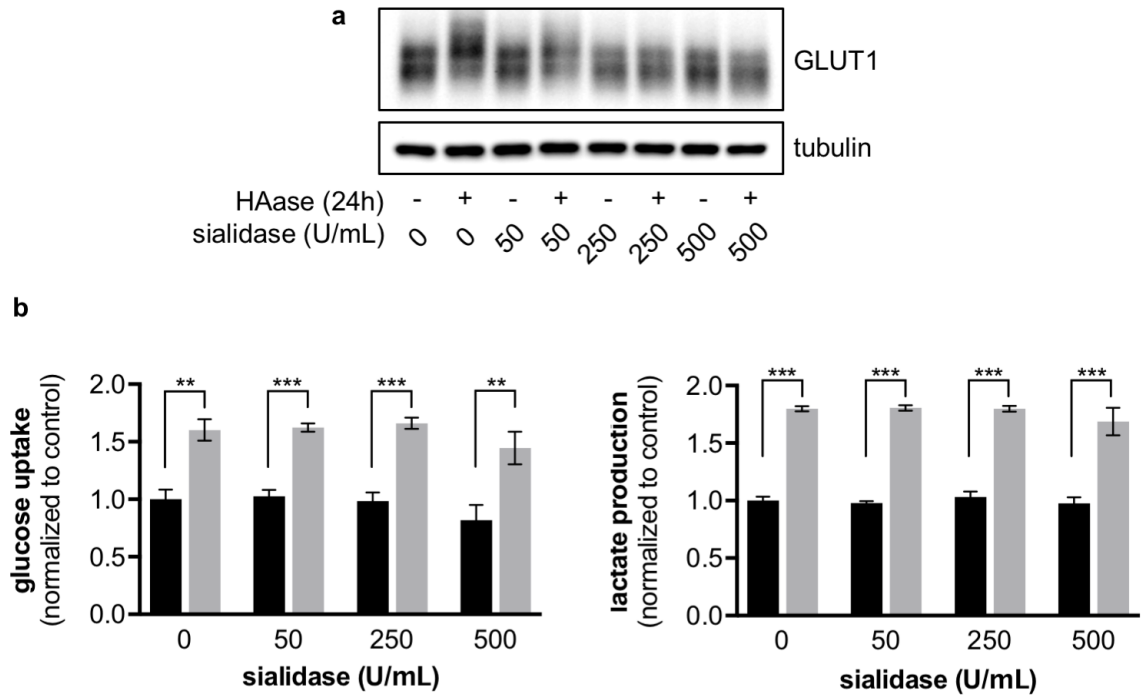

Figure 3-4. Cleavage of sialic acid from exofacial glycans does not diminish the acute glycolytic response to HAase. (a) Immunoblots showing GLUT1 levels in whole-cell lysates of LiSa-2 cells treated for 24h with α2-3,6,8 neuraminidase (sialidase) at indicated concentrations (0, 50, 250, 500U/mL), as well as with either PBS or HAase. **(b)** Glucose uptake and lactate production rates in LiSa-2 cells treated for 24h with α2-3,6,8 neuraminidase (sialidase) at indicated concentrations (0, 50, 250, 500U/mL), as well as with either PBS or HAase. Values are all normalized to the sialidase 0U/mL + PBS condition. Error bars denote SD (n=3). **$p<0.01$; ***$p< 0.001$.

DISCUSSION

In summary, we have shown here that GLUT1 is a target of sialylation. In the previous chapter, we found that the induction of glycolysis by HAase treatment was necessary not for the proliferative but for the migratory response of cells—albeit *in vitro*. It is interesting, then, that sialylation, which is so well correlated with cancer cell migration, also targets GLUT1. Could sialylation of GLUT1 reinforce the connection between migration and the rapid generation of ATP through glycolysis? Because downregulation of TXNIP is an acute response to extracellular stimuli, perhaps sialylation of GLUT1 increases plasma membrane trafficking in a more sustained way, to buttress pathologically (constitutively) migratory cancer cell behavior?

Unfortunately, these are somewhat intractable questions given the paucity of chemical inhibitors, and the difficulty of using a genetic approach on the large network of enzymes involved in sialylation. We did, however, attempt to explore 3 possible effects of sialylation on GLUT1: higher affinity for glucose, increased trafficking to the plasma membrane, and increased stability at the plasma membrane. From this work, we cannot make inferences regarding the effects of sialylation on GLUT1 trafficking, nor regarding its biochemical effects on transporter kinetics, as the GLUT1 response to HAase may be saturated. If there is an excess of glucose transport capacity at the plasma membrane beyond the glucose demands of the cell, changes in affinity for glucose may not impact net glucose uptake. Our work does suggest, however, that stability of GLUT1 at the plasma membrane is not substantially altered by sialylation. Our results also suggest that the possible effects of sialylation on glucose affinity and plasma membrane stability of GLUT1 are not substantial in mediating the glycolytic response to HAase in LiSa-2 cells.

One limitation to these experiments, however, is that the metabolic measurements and membrane fractionation were performed after a 24h HAase treatment interval. It would be informative to repeat these measurements on cells that have been treated for 5d, to disentangle the

acute and the sustained glycolytic response to HAase. It is possible that there is redundancy in GLUT1 regulation during the 24h treatment interval, and that once TXNIP levels return to baseline, sustained sialylation of GLUT1 may become more important in maintenance of the glycolytic phenotype in response to HAase.

While HAase treatment was a valuable system for identifying the sialylation event—and while this modification may be in involved in the sustained glycolytic response to HAase—use of the enzyme is not the most effective way to assess the biochemical impacts of GLUT1 sialylation, as HAase has multivariate metabolic effects. A better approach to understand the impact of the modification beyond the context of HAase treatment would be through identification and overexpression of the ST responsible for targeting GLUT1.

CHAPTER 4

•

Sustained metabolic reprogramming by hyaluronidase in a subset of cells is accompanied by broad changes in the state of the cell.

INTRODUCTION

Engagement with the ECM has been shown to exert an important role in changing cellular states. Expression of the matrix metalloproteinase (MMP)-3 in breast epithelial cells can stimulate the production of reactive oxygen species, which in turn promote EMT and cause genomic instability (Radisky et al., 2005). Although often discussed in the context of tumorigenesis and the escape of cancer cells from ordered epithelial tissue, EMT is also a fundamental aspect of processes such as embryogenesis and wound healing (Li and Li, 2015). One of the hallmarks of EMT and metastatic dissemination is the loss of E-cadherin, which is involved in maintaining strong intercellular adhesion within tissue (Onder et al., 2008). Indeed, many non-redundant transcription factors involved in EMT converge on suppression of E-cadherin (Moreno-Bueno et al., 2006). Interestingly, MMP expression has also been shown to more directly promote migration and EMT though direct proteolysis of E-cadherin (Kessenbrock et al., 2010). There is clearly an important relationship between ECM contacts and both the identity and behavior of the cell.

EMT and dedifferentiation of cancer cells have been linked to upregulation of glycolytic metabolism. Although cancer stem cells (CSCs) are often less proliferative than their better differentiated counterparts, they still exhibit higher rates of glycolytic metabolism, which has been suggested to be vital for maintenance of the stem-like state (Agathocleous and Harris, 2013; Li and Li, 2015)—a theory that is supported by our work on human embryonic stem cells (Gu et al., 2016). Reprogramming of metabolism during EMT occurs, at least in part, as a result of widespread chromatin reorganization. Promoter methylation and subsequent epigenetic silencing of genes such as *FBP1*—which encodes gluconeogenic enzyme fructose-1,6-bisphosphatase—can significantly increase glycolytic flux (Dong et al., 2013).

Various data presented in previous chapters suggest that HAase may alter the state of some cells beyond simple upregulation of glycolysis. HAase treatment of LiSa-2 cells, for example, causes

a change in morphology that resembles that of the canonical EMT program, with cells transitioning from fibroblastoid to a much more elongated form (Figure 2-16) (Yang and Weinberg, 2008). MEFs, too, show a morphological shift from cobblestone-like at high density to intercalating spindles when treated with HAase. Although LiSa-2 cells are already transformed and of mesenchymal origin, the parallel is striking, as is the increase in migratory behavior that accompanies this change in morphology (Figures 2-16 & 2-17). Although LiSa-2 cells are not undergoing true EMT, it is possible that they experience elements of this transition of identity in response to HAase.

HAase treatment causes an unsurprising increase in the HA receptor CD44, which is an established marker of CSCs (Figure 1-9). CSCs are defined by their relative dedifferentiation and their ability to reestablish the full phenotype range of cells within a tumor if re-seeded (Collins et al., 2005; Li et al., 2007; Prince et al., 2007). We hypothesized that the dramatic increase in CD44 upon HAase treatment may have global impacts on the state of the cell and push it towards a more de-differentiated state that may parallel EMT. We therefore decided to investigate whether HAase treatment can reprogram both the metabolism and the behavior of LiSa-2 cells, pushing them towards a more stem-like state. Here, we show that HAase treatment does, in fact, stably reprogram the metabolism of these cells, and that this reprogramming is accompanied by profound changes in the transcriptional and epigenetic state of the cell.

RESULTS

HAase treatment stably reprograms glycolytic metabolism in LiSa-2 cells.

To determine whether the sustained glycolytic response to HAase treatment in LiSa-2 cells represents stable reprogramming of metabolism or whether it requires continuous stimulation with the enzyme, we treated cells with HAase for 5d and then thoroughly washed off the enzyme. We then measured glucose uptake and lactate production 5d and 10d after release of the enzyme (Figure 4-1a). Both variables are strikingly stable after the withdrawal of HAase, confirming a reprogramming effect that becomes independent of ECM engagement. To determine if there is a temporal limit to this elevated rate of glycolysis, we treated LiSa-2 cells with HAase for 40d and found that both glucose uptake and lactate production continue to be elevated (Figure 4-1b) with no effect on cell viability (data not shown).

Transcriptional profile of HAase-treated cells suggests change in cell identity.

Because ECM disengagement has been associated with EMT and dedifferentiation, and because both of these events are closely connected to metabolism, we performed rank-rank hypergeometric overlap analyses to examine possible correlations between gene expression signatures associated with HAase treatment, induction of EMT, and the dedifferentiated state. The expression profile of LiSa-2 cell treated with HAase for 24h strongly overlaps with that of MCF-10A breast epithelial cells treated with TGF-β and irradiation (Andarawewa et al., 2007) (Figure 4-2a), as well as that of A549 lung adenocarcinoma cells treated with just TGF-β (Sartor et al., 2010) (Figure 4-2b). The HAase expression profile also strongly correlates with the dedifferentiated state in melanoma (Figure 4-2c) (Tsoi & Graeber, unpublished). To examine the specificity of correlation between HAase and TGF-β, we also compared the HAase expression profile to mammary epithelial cells genetically transduced with a number of established EMT-promoting constructs (Taube et al., 2010). There is

also strong overlap between the HAase and TGF-β1 expression signature in this genetic system, validating previous findings (Figure 4-3a). There is not, however, strong correlation between the HAase expression profile and that of E-cadherin knockdown (Figure 4-3b), or that of Goosecoid (Figure 4-3c), Snail (Figure 4-3d), or Twist (Figure 4-3e) overexpression. Together, these data support the notion that HAase treatment of LiSa-2 cells shifts the cell towards a less differentiated state, a process that may specifically overlap with aspects of TGF-β-driven EMT.

It is not clear, however, whether this dedifferentiation- and EMT-correlated HAase expression signature is a direct effect of the enzyme treatment and the signaling events it triggers, or whether it is the result of secondary effects on the ECM. Among the 15 genes most upregulated with 24h HAase treatment are MMP-1 and MMP-3 (Figure 4-4). Given the reported direct effects of these MMPs on EMT, it is possible that HAase treatment initiates further remodeling of the ECM, and that it is this secondary effect that drives the transcriptional change in cell identity.

HAase treatment alters the structure of both the genome and the epigenome.

To determine whether the stable reprogramming of metabolism by HAase in LiSa-2 cells coincides with changes in the epigenetic state of the cell, we extracted histones from cells treated with HAase for 24h and 5d. We then probed for trimethylation marks on various lysine residues on histone H3, but did not observe any substantial differences between either HAase time point and the PBS control (data not shown). We did, however, see a specific reduction in trimethylation of Lys20 on histone H4 (H4K20me3) at 5d compared to both PBS and 24h of HAase; there is no change in the monomethylated form (Figure 4-5). There is also a reduction in total H4 levels by immunoblot, which was confirmed to be specific to this histone by Coomassie staining, as total levels of H2A, H2B, and H3 appear unaffected by HAase. Levels of trimethylation of H4K20 have been reported to have a strong inverse correlation with clinical stage in squamous cell lung carcinoma, and loss of

this mark is associated with both a poor prognosis and invasive behavior in breast cancer (Van Den Broeck et al., 2008; Yokoyama et al., 2014). Because trimethylated H4K20 is enriched in heterochromatin, telomeres, and imprinted loci, it is thought to be largely involved in transcriptional silencing (Jørgensen et al., 2013). Loss of this mark, then, is consistent with broad activation of the genome and reversion to a stem-like state suggested by the transcriptional signature associated with HAase treatment of LiSa-2 cells (Figure 4-2c).

Because H4K20me3 has been reported to be important for the recruitment of the origin recognition complex to the origin of replication during DNA replication, we examined the possibility that HAase treatment and subsequent loss of this trimethylation mark alters progression through the cell cycle (Beck et al., 2012). DNA content of LiSa-2 cells treated with HAase for 24h or 5d was assessed by propidium iodide staining and subsequent flow cytometry analysis; representative histograms are shown here (Figure 4-6). After 24h of HAase treatment, there is a relative increase in the peak corresponding with 4N DNA content, suggesting G_2 arrest. This is an acute effect of HAase in LiSa-2 cells and can be rescued by co-treating cells with a MEK inhibitor (1μM PD 0325901, data not shown). Surprisingly, however, after 5d of HAase treatment, peaks appear that correspond with atypically high DNA content, suggesting that sustained HAase treatment triggers genomic instability and the induction of polyploidy in these cells. These data suggest polyploidy rather than aneuploidy because of the distinct peaks; aneuploidy would presumably show higher cell-to-cell variation in DNA content in excess of 4N. The experiment was repeated with particularly rigorous dissociation to ensure that the DNA peaks >4N were not the result of increased intercellular adhesion and possible clumping that might result from it. Additionally, nuclei were visually inspected after resuspension to confirm thorough dissociation. Although it is unclear if this change in cellular DNA content is mediated by loss of trimethylated H4K20, it is interesting that the temporalities of these observations overlap. Tetraploidy has been hypothesized to precede the more

disorganized chromosomal rearrangement characteristic of aneuploidy, which is an established driving feature of tumorigenesis (Kops et al., 2005; Storchova and Pellman, 2004). The extent and degree of aneuploidy have been shown to correlate with both tumor stage and level of dedifferentiation (Frankfurt et al., 1985; Oriyama et al., 1998).

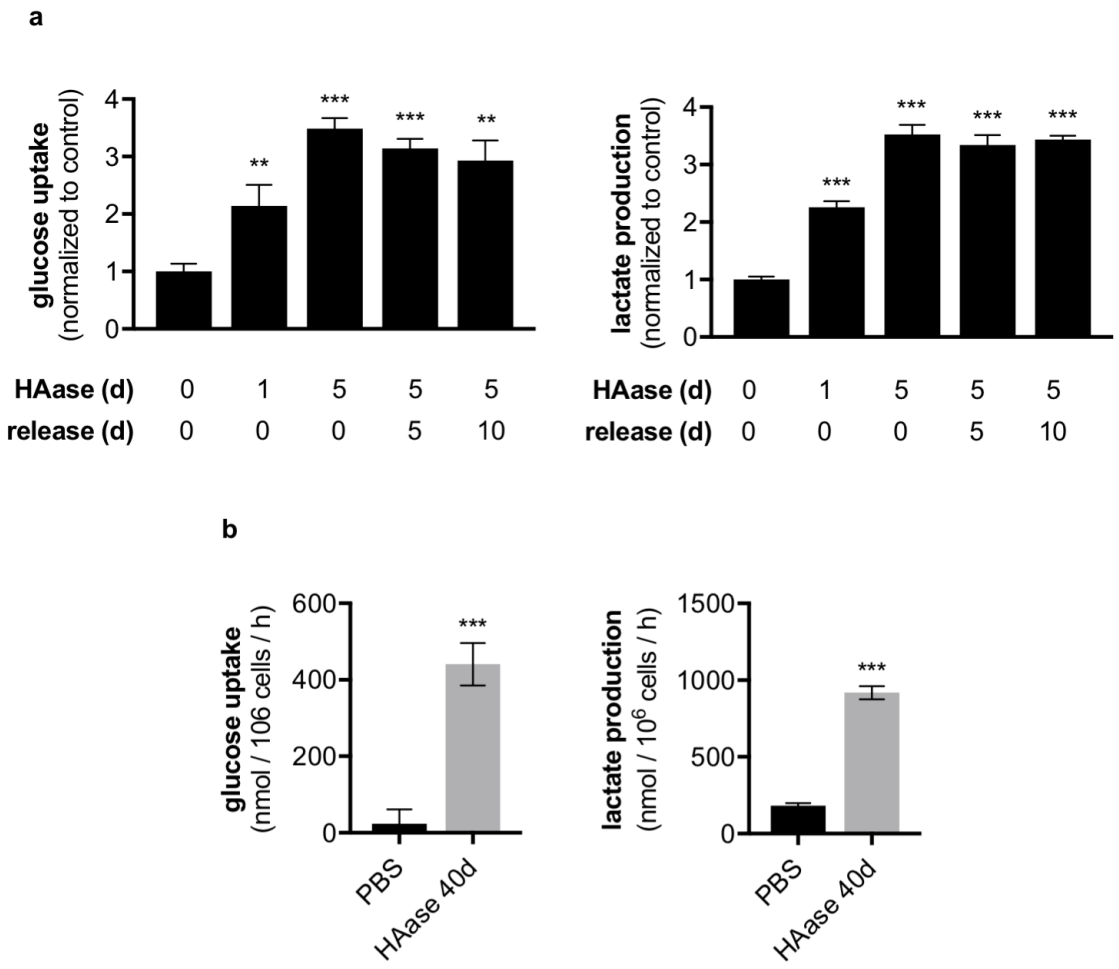

Figure 4-1. HAase treatment causes stable reprogramming of glycolytic metabolism in LiSa-2 cells. (a) Glucose uptake and lactate production rates in LiSa-2 cells treated with PBS or HAase (24h or 5d); additional cells were treated with HAase for 5d before being released of the enzyme—by thorough washing and replacement with PBS—and allowed to recover for indicated interval (5d or 10d) before measurement. Rates were normalized to PBS control. **(b)** Glucose uptake and lactate production rates in LiSa-2 cells continuously treated with HAase for 40d. Error bars denote SD (n=3). **p<0.01; ***p< 0.001.

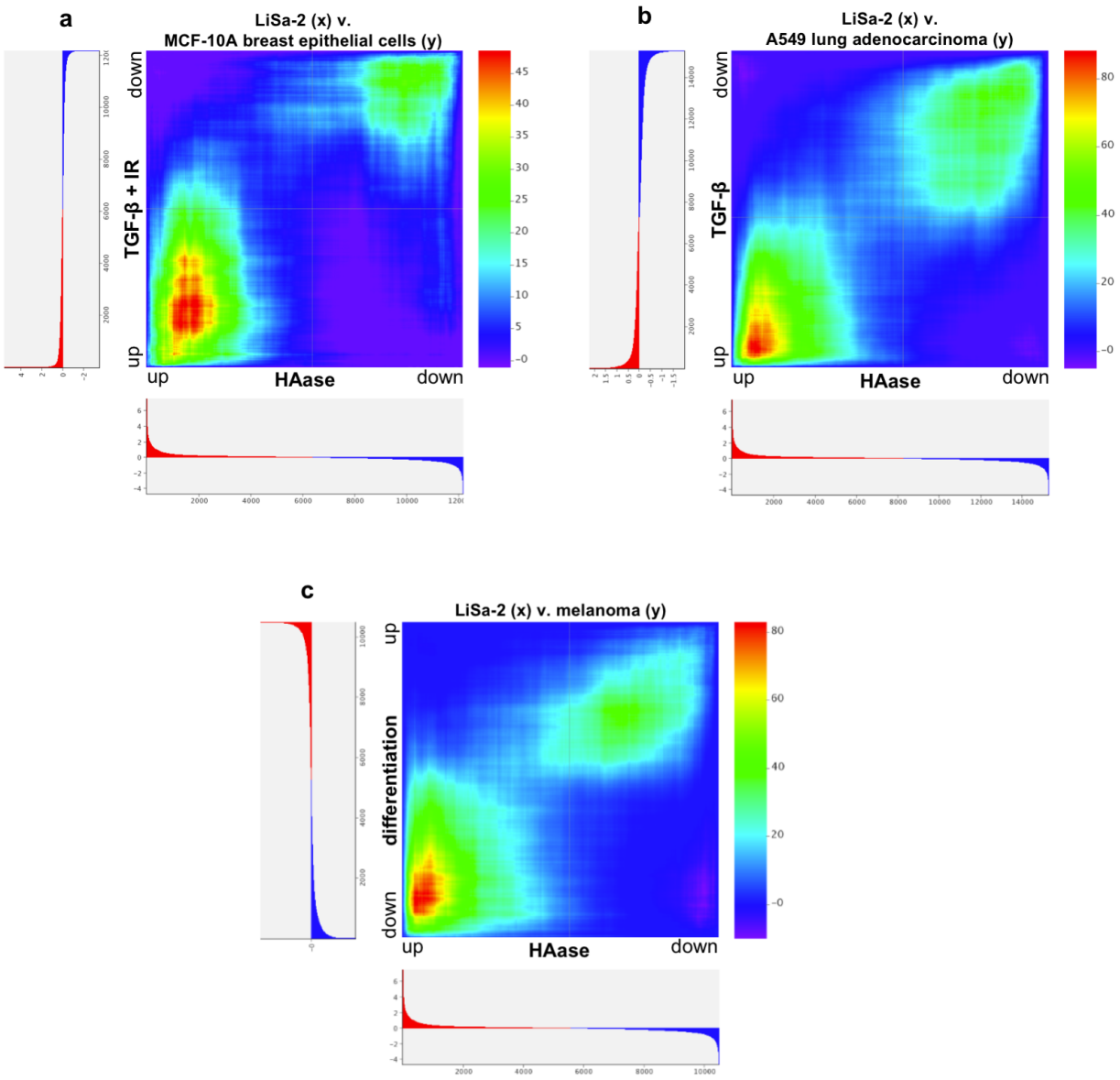

Figure 4-2. HAase treatment causes changes in gene expression signature than parallel that of TGF-β-induced EMT. Rank-rank hypergeometric overlap plots comparing genes ranked by differential expression in LiSa-2 cells treated for 24h with PBS or HAase and in **(a)** MCF-10A breast epithelial cells treated with TGF-β (400pg/mL) and irradiation (2Gy total dose) for 8d (GEO: GSE8240) (Andarawewa et al., 2007); **(b)** A549 lung adenocarcinoma cells treated with TGF-β (5ng/mL) for 72h (GEO: GSE17708) (Sartor et al., 2010); and **(c)** the principle component that defines the differentiation state of melanoma (Tsoi & Graeber, unpublished).

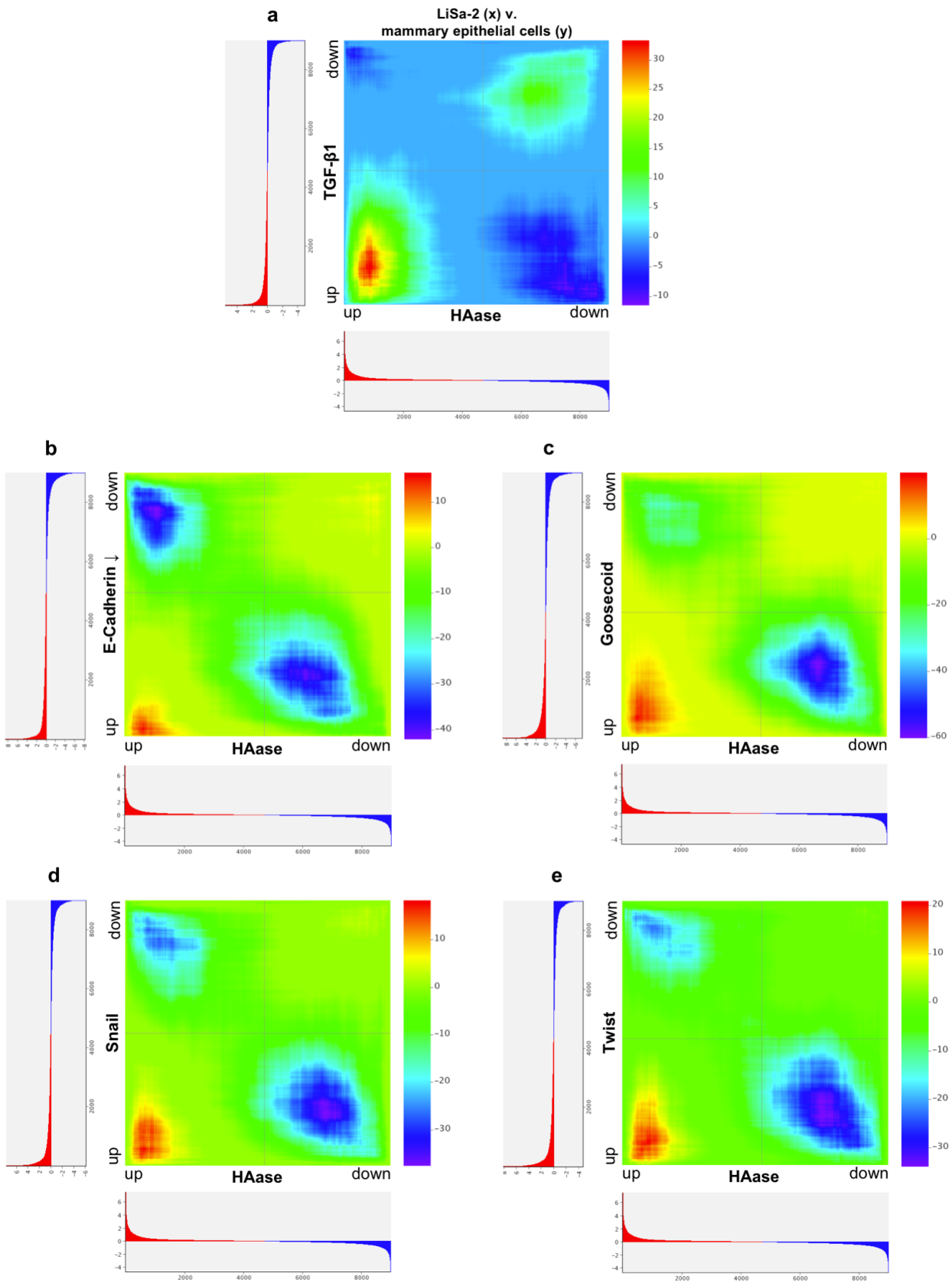
a
LiSa-2 (x) v.
mammary epithelial cells (y)
down
TGF-β1
up
up
HAase
down
b
down
E-Cadherin ↓
up
up
HAase
down
c
down
Goosecoid
up
up
HAase
down
d
down
Snail
up
up
HAase
down
e
down
Twist
up
up
HAase
down

(previous page)

Figure 4-3. Expression signature of HAase overlaps with that of TGF-β far more than other established mediators of EMT. Rank-rank hypergeometric overlap plots comparing genes ranked by differential expression in LiSa-2 cells treated for 24h with PBS or HAase and in immortalized human mammary epithelial cells retrovirally transduced with stable expression or knockdown (↓) constructs of various factors known to be involved in EMT: **(a)** TGF-β1, **(b)** E-cadherin, **(c)** Goosecoid, **(d)** Snail, **(e)** Twist (GEO: GSE24202) (Taube et al., 2010).

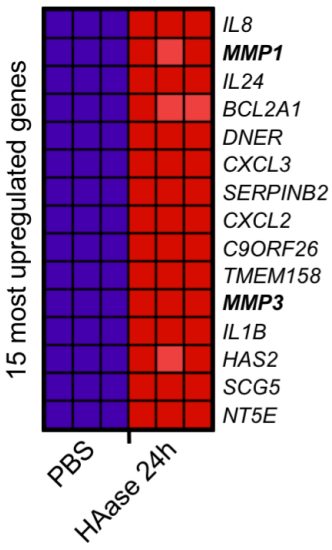

Figure 4-4. MMPs 1 & 3 are among the most upregulated genes upon HAase treatment. Heatmap showing the 15 most upregulated genes in LiSa-2 cells upon treatment with HAase for 24h. Genes were ranked by signal-to-noise ratio (SNR) on the GSEA platform (Broad Institute).

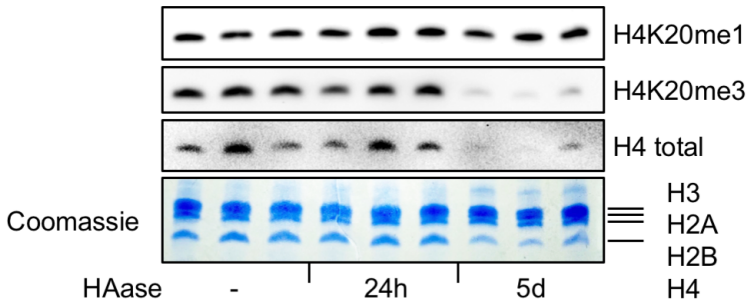

Figure 4-5. HAase treatment alters the epigenetic state of the cell. Immunoblots and Coomassie staining (bottom) of histones extracted in triplicate from LiSa-2 cells treated with PBS or HAase (24h or 5d). Extracts were probed for H4K20me1, H4K20me3, and total H4. Coomassie stain is also presented to address possible nonlinearity of histone-specific antibodies.

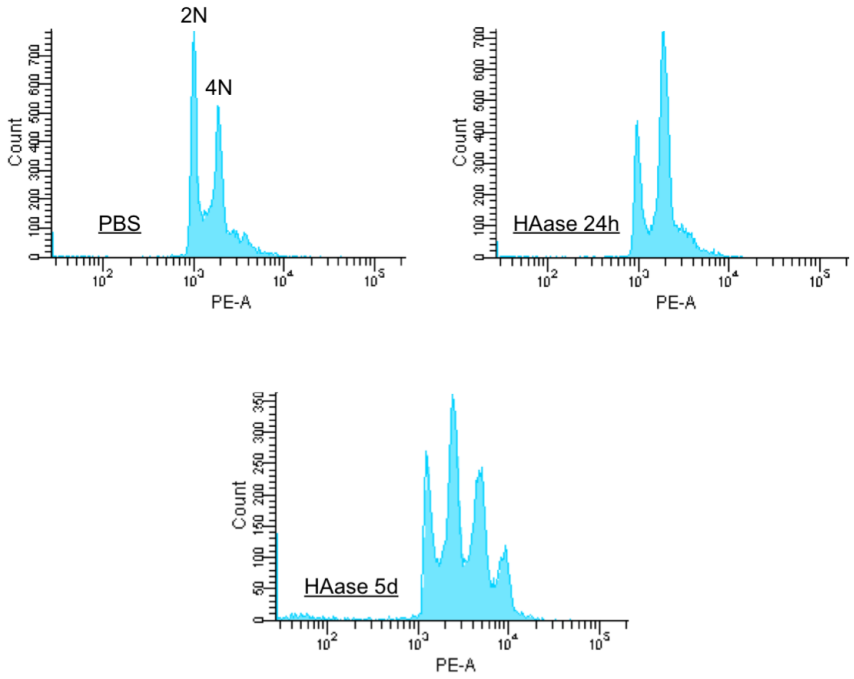

Figure 4-6. HAase treatment results in hyperploidy after 5d of treatment. Representative histograms of propidium iodide (PI) DNA staining in LiSa-2 cells. Unsynchronized, subconfluent LiSa-2 cells were resuspended in hypotonic PI staining buffer and analyzed by flow cytometry. Cells were gated to remove signal from debris. Signal on the PE channel corresponds with amount of DNA content. Prior to preparation, cells were treated with PBS or HAase for times indicated.

DISCUSSION

We have shown here that HAase treatment of LiSa-2 cells not only stably reprograms glycolytic metabolism, but that this reprogramming is accompanied by global changes to the genome, the epigenome, and the transcriptome. Consistent with previous reports on the impact of MMP expression on EMT, HAase treatment pushes LiSa-2 cells to what appears to be a more dedifferentiated state. Whether this is a direct effect of HAase, however, is not clear and could be explored further by co-treatment with HAase and a well-established MMP inhibitor, such as GM 6001. It would also be interesting to express MMPs in the contexts in which they have been shown to promote EMT to determine whether this change in cell identity is necessarily accompanied by an upregulation of glycolytic metabolism, or whether they are uniquely coincident aspects of HAase treatment.

Do epigenetic changes underpin the sustained glycolytic response to HAase? Further unbiased assessment of histone modifications should be performed on LiSa-2 cells to comprehensively catalog the changes in response to HAase. Such an assessment could then be coupled with transcriptional data to identify methyltransferases or demethylases that may be responsible for mediating these specific histone mark alterations. Levels of these enzymes could then be modulated to test possible rescue of the sustained effects of HAase on these cells. These marks can be much more systematically targeted than the broad downstream transcriptional changes.

Collectively, these results, albeit preliminary, suggest the possibly that detachment from HA—or from the ECM more generally—may have an important impact on cell identity and stable effect on the biology of a subset of cells. But why do some cells show only an acute metabolic response to HAase, whereas other show a more sustained response accompanied by global changes in the cell state? Stratifying cell types by the nature and duration of their response to HAase during

longer treatment intervals might be an informative way to identify the predispositions to the sustained effects of HAase. This might also inform our understanding of the biological contexts in which sustained reprogramming occurs. Although it might be an advantageous response for an early or pre-cancerous cell, such a sustained response might be pathological when temporally defined transitions are required, such as in development and wound healing.

UNANSWERED QUESTIONS & FUTURE DIRECTIONS

What receptor(s) and subsequent signaling events are responsible for initiating the acute metabolic response to HAase?

How does the extracellular digestion of HA culminate in the acute upregulation of ZFP36 and subsequent downregulation of TXNIP? As described previously, the canonical HA receptors do not seem to be involved in the response to HAase. We have observed activation of all three branches of the MAPK pathway—MEK, JNK, and p38—in response to HAase in LiSa-2 cells, but inhibition of these pathways does not block the glycolytic response. Antibody array profiling of phosphorylated receptor tyrosine kinases after 30min of HAase treatment shows activation of different receptors in each cell line tested: FGFR in 293T cells; PDFGR-β and EphA4 in LiSa-2 cells; EGFR in MDA-686 cells; and ALK and EphB3 in MEFs. This suggest three possibilities: that there is a high degree of cell-type specificity, and that the receptor activated is largely dependent on the composition and levels of different receptors embedded in the plasma membrane at baseline; that these receptors are transactivated by another common receptor with which they are complexed at the plasma membrane; and finally, that these are off-target signals. Because ZFP36 has been shown to be activated by a range of mitogenic signals, we are actively investigating whether blockage of growth factor signaling can block the induction of glycolysis upon HAase. We are also actively assessing whether there is activation of the Rho family GTPases downstream of integrin (trans)activation, as it is a common pathway for signals to be relayed from the ECM to the cell.

Can expression of a conditional hyaluronidase allele in the epidermis recapitulate correlational findings?

Our investigations of matrix remodeling *in vivo* are limited to cross-sectional comparisons within an early cutaneous neoplasm, as well as observational measurements of early murine embryos. While there are informative gradients of matrix deposition and intracellular protein expression that support the model we have proposed, it would be valuable to generate a mouse model with a conditional allele of one of the hyaluronidase genes to experimentally recapitulate our findings. If crossed with a *K15CrePR* mouse, we could induce HAase activity in the hair follicle stem cells—from which the neoplasm arose—for ease of comparison. In addition to immunohistochemical analysis of the skin after induction of HAase, we could perform an *in situ* colorimetric lactate dehydrogenase activity assay to functionally read out the levels and spatial distribution of glycolysis in the tissue, as has been previously described (Flores et al., 2017).

-

What are the consequences of GLUT1 sialylation?

More direct sialylation of GLUT1 should be attempted by individually overexpressing the STs shown to be upregulated upon HAase treatment. Given the difficulty of disentangling the broad effects of HAase treatment on GLUT1 from those of the sialylation event specifically, this would be a powerful way to reduce background metabolic noise. More precise assessment could be performed on the impact of GLUT1 sialylation on its trafficking, affinity for glucose, and stability at the plasma membrane by comparing ST-overexpressing cells to the control condition.

Does sialylation contribute to the sustained glycolytic response to HAase?

The most easily targeted node in the sialylation of GLUT1 is *GNE*, which encodes a bifunctional enzyme that regulates sialic acid biosynthesis, UDP-GlcNAc 2-epimerase/N-acetylmannosamine

kinase. CRISPR/Cas9 could be used to delete the gene with presumably little consequence if selection were performed in full-serum media so that cells could scavenge sialic acid from the media through monosaccharide salvage pathways. Once selected, the cells could be switched to serum-free conditions and their sustained metabolic response to HAase assessed. One drawback of this approach is the possibility that sialic acid pools and/or sialylation are involved in or feed back on glycolytic metabolism in unforeseen ways, which would confound the results.

Is sialylation of GLUT1 associated with transformation or pluripotency?

Glycolytic metabolism is a hallmark of rapidly proliferating cells, with cancer cells and stem cells being the canonical cases in point. As both states are characterized by sustained reprogramming of metabolism, they are compelling systems to examine possible associations with GLUT1 sialylation, as this would suggest a functional role for this modification and contexts in which it may be important. To test this possibility, comparison of GLUT1 mobility via SDS/PAGE could be made on embryonic stem cells in varying stages of (de)differentiation, and on epithelial cells transformed *in vitro* using either a chemical or a genetic approach. Sialidase digestions of lysates could confirm sialylation to be responsible for the observed mobility shifts. Additionally, a panel of lysates could be assembled from different cancer cells and then subject to sialidase digestion to determine the extent of sialylation among transformed cells, and whether there is any cell-type determinant of GLUT1 sialylation.

-

Do expression or treatment with other matrix remodeling enzymes recapitulate the metabolic effects of HAase treatment?

Matrix remodeling enzymes such as MMPs have been implicated in the promotion of EMT, which transcriptionally parallels HAase treatment (Radisky et al., 2005). But do they exert a similar

metabolic effect on cells—in either an acute or chronic fashion? Is the ECM broadly a node of cell-extrinsic metabolic regulation, or are elements of the metabolic response to HAase specific to this ECM constituent? These questions could be addressed in a rather straightforward way by expressing a panel of MMPs in the model cell lines metabolically characterized here. The one limitation of this approach, however, is that it is more difficult to define an "acute" response to gene induction, compared to addition of an exogenously purified enzyme. To better control temporality of expression, genes of interest could be subcloned into doxycycline-inducible vectors. Treatment with enzymes isolated from bacteria (collagenase, for instance) is not recommended due to the possibility of off-target metabolic effects of endotoxin. We were unable to heat-inactivate such enzymes.

Is loss of trimethylated H4K20 necessary for the sustained reprogramming of glycolytic metabolism?

Although 5d of HAase treatment pushes LiSa-2 cells towards what appears to be a dedifferentiated state—with parallel reprogramming of glycolytic metabolism that becomes independent of the activity of HAase—the global nature of these changes means there are relatively few opportunities to experimentally probe the mechanism by which they occur. Loss of trimethylated H4K20, however, is an attractive potential target. Lysates of LiSa-2 cells treated with HAase for 5d could be probed for levels of SUV4-20H1, SUV4-20H2, and SMYD5—methyltransferases known to be responsible for H4K20 *tri*methylation marks—to determine whether their levels track with the decrease in the trimethylation mark (Jørgensen et al., 2013; Stender et al., 2012). In parallel, levels of demethylases such as PHF2 could be assessed for possible anti-correlation with H4K20me3 (Stender et al., 2012). Candidate genes could then be overexpressed or knocked down, respectively, in the context of HAase treatment to determine if the global transcriptional and metabolic changes can be rescued.

EXPERIMENTAL PROCEDURES

Cell culture

An annotated inventory of all cells and cell lines used, as well as respective culture conditions can be found in Table 1. LiSa-2 liposarcoma cells were generated and provided by Dr. Peter Möller (University of Ulm) (Wabitsch et al., 2000), and are a compelling model to study glycolytic activation as they have the lowest baseline glucose uptake rate of any cell line we have tested. All experiments reported here have been performed with these cells unless otherwise indicated.

The provenance of all other cells used is as follows—liposarcoma cell lines LPS2 and LPS3 were established as previously described (Smith et al., 2013). Immortalized human pancreatic stellate cells (HPSC) were provided by Dr. Rosa Hwang (MD Anderson Cancer Center) (Hwang et al., 2008), Txnip knockout MEFs by Dr. Donald Ayer (University of Utah) (Elgort et al., 2010), and U-87 cells by Dr. Paul Mischel (University of California, San Diego). All breast lines were gifts from Dr. Frank McCormick (University of California, San Francisco). The following cells were obtained from University of California, Los Angeles, investigators: the lung cancer cell lines from the NCI series and A549 cells from Dr. Steven Dubinett, 293T and HeLa cells from Dr. Steven Bensinger, 3T3-L1 cells from Dr. Peter Tontonoz, A431 cells from Dr. Thomas Graeber, HCT116 cells (both WT and $p53^{-/-}$) from Dr. Cun-Yu Wang, MIA-PaCa-2 and PANC-1 cells from Dr. Timothy Donahue, MDA-686 cells from Dr. William Lowry. HFF-1 and SNL76/6 cells were purchased from ATCC, and NHBE cells from Lonza.

Cells were maintained using standard tissue culture procedures in a humidified incubator with 5% CO_2 and atmospheric oxygen. DMEM, DMEM/F12, Ham's F12, and RPMI 1640 base media were supplemented with fetal bovine serum (FBS), bovine serum (BS), or horse serum (HS) as indicated, as well as with 1x penicillin-streptomycin (all Gibco). Additional mitogens were added

as indicated in Table 1. NBHE cells were grown in proprietary serum-free growth media without antibiotics (Lonza).

Enzyme & drug treatments

Hyaluronidase (HAase) from bovine testes (Sigma) was reconstituted in PBS at 40mg/mL and treated at 1:100 for a final concentration of 400μg/mL. This concentration of HAase was determined based on the dose-response relationship established in LiSa-2 cells (Figure S1A). This concentration is above the minimum dose needed to achieve the maximum glycolytic response in these cells, but was selected to buffer against variations in enzymatic activity between lots of HAase and to account for the possibility of decreased sensitivity in other cells. PBS was used as the vehicle control, paired with the longest HAase treatment when multiple time points were assayed. For multi-day time points, media and enzyme were refreshed every other day as appropriate. Heat-inactivated (HI) HAase was prepared by boiling for 15min at 95°C; the resulting preparation was then quickly centrifuged to remove protein aggregates.

Hyaluronic acid (HA) oligomers (oligoHA) were prepared by hydrating HA from *Streptococcus equi* (Sigma) in serum-free cell culture media, followed by treatment with HAase. Media with HAase alone was prepared as a control. Preparations were incubated at 37°C for 72h with occasional agitation to fully digest the HA. HAase was then inactivated by boiling for 15min. After diluting oligoHA to assay concentrations in normal growth media, cells were trypsinized and plated for metabolic measurements in oligoHA-enriched media (or HI HAase control) to ensure exposure to receptors before reestablishment of the pericellular coat of HA.

HA digestion was non-quantitatively confirmed by visualization with Stains-All (Sigma). Briefly, both full-length HA and oligoHA were resolved on a 1% agarose gel for 45min at 100V. Gel was equilibrated in 30% ethanol solution for 1h and then replaced with 1x Stains-All solution in 30%

ethanol and allowed to incubate overnight, rocking and protected from light. Staining solution was washed off by rocking in dH_2O for 1h. Gel was imaged after sufficient exposure to light to cause pink background stain to fade (~1h).

Apigenin (Tocris), A-769662 (Tocris), erlotinib (Cayman), and SP600125 (Tocris) were dissolved in DMSO. HAase and apigenin (or DMSO) were co-incubated in media for 1h before treating cells. Erlotinib and SP600125 were added to cells 1h prior to addition of HAase. Before interrogation of signaling events, cells were serum starved overnight as indicated.

Metabolic rate measurements

Media glucose, glutamine, and lactate concentrations were measured using a Bioprofile Basic Analyzer (Nova Biomedical). Cells were seeded in 6-well plates at densities such that measurements would be made on subconfluent cells. Media was refreshed 24h after seeding cells; media was also added to empty wells as blank controls. After 24h incubation, 1mL media was removed from each sample and the blanks, and metabolite levels were assessed. Cell number was then determined using a Z1 Particle Counter (Beckman Coulter). Rates were calculated by dividing the difference in metabolite levels between samples and blanks by both the measurement interval (24h) and cell number.

We are cautious about making quantitative inferences regarding the magnitude of the fold changes in glucose uptake and lactate production across cell lines and across experiments. Though these are informative metrics for comparisons across *conditions*, cell lines with very low levels of baseline glycolytic activity (like LiSa-2 cells) can appear to respond with dramatically different magnitude between experiments due to small absolute differences in the denominator of the fold-change calculations (which is to say, the rate in the control condition). These differences are both technical (insensitivity of the instrument in measurement of small changes) and biological (e.g., changes in baseline rate due to passage number, serum lot, sensitivity to solvents such as DMSO). In

this report, we focus on internal comparisons of magnitude across conditions but within individual experiments and cell lines.

Extracellular acidification rate (ECAR) measurement

Real-time measurements of extracellular pH were completed on a Seahorse XF96 Extracellular Flux Analyzer. LiSa-2 cells were seeded in a XF96 microplate at a density of 5,000 cells/well 48h prior to experiment and maintained under standard tissue culture conditions with treatments of HAase as indicated. Cells were then washed twice with assay media (XF Base Medium supplemented with 17mM glucose and 2.5mM glutamine, pH 7.4) and brought to a final volume of 175μL per well. The microplate was placed in a 37°C incubator without CO_2 for 30min prior to loading the plate into the instrument. The extracellular acidification rate was measured over the course of 75min; midpoint measurements are presented.

Immunoblotting

Whole-cell lysates were prepared with RIPA buffer supplemented with phosphatase inhibitors (20mM sodium fluoride and 1mM sodium orthovanadate) and protease inhibitors (aprotinin, leupeptin, pepstatin – all at 4μg/mL). A Plasma Membrane Protein Extraction Kit (Abcam) was used for fractionation of the plasma membrane and the cytosol according to manufacturer's protocol, but with additional centrifugation steps to ensure maximal phase separation. Because we observed that boiling caused aggregation of membrane proteins and poor resolution by SDS/PAGE, lysates were denatured at room temperature for 30min following the addition of sample buffer as this prevented the aggregation of membrane proteins.

The following primary antibodies were used: ALDOA (Cell Signaling 3188, 1:1,000), CD44 (Cell Signaling 3578, 1:1,000), ENO1 (Cell Signaling 3810, 1:1,000), GAPDH (Invitrogen AM4300, 1:1,000), GLUT1 (Abcam ab115730, 1:1,000 for whole-cell lysates, 1:5,000 for plasma membrane

fractions), GLUT3 (Abcam ab191071, 1:1,000), HK2 (Cell Signaling 2867, 1:1,000), LDHA (Cell Signaling 3582, 1:1,000), LDHB (Abcam ab75167, 1:500), MCT1 (Abcam ab85021, 1:1,000), Na,K-ATPase (Cell Signaling 3010, 1:1,000), PFKFB3 (Cell Signaling 13123, 1:1,000), HMMR/CD168 (Abcam ab108339, 1:1,000), ZFP36/tristetraprolin (Cell Signaling 71632, 1:1000), α-tubulin (Sigma T6074, 1:10,000), TXNIP (Cell Signaling 14715, 1:1000). Antibodies towards histone H4, H4K20me1, and H4K20me3 were gifts from Dr. Hilary Coller (University of California, Los Angeles). Where shown, bands were quantified using ImageJ (NIH).

Screening for activation (phosphorylation) of receptor tyrosine kinases was performed using the Human Phospho-Receptor Tyrosine Kinase Array Kit (R&D Systems) per manufacturer's protocol. 100-300μg of cell lysate was used from cells treated with PBS or HAase for 30min.

Fluorescence microscopy

Cells were seeded at subconfluent densities on acid-washed coverslips. After indicated treatment, cells were fixed in 4% paraformaldehyde for 20min. For GLUT1 staining, cells were permeabilized for 5min in 0.1% Triton X-100 in PBS then blocked in 10% goat serum in PBS for 30min. For HABP staining, cell membranes remained intact and were blocked using an avidin/biotin blocking kit (Vector Laboratories). Cells were probed with a GLUT1 antibody (Abcam ab115730, 1:100) or biotinylated hyaluronan binding protein (HABP, EMD Millipore, 1:100) overnight at 4°C, then incubated with Alexa Fluor 488-conjugated goat anti-rabbit IgG and Alexa Fluor 555-conjugated streptavidin (both Invitrogen), respectively, at a dilution of 1:500 in blocking buffer for 1h at room temperature. Coverslips were then mounted with ProLong Gold Antifade (Invitrogen) and cured overnight before sealing. GLUT1 was then imaged on a Nikon Eclipse 90i microscope and HABP on a Zeiss AxioImager M1 microscope.

Intracellular metabolite extraction and mass spectrometry-based metabolomics

Cells were seeded in 6-well plates such that they were at ~75% confluency at the time of metabolite extraction. Media containing 10mM U-$^{13}C_6$-glucose (Cambridge Isotope Labs) and PBS or HAase was added to cells 6h and 24h before extraction. Cells were washed with 150mM ammonium acetate and scraped into 800µL chilled 50% methanol. 10nM norvaline was added to the suspension as an internal standard, followed by 400µL chloroform. After repeated vortexing, the aqueous layer containing metabolites was transferred to a glass vial and dried under vacuum. Metabolites were resuspended in 100µL 70% acetonitrile (ACN) and 5µL of this solution used for the mass spectrometer- based analysis. The analysis was performed on a Q Exactive (Thermo Scientific) in polarity-switching mode with positive voltage 3.0 kV and negative voltage 2.25 kV. The mass spectrometer was coupled to an UltiMate 3000RSLC (Thermo Scientific) UHPLC system. Mobile phase A was 5mM NH4AcO, pH 9.9, B) was ACN, and the separation achieved on a Luna 3mm NH2 100A (150 x 2.0mm) (Phenomenex) column. The flow was 300µL/min, and the gradient ran from 15% A to 95% A in 18min, followed by an isocratic step for 9min and re-equilibration for 7min. Metabolites were detected and quantified as area under the curve (AUC) based on retention time and accurate mass (≤ 3ppm) using the TraceFinder 3.1 (Thermo Scientific) software. Relative amounts of metabolites between conditions, as well as percentage of labeling, were calculated and corrected for naturally occurring ^{13}C abundance.

Gene expression knockdown & overexpression

Stable knockdown of gene expression was achieved using targeted shRNA sequences in the pLKO.1-puro backbone (Sigma); a nonspecific 'scramble' sequence was used as a control. shRNA sequences can be found in Table 2. A CMV-driven N-terminal 3xFLAG-tagged human TXNIP expression vector with a blasticidin-resistance cassette (pLV[Exp]-Bsd-CMV>3xFLAG/hTXNIP[NM_006472.4]) was obtained from VectorBuilder (Cyagen Biosciences).

Lentiviral particles were produced by co-transfecting 293T cells with these constructs along with the *gag/pol*, *rev*, and *vsvg* packaging plasmids using PolyFect Transfection Reagent (Qiagen). Virus was collected 48h later, filtered through .45μm pores, and added to subconfluent target cells with 4μg/mL polybrene overnight. Transduced cells were allowed to recover in regular growth media for 24h and then were selected with the appropriate resistance marker: 1μg/mL puromycin or 10μg/mL blasticidin.

TXNIP UTR reporter analysis

The human *TXNIP* 3' UTR (1.4kb) was amplified from genomic DNA isolated from Hela cells using KAPA HiFi polymerase (Kapa). The human *TXNIP* UTR sequence was cloned upstream of a luciferase gene (luc2 gene, Promega) in a pcDNA3.1(+) backbone. Human *ZFP36* cDNA (GE Dharmacon) was subcloned into an M4 expression vector backbone, where it is driven by a CMV promoter. The luciferase reporter construct (100ng) was transfected alongside transfection control plasmid (pCMX β-gal, 50ng) and either increasing amounts of the M4-ZFP36 expression plasmid or pcDNA3.1(+) (up to 50ng) per well of a 48-well plate. Transfection was carried out using Fugene HD (Promega) according to manufacturer's instructions into HEK293 cells plated onto 48-well dishes (n=6 wells/condition). After overnight incubation with the transfection mixture, media was replaced for further 24h before cells were harvested. Cells were then treated for 0.5-6h with HAase-containing media before being harvested. Cell lysates were assayed for luciferase activity using the Luciferase Assay Reagent (Promega) and luciferase activity was normalized to β-gal activity to correct for differences in transfection efficiency. Data are expressed as fold change relative to *TXNIP* UTR luciferase activity with no experimental treatments.

Quantitative Real-Time PCR

Total RNA was isolated using the Qiagen RNeasy Kit and 700ng was used as template for each cDNA synthesis reaction with the iScript Kit (Bio-Rad). Each reaction was then diluted to a total volume of 100μL with ultrapure water. For qPCR, 2μL of the diluted cDNA was combined with 0.5μM primers and KAPA SYBR FAST master mix (Kapa Biosystems) and amplified on a LightCycler 480 (Roche). Relative quantification was then performed using the $\Delta\Delta C_t$ method with RPLP0 as the reference gene. Primer sequences can be found in Table 3.

Cell proliferation

Cells were seeded in 6-well plates such that triplicate measurements could be made at each indicated time point. Media was refreshed every other day as appropriate. Cells were trypsinized and counted using a Z1 Particle Counter (Beckman Coulter). Phase-contrast images were captured at indicated time points using a Zeiss Axiovert 40 CFL live-cell microscope.

Scratch assay

MEFs were grown to confluency in 6-well plates and inactivated with mitomycin C (10μg/mL) for 2h to rule out the possibility that differences in proliferation could confound the results. Following 12h treatment with PBS or HAase, a P20 tip was then used to make two intersecting scratches in the monolayer of each triplicate well. After numerous washes with media to remove cell debris, media was replaced with PBS or HAase, as originally treated. Phase-contrast images were captured for each well using a Zeiss Axiovert 40 CFL live-cell microscope at 0h, 6h, and 12h following disruption of the monolayer. Images were centered on the intersection point of the two scratches. Absolute area closed at each time point was determined using the MRI Wound Healing Tool for ImageJ.

Animals

Mice were acquired from Jackson Labs (*K15CrePR*) and from the National Cancer Institute Mouse Models of Human Cancers Consortium repository (*LSL-KrasG12D* and *p53ff*) and maintained in accordance with standards established by the Institutional Animal Care and Use Committee and the Animal Research Committee (University of California, Los Angeles). *K15CrePR* mice express mifepristone-inducible cre recombinase driven by the promoter of *Krt15*, a member of the keratin family whose expression is pronounced in epithelial stem cells located in the bulge of the hair follicle. *K15CrePR; KrasG12D; p53ff* animals were treated with intraperitoneal injections of mifepristone (10mg/mL dissolved in sunflower seed oil; 2mg per day) for 3–5d before the start of the second adult hair cycle (10wk postnatal). Papillomas followed by bona fide squamous cell carcinomas developed in treated animals 6–10wk after anagen.

Immunohistochemistry

Isolated tissues were fixed overnight in 4% formalin and embedded in paraffin. Sections were then de-paraffinized, prepared for histology, and blocked in staining buffer containing appropriate IgG control. Immunohistochemistry was performed with citrate or Tris buffer antigen retrieval with the following antibodies: collagen IV (Abcam ab6586, 1:500), Glut1 (Abcam ab115730; 1:250), Glut3 (Abcam ab15311; 1:50), Ki-67 (Abcam ab16667; 1:50), ZFP36/tristetraprolin (LSBio LS-B1572, 1:200), and Txnip (Abcam ab188865; 1:100). The DAKO EnVision+ HRP Peroxidase System and Dako AEC Substrate Chromogen was used for detection. Biotinylated hyaluronan binding protein (EMD Millipore, 1:50) was also used as a probe, and detected with the Vectastain ABC Kit. Images were collected on an Olympus upright microscope.

RNA-Seq library construction & analysis

Total RNA was isolated from embryos derived as previously described (Nagaraj et al., 2017) using the Quick-RNA microprep kit (Zymo) according to manufacturer's protocol. Total RNA fraction was processed and libraries generated using the Ovation® Ultralow Library System V2. The resulting purified cDNA library was sequenced on the Illumina Hiseq 2000. 50 bp single-end RNA-seq reads were obtained, and sequence files were generated in FASTQ format. The quality score of RNA-seq reads was obtained by using the FastQC. Reads were then aligned to the *Mus musculus* Reference Sequences UCSC dm6 from Illumina iGenome files using TopHat v2.0.10.Transcript assembly and estimation of their abundances were calculated with Cufflinks 2.1.1 by using the *Mus musculus*. Reference annotation dataset UCSC dm6 from Illumina iGenome files. Differential expression for genes across the different conditions was calculated with Cuffdiff 2.1.1. Data were visualized using the Morpheus software developed by the Broad Institute.

Enrichment analyses

Total RNA was isolated with the Qiagen RNeasy Kit and used by the UCLA Clinical Microarray Core to perform whole-genome expression analysis with the GeneChip Human Genome U133 Plus 2.0 array (Affymetrix). Gene set enrichment analysis (Subramanian et al., 2005) was performed using annotations in the Molecular Signatures Database (MSigDB) C2 collection. A ranked list of genes was generated based on differential expression with HAase treatment and then compared to that of existing expression data sets using the rank-rank hypergeometric overlap(Plaisier et al., 2010) algorithm.

Enzymatic activity assays

The Hexokinase Colorimetric Assay Kit and Phosphofructokinase Activity Colorimetric Assay Kit (both BioVision) were used per manufacturer's protocol with 5µg and 0.1µg cell lysate, respectively.

Readout absorbance at 450nm is proportional to NADH production. Lactate dehydrogenase activity was measured by NADH fluorescence (absorption: 340nm, emission: 465nm) when 2μg lysate was combined with 100μL kinetic buffer (50mM Tris pH 7.5, 100mM KCl, 5mM $MgCl_2$, 1mM pyruvate). In all cases, enzyme activity was calibrated against an NADH standard curve.

GLUT1 digestions

All enzymes and buffers were acquired from New England Biolabs. For calf intestinal alkaline phosphatase, 15μg lysate was incubated with 50 units of enzyme in CutSmart buffer for 1h at 37°C; for Peptide:N-glycosidase F (PNGase F), with 1,000 units of enzyme in Glycoprotein Denaturing Buffer with GlycoBuffer 2 and 1% NP-40 for 1h at 37°C; for α2-3,6,8 neuraminidase (sialidase), with 450 units of enzyme in GlycoBuffer 1 for 3h at 37°C.

Cell cycle analysis

Cell cycle analysis was performed using propidium iodide (PI) staining. In brief, cells were trypsinized and resuspended in hypotonic DNA staining buffer (3.5mM sodium citrate, 0.1 g/L propidium iodide, 0.3% Triton X-100, 20 mg/L Ribonuclease A) at a concentration of 10^6 cells/mL and incubated for 20 minutes at room temperature in the dark. Analysis was performed using the BD FACSDiva software on an LSR II flow cytometer (BD Biosciences). PI fluorescence was recorded in the PE channel.

Histone extraction

DNA-histone complexes were pelleted in lysis buffer (10mM Tris-HCl pH 7.5, 1mM $MgCl_2$, 0.5% NP-40) and then resuspended in 5 volumes of extraction solution (1μL βME, 6μL concentrated H_2SO_4, 50μL glycerol, 443μL water). After incubation, histones were precipitated from the supernatant by adding enough 100% trichloroacetic acid (TCA) such that the final concentration is

20%. Pellet was washed in 5% TCA followed by cold ethanol; histones were incubated in ethanol at -80°C for 10min before spinning down and drying. Histones were resuspended in 1X sample buffer.

Statistical analysis

All experiments were performed in triplicate unless otherwise indicated. Data are presented as mean ± standard deviation, with asterisks indicating the significance of the p-value generated by a two-tailed Student's t-test.

DESIGNATION	species	origin	culture media
293T	human	embryonic kidney cells	DMEM, 10% FBS
3T3-L1	mouse	embryonic fibroblasts	DMEM, 10% FBS
A431	human	epidermoid carcinoma	DMEM, 10% FBS
A549	human	lung adenocarcinoma	RPMI 1640, 10% FBS
HCT116	human	colorectal carcinoma	DMEM, 10% FBS
HCT116 (p53 -/-)	human	colorectal carcinoma [isogenic p53 null]	DMEM, 10% FBS
HeLa	human	cervical adenocarcinoma	DMEM, 10% FBS
HFF-1	human	foreskin fibroblasts	DMEM, 10% FBS
HPSC	human	immortalized human pancreatic stellate cells	DMEM, 10% FBS
Hs578T	human	breast carcinoma	DMEM, 10% FBS
LiSa-2	human	liposarcoma	DMEM/F12, 10% BS
LPS2	human	liposarcoma	DMEM, 10% FBS
LPS3	human	liposarcoma	DMEM/F12, 10%FBS
MCF-10A	human	breast epithelial cells	DMEM/F12, 5% HS, 10µg/mL insulin, 10µg/mL cholera toxin, 500ng/mL hydrocortisone, 20ng/mL EGF
MCF-12A	human	breast epithelial cells	DMEM/F12, 5% HS, 10µg/mL insulin, 10µg/mL cholera toxin, 500ng/mL hydrocortisone, 20ng/mL EGF
MDA-686	human	oropharyngeal squamous cell carcinoma	DMEM, 10% FBS
MDA-MB-453	human	breast carcinoma	DMEM, 10% FBS
MEF (Txnip-/-)	mouse	embryonic fibroblasts (immortalized)	DMEM, 10% FBS
MEF (WT)	mouse	embryonic fibroblasts (immortalized)	DMEM, 10% FBS
MIA-PaCa-2	human	pancreatic carcinoma	DMEM, 10% FBS
NCI-H1437	human	lung adenocarcinoma	RPMI 1640, 10% FBS
NCI-H157	human	squamous cell lung carcinoma	RPMI 1640, 10% FBS
NCI-H1792	human	lung adenocarcinoma	RPMI 1640, 10% FBS
NCI-H358	human	bronchioloalveolar carcinoma	RPMI 1640, 10% FBS
NCI-H441	human	lung adenocarcinoma	RPMI 1640, 10% FBS
NCI-H460	human	large celll lung carcinoma	RPMI 1640, 10% FBS
NCI-H520	human	squamous cell lung carcinoma	RPMI 1640, 10% FBS
NCI-H661	human	large celll lung carcinoma	RPMI 1640, 10% FBS
NHBE	human	primary normal human bronchial epithelial cells	BEGM BulletKit
PANC-1	human	pancreatic epithelioid carcinoma	DMEM, 10% FBS
SNL76/7	mouse	embryonic fibroblasts	DMEM, 10% FBS
SUM149PT	human	breast carcinoma	Ham's F12, 5% FBS, 5µg/mL insulin, 1µg/mL hydrocortisone, 10ng/mL EGF
SUM159PT	human	breast carcinoma	Ham's F12, 5% FBS, 5µg/mL insulin, 1µg/mL hydrocortisone, 10ng/mL EGF
U-87	human	glioblastoma	DMEM, 10% FBS

Table 1. Glossary of cells and cell lines.

construct	sequence (5' - 3')
scramble	CCGGCAACAAGATGAAGAGCACCAACTCGAGTTGGTGCTCTTCATCTTGTTGTTTTT
shCD44-1	CCGGGGACCAATTACCATAACTATTCTCGAGAATAGTTATGGTAATTGGTCCTTTTTG
shCD44-2	CCGGCGCTATGTCCAGAAAGGAGAACTCGAGTTCTCCTTTCTGGACATAGCGTTTTTG
shHMMR-1	CCGGGCAGACCAAGTCAGCACTAAACTCGAGTTTAGTGCTGACTTGGTCTGCTTTTTG
shHMMR-2	CCGGGCCAACTCAAATCGGAAGTATCTCGAGATACTTCCGATTTGAGTTGGCTTTTTG
shZFP36-1	CCGGCCCATCTTCAATCGCATCTCTCTCGAGAGAGATGCGATTGAAGATGGGTTTTT
shZFP36-2	CCGGATCTGTCTCCTAGAATCTTATCTCGAGATAAGATTCTAGGAGACAGATTTTTTTG

Table 2. shRNA sequences.

GENE	Forward Primer (5' - 3')	Reverse Primer (5' - 3')
RPLP0	TCTACAACCCTGAAGTGCTTGAT	CAATCTGCAGACAGACACTGG
SLC2A1 (GLUT1)	GGCCAAGAGTGTGCTAAAGAA	ACAGCGTTGATGCCAGACAG
SLC2A2 (GLUT2)	GCTGCTCAACTAATCACCATGC	TGGTCCCAATTTTGAAAACCCC
SLC2A3 (GLUT3)	GCTGGGCATCGTTGTTGGA	GCACTTTGTAGGATAGCAGGAAG
SLC2A4 (GLUT4)	TGGGCGGCATGATTTCCTC	GCCAGGACATTGTTGACCAG
ST3GAL1	GGAGGACGACACCTACCGAT	CCACCGACCTCTTCTCCAG
ST3GAL2	TGGACGGGCACAACTTCATC	GGCAGGTTCTTGGCACTCTC
ST3GAL3	AACATCCCTACCCTTGGCAG	TGCGTCCAGGACTCTTTGAT
ST3GAL4	CTTCCTGCGGCTTGAGGATTA	CTCACTCCCCTTGGTCCCATA
ST3GAL5	TATAGCGTGGACTTACTCCCTTT	AGGAGGATCGTACTTGGACTC
ST3GAL6	ATTGCCATCACATTGGCGTTT	GCAAAGGACTCTTGAGGTCAG
ST6GAL1	ACCCCAATCAGCCCTTTTACA	CTGGTCACACAGCGTCATCA
ST6GAL2	TGCGCTGTCGTCATGTCTG	GCGTATGGTGGTTTTATTCCCAA
ST6GALNAC1	CACAGCCAAGACGCTCATTC	CCTTTCTGTCTCGTCCTTGTTG
ST6GALNAC2	ACTCCCTCGTCTCCTACTGGA	ACATAGTCGCGGATGTCTGAG
ST6GALNAC3	CAACTGGACTGTGACCTTTGT	GGCCGACATCTTCTTCATAACC
ST6GALNAC4	TGTGAGGAGATCGTGGTCTATG	CAAAGTAGTGGTAAGGCACTGAG
ST6GALNAC5	CTGAGGGTCATCGCGCATT	GGAGATGCAGGTTGTTGTAGAC
ST6GALNAC6	ATCCGCATGAATGATGCACC	GGGGTCCGGTTGACAAACTC
ST8SIA1	CATGCGATGCAATCTCCCTC	CTGGGATTAGCTGTCACTAACTG
ST8SIA2	GGCAGAGGTACAATCAGATCAGC	ATGTCTCCATTTGGACGAGGC
ST8SIA3	CACAATTTGCGCTGAAGTTTCT	TGATGTAAAAACGCTGTCCGATT
ST8SIA4	ACGAGATGTGTCAGTGGTCAA	AACTTCAGGTAGGAGGCTATGT
ST8SIA5	ACCGGGATTTGTTGGGGAG	CATACAGGATCTGTTGCAGCA
ST8SIA6	CGCCACTAACAGCACATATCTG	ATCTGAAGGTAGTCGTTCTCTGA
TXNIP	TGTGTGAAGTTACTCGTGTCAAA	GCAGGTACTCCGAAGTCTGT
ZFP36	GACTGAGCTATGTCGGACCTT	GAGTTCCGTCTTGTATTTGGGG
ZFP36L1	GATGACCACCACCCTCGT	TGGGAGCACTATAGTTGAGCATC
ZFP36L2	CTGCTGCTGACTGCGGTA	ATCCAGACCCACAACTTTGC

Table 3. qPCR primer sequences.

REFERENCES

Adams, J.C., and Watt, F.M. (1993). Regulation of development and differentiation by the extracellular matrix. Development *117*, 1183-1198.

Agathocleous, M., and Harris, W.A. (2013). Metabolism in physiological cell proliferation and differentiation. Trends in Cell Biology *23*, 484-492.

Ahmed, N., and Berridge, M.V. (1999). N-Glycosylation of glucose transporter-1 (Glut-1) is associated with increased transporter affinity for glucose in human leukemic cells. Leukemia Research *23*, 395-401.

Almaraz, R.T., Tian, Y., Bhattarcharya, R., Tan, E., Chen, S.-H., Dallas, M.R., Chen, L., Zhang, Z., Zhang, H., Konstantopoulos, K.*, et al.* (2012). Metabolic Flux Increases Glycoprotein Sialylation: Implications for Cell Adhesion and Cancer Metastasis. Molecular & Cellular Proteomics *11*, M112.017558.

Andarawewa, K.L., Erickson, A.C., Chou, W.S., Costes, S.V., Gascard, P., Mott, J.D., Bissell, M.J., and Barcellos-Hoff, M.H. (2007). Ionizing Radiation Predisposes Nonmalignant Human Mammary Epithelial Cells to Undergo Transforming Growth Factor β–Induced Epithelial to Mesenchymal Transition. Cancer Research *67*, 8662-8670.

Aruffo, A., Stamenkovic, I., Melnick, M., Underhill, C.B., and Seed, B. (1990). CD44 is the principal cell surface receptor for hyaluronate. Cell *61*, 1303-1313.

Asano, T., Katagiri, H., Takata, K., Lin, J.L., Ishihara, H., Inukai, K., Tsukuda, K., Kikuchi, M., Hirano, H., and Yazaki, Y. (1991). The role of N-glycosylation of GLUT1 for glucose transport activity. Journal of Biological Chemistry *266*, 24632-24636.

Asano, T., Takata, K., Katagiri, H., Ishihara, H., Inukai, K., Anai, M., Hirano, H., Yazaki, Y., and Oka, Y. (1993). The role of N-glycosylation in the targeting and stability of GLUT1 glucose transporter. FEBS Letters *324*, 258-261.

Barthel, A., Okino, S.T., Liao, J., Nakatani, K., Li, J., Whitlock, J.P., and Roth, R.A. (1999). Regulation of GLUT1 Gene Transcription by the Serine/Threonine Kinase Akt1. Journal of Biological Chemistry *274*, 20281-20286.

Beck, D.B., Burton, A., Oda, H., Ziegler-Birling, C., Torres-Padilla, M.-E., and Reinberg, D. (2012). The role of PR-Set7 in replication licensing depends on Suv4-20h. Genes & Development *26*, 2580-2589.

Bensinger, S.J., and Christofk, H.R. (2012). New aspects of the Warburg effect in cancer cell biology. Seminars in Cell & Developmental Biology *23*, 352-361.

Bissell, M.J., and Radisky, D. (2001). Putting tumours in context. Nat Rev Cancer *1*, 46-54.

Blackshear, P.J. (2002). Tristetraprolin and other CCCH tandem zinc-finger proteins in the regulation of mRNA turnover. Biochemical Society Transactions *30*, 945-952.

Büll, C., Stoel, M.A., den Brok, M.H., and Adema, G.J. (2014). Sialic Acids Sweeten a Tumor's Life. Cancer Research *74*, 3199-3204.

Camenisch, T.D., Spicer, A.P., Brehm-Gibson, T., Biesterfeldt, J., Augustine, M.L., Calabro, A., Jr., Kubalak, S., Klewer, S.E., and McDonald, J.A. (2000). Disruption of hyaluronan synthase-2 abrogates normal cardiac morphogenesis and hyaluronan-mediated transformation of epithelium to mesenchyme. The Journal of Clinical Investigation *106*, 349-360.

Chang, L., Kamata, H., Solinas, G., Luo, J.-L., Maeda, S., Venuprasad, K., Liu, Y.-C., and Karin, M. (2006). The E3 Ubiquitin Ligase Itch Couples JNK Activation to TNFα-induced Cell Death by Inducing c-FLIPL Turnover. Cell *124*, 601-613.

Christofk, H.R., Vander Heiden, M.G., Harris, M.H., Ramanathan, A., Gerszten, R.E., Wei, R., Fleming, M.D., Schreiber, S.L., and Cantley, L.C. (2008). The M2 splice isoform of pyruvate kinase is important for cancer metabolism and tumour growth. Nature *452*, 230-233.

Clarke, J.F., Young, P.W., Yonezawa, K., Kasuga, M., and Holman, G.D. (1994). Inhibition of the translocation of GLUT1 and GLUT4 in 3T3-L1 cells by the phosphatidylinositol 3-kinase inhibitor, wortmannin. Biochemical Journal *300*, 631-635.

Cohen, M., Klein, E., Geiger, B., and Addadi, L. (2003). Organization and Adhesive Properties of the Hyaluronan Pericellular Coat of Chondrocytes and Epithelial Cells. Biophysical Journal *85*, 1996-2005.

Collins, A.T., Berry, P.A., Hyde, C., Stower, M.J., and Maitland, N.J. (2005). Prospective Identification of Tumorigenic Prostate Cancer Stem Cells. Cancer Research *65*, 10946-10951.

DeBerardinis, R.J., Lum, J.J., Hatzivassiliou, G., and Thompson, C.B. (2008). The Biology of Cancer: Metabolic Reprogramming Fuels Cell Growth and Proliferation. Cell Metabolism *7*, 11-20.

Dong, C., Yuan, T., Wu, Y., Wang, Y., Fan, Teresa W.M., Miriyala, S., Lin, Y., Yao, J., Shi, J., Kang, T.*, et al.* (2013). Loss of FBP1 by Snail-Mediated Repression Provides Metabolic Advantages in Basal-like Breast Cancer. Cancer Cell *23*, 316-331.

DuBois, R.N., McLane, M.W., Ryder, K., Lau, L.F., and Nathans, D. (1990). A growth factor-inducible nuclear protein with a novel cysteine/histidine repetitive sequence. Journal of Biological Chemistry *265*, 19185-19191.

Elgort, M.G., O'Shea, J.M., Jiang, Y., and Ayer, D.E. (2010). Transcriptional and Translational Downregulation of Thioredoxin Interacting Protein Is Required for Metabolic Reprogramming during G(1). Genes & Cancer *1*, 893-907.

Elson, D.A., Ryan, H.E., Snow, J.W., Johnson, R., and Arbeit, J.M. (2000). Coordinate Up-Regulation of Hypoxia Inducible Factor (HIF)-1α and HIF-1 Target Genes during Multi-Stage Epidermal Carcinogenesis and Wound Healing. Cancer Research *60*, 6189-6195.

Evanko, S.P., Angello, J.C., and Wight, T.N. (1999). Formation of Hyaluronan- and Versican-Rich Pericellular Matrix Is Required for Proliferation and Migration of Vascular Smooth Muscle Cells. Arteriosclerosis, Thrombosis, and Vascular Biology *19*, 1004-1013.

Flores, A., Schell, J., Krall, A.S., Jelinek, D., Miranda, M., Grigorian, M., Braas, D., White, A.C., Zhou, J.L., Graham, N.A., *et al.* (2017). Lactate dehydrogenase activity drives hair follicle stem cell activation. Nat Cell Biol *advance online publication*.

Frankfurt, O.S., Chin, J.L., Englander, L.S., Greco, W.R., Pontes, J.E., and Rustum, Y.M. (1985). Relationship between DNA Ploidy, Glandular Differentiation, and Tumor Spread in Human Prostate Cancer. Cancer Research *45*, 1418-1423.

Gallagher, E., Gao, M., Liu, Y.-C., and Karin, M. (2006). Activation of the E3 ubiquitin ligase Itch through a phosphorylation-induced conformational change. Proceedings of the National Academy of Sciences *103*, 1717-1722.

Gardner, D.K., Pool, T.B., and Lane, M. (2000). Embryo Nutrition and Energy Metabolism and Its Relationship to Embryo Growth, Differentiation, and Viability. Semin Reprod Med *18*, 205-218.

Gu, W., Gaeta, X., Sahakyan, A., Chan, Alanna B., Hong, Candice S., Kim, R., Braas, D., Plath, K., Lowry, William E., and Christofk, Heather R. (2016). Glycolytic Metabolism Plays a Functional Role in Regulating Human Pluripotent Stem Cell State. Cell Stem Cell *19*, 476-490.

Haber, R.S., Rathan, A., Weiser, K.R., Pritsker, A., Itzkowitz, S.H., Bodian, C., Slater, G., Weiss, A., and Burstein, D.E. (1998). GLUT1 glucose transporter expression in colorectal carcinoma. Cancer *83*, 34-40.

Hanahan, D., and Weinberg, Robert A. (2011). Hallmarks of Cancer: The Next Generation. Cell *144*, 646-674.

Harduin-Lepers, A., Mollicone, R., Delannoy, P., and Oriol, R. (2005). The animal sialyltransferases and sialyltransferase-related genes: a phylogenetic approach. Glycobiology *15*, 805-817.

Havula, E., and Hietakangas, V. (2012). Glucose sensing by ChREBP/MondoA–Mlx transcription factors. Seminars in Cell & Developmental Biology *23*, 640-647.

Hayen, W., Goebeler, M., Kumar, S., Riessen, R., and Nehls, V. (1999). Hyaluronan stimulates tumor cell migration by modulating the fibrin fiber architecture. Journal of Cell Science *112*, 2241-2251.

Hensley, Christopher T., Faubert, B., Yuan, Q., Lev-Cohain, N., Jin, E., Kim, J., Jiang, L., Ko, B., Skelton, R., Loudat, L., *et al.* (2016). Metabolic Heterogeneity in Human Lung Tumors. Cell *164*, 681-694.

Hong, C.S., Graham, N.A., Gu, W., Espindola Camacho, C., Mah, V., Maresh, E.L., Alavi, M., Bagryanova, L., Krotee, P.A.L., Gardner, B.K., *et al.* (2016). MCT1 Modulates Cancer Cell Pyruvate Export and Growth of Tumors that Co-express MCT1 and MCT4. Cell Reports *14*, 1590-1601.

Hsu, P.P., and Sabatini, D.M. (2008). Cancer Cell Metabolism: Warburg and Beyond. Cell *134*, 703-707.

Hu, H., Juvekar, A., Lyssiotis, Costas A., Lien, Evan C., Albeck, John G., Oh, D., Varma, G., Hung, Yin P., Ullas, S., Lauring, J.*, et al.* (2016). Phosphoinositide 3-Kinase Regulates Glycolysis through Mobilization of Aldolase from the Actin Cytoskeleton. Cell *164*, 433-446.

Hwang, R.F., Moore, T., Arumugam, T., Ramachandran, V., Amos, K.D., Rivera, A., Ji, B., Evans, D.B., and Logsdon, C.D. (2008). Cancer-Associated Stromal Fibroblasts Promote Pancreatic Tumor Progression. Cancer Research *68*, 918-926.

Itano, N., Atsumi, F., Sawai, T., Yamada, Y., Miyaishi, O., Senga, T., Hamaguchi, M., and Kimata, K. (2002). Abnormal accumulation of hyaluronan matrix diminishes contact inhibition of cell growth and promotes cell migration. Proceedings of the National Academy of Sciences *99*, 3609-3614.

Jiang, D., Liang, J., and Noble, P.W. (2007). Hyaluronan in Tissue Injury and Repair. Annual Review of Cell and Developmental Biology *23*, 435-461.

Jørgensen, S., Schotta, G., and Sørensen, C.S. (2013). Histone H4 Lysine 20 methylation: key player in epigenetic regulation of genomic integrity. Nucleic Acids Research *41*, 2797-2806.

Julien, S., Ivetic, A., Grigoriadis, A., QiZe, D., Burford, B., Sproviero, D., Picco, G., Gillett, C., Papp, S.L., Schaffer, L.*, et al.* (2011). Selectin Ligand Sialyl-Lewis x Antigen Drives Metastasis of Hormone-Dependent Breast Cancers. Cancer Research *71*, 7683-7693.

Kang, S.S., Chun, Y.K., Hur, M.H., Lee, H.K., Kim, Y.J., Hong, S.R., Lee, J.H., Lee, S.G., and Park, Y.K. (2002). Clinical Significance of Glucose Transporter 1 (GLUT1) Expression in Human Breast Carcinoma. Japanese Journal of Cancer Research *93*, 1123-1128.

Kessenbrock, K., Plaks, V., and Werb, Z. (2010). Matrix Metalloproteinases: Regulators of the Tumor Microenvironment. Cell *141*, 52-67.

Kidder, G.M., and Mhawi, A.A. (2002). Gap junctions and ovarian folliculogenesis. Reproduction *123*, 613-620.

Kitagawa, T., Tsuruhara, Y., Hayashi, M., Endo, T., and Stanbridge, E.J. (1995). A tumor-associated glycosylation change in the glucose transporter GLUT1 controlled by tumor suppressor function in human cell hybrids. Journal of Cell Science *108*, 3735-3743.

Koppenol, W.H., Bounds, P.L., and Dang, C.V. (2011). Otto Warburg's contributions to current concepts of cancer metabolism. Nat Rev Cancer *11*, 325-337.

Kops, G.J.P.L., Weaver, B.A.A., and Cleveland, D.W. (2005). On the road to cancer: aneuploidy and the mitotic checkpoint. Nat Rev Cancer *5*, 773-785.

Kuppusamy, U.R., Khoo, H.E., and Das, N.P. (1990). Structure-activity studies of flavonoids as inhibitors of hyaluronidase. Biochemical Pharmacology *40*, 397-401.

Lai, W.S., Stumpo, D.J., and Blackshear, P.J. (1990). Rapid insulin-stimulated accumulation of an mRNA encoding a proline-rich protein. Journal of Biological Chemistry *265*, 16556-16563.

Lee, Eunice E., Ma, J., Sacharidou, A., Mi, W., Salato, Valerie K., Nguyen, N., Jiang, Y., Pascual, Juan M., North, Paula E., Shaul, Philip W.*, et al.* (2015). A Protein Kinase C Phosphorylation Motif in GLUT1 Affects Glucose Transport and is Mutated in GLUT1 Deficiency Syndrome. Molecular Cell *58*, 845-853.

Lee, S.-Y., Lee, H.-S., Kim, E.-Y., Ko, J.-J., Yoon, T.K., Lee, W.-S., and Lee, K.-A. (2013). Thioredoxin-Interacting Protein Regulates Glucose Metabolism and Affects Cytoplasmic Streaming in Mouse Oocytes. PLOS ONE *8*, e70708.

Leese, H.J., and Barton, A.M. (1984). Pyruvate and glucose uptake by mouse ova and preimplantation embryos. Journal of Reproduction and Fertility *72*, 9-13.

Lerner, Alana G., Upton, J.-P., Praveen, P.V.K., Ghosh, R., Nakagawa, Y., Igbaria, A., Shen, S., Nguyen, V., Backes, Bradley J., Heiman, M.*, et al.* (2012). IRE1α Induces Thioredoxin-Interacting Protein to Activate the NLRP3 Inflammasome and Promote Programmed Cell Death under Irremediable ER Stress. Cell Metabolism *16*, 250-264.

Li, C., Heidt, D.G., Dalerba, P., Burant, C.F., Zhang, L., Adsay, V., Wicha, M., Clarke, M.F., and Simeone, D.M. (2007). Identification of Pancreatic Cancer Stem Cells. Cancer Research *67*, 1030-1037.

Li, L., and Li, W. (2015). Epithelial–mesenchymal transition in human cancer: Comprehensive reprogramming of metabolism, epigenetics, and differentiation. Pharmacology & Therapeutics *150*, 33-46.

Lim, R.W., Varnum, B.C., O'Brien, T.G., and Herschman, H.R. (1989). Induction of tumor promotor-inducible genes in murine 3T3 cell lines and tetradecanoyl phorbol acetate-nonproliferative 3T3 variants can occur through protein kinase C-dependent and -independent pathways. Molecular and Cellular Biology *9*, 1790-1793.

Lin, Y., Mahan, K., Lathrop, W.F., Myles, D.G., and Primakoff, P. (1994). A hyaluronidase activity of the sperm plasma membrane protein PH-20 enables sperm to penetrate the cumulus cell layer surrounding the egg. The Journal of Cell Biology *125*, 1157-1163.

Lu, P., Weaver, V.M., and Werb, Z. (2012). The extracellular matrix: A dynamic niche in cancer progression. The Journal of Cell Biology *196*, 395-406.

Lunt, S.Y., and Vander Heiden, M.G. (2011). Aerobic Glycolysis: Meeting the Metabolic Requirements of Cell Proliferation. Annual Review of Cell and Developmental Biology *27*, 441-464.

Lykke-Andersen, J., and Wagner, E. (2005). Recruitment and activation of mRNA decay enzymes by two ARE-mediated decay activation domains in the proteins TTP and BRF-1. Genes & Development *19*, 351-361.

Martin, K.L., and Leese, H.J. (1995). Role of glucose in mouse preimplantation embryo development. Molecular Reproduction and Development *40*, 436-443.

Martin, P. (1997). Wound Healing—Aiming for Perfect Skin Regeneration. Science *276*, 75-81.

Masumi, A., Akamatsu, Y., and Kitagawa, T. (1993). Modulation of the synthesis and glycosylation of the glucose transporter protein by transforming growth factor-β1 in Swiss 3T3 fibroblasts. Biochimica et Biophysica Acta (BBA) - Biomembranes *1145*, 227-234.

Matzuk, M.M., Burns, K.H., Viveiros, M.M., and Eppig, J.J. (2002). Intercellular Communication in the Mammalian Ovary: Oocytes Carry the Conversation. Science *296*, 2178-2180.

Maupin, K.A., Sinha, A., Eugster, E., Miller, J., Ross, J., Paulino, V., Keshamouni, V.G., Tran, N., Berens, M., Webb, C.*, et al.* (2010). Glycogene Expression Alterations Associated with Pancreatic Cancer Epithelial-Mesenchymal Transition in Complementary Model Systems. PLOS ONE *5*, e13002.

Meacham, C.E., and Morrison, S.J. (2013). Tumour heterogeneity and cancer cell plasticity. Nature *501*, 328-337.

Moreno-Bueno, G., Cubillo, E., Sarrió, D., Peinado, H., Rodríguez-Pinilla, S.M., Villa, S., Bolós, V., Jordá, M., Fabra, A., Portillo, F.*, et al.* (2006). Genetic Profiling of Epithelial Cells Expressing E-Cadherin Repressors Reveals a Distinct Role for Snail, Slug, and E47 Factors in Epithelial-Mesenchymal Transition. Cancer Research *66*, 9543-9556.

Mueckler, M. (1994). Facilitative glucose transporters. European Journal of Biochemistry *219*, 713-725.

Nagaraj, R., Sharpley, M.S., Chi, F., Braas, D., Zhou, Y., Kim, R., Clark, A.T., and Banerjee, U. (2017). Nuclear Localization of Mitochondrial TCA Cycle Enzymes as a Critical Step in Mammalian Zygotic Genome Activation. Cell *168*, 210-223.

Onder, T.T., Gupta, P.B., Mani, S.A., Yang, J., Lander, E.S., and Weinberg, R.A. (2008). Loss of E-Cadherin Promotes Metastasis via Multiple Downstream Transcriptional Pathways. Cancer Research *68*, 3645-3654.

Onetti, R., Baulida, J., and Bassols, A. (1997). Increased glucose transport in ras-transformed fibroblasts: a possible role for N-glycosylation of GLUT1. FEBS Letters *407*, 267-270.

Oriyama, T., Yamanaka, N., Fujimoto, J., Ichikawa, N., and Okamoto, E. (1998). Progression of hepatocellular carcinoma as reflected by nuclear DNA ploidy and cellular differentiation. Journal of Hepatology *28*, 142-149.

Patwari, P., Chutkow, W.A., Cummings, K., Verstraeten, V.L.R.M., Lammerding, J., Schreiter, E.R., and Lee, R.T. (2009). Thioredoxin-independent Regulation of Metabolism by the α-Arrestin Proteins. Journal of Biological Chemistry *284*, 24996-25003.

Perkins, S.J., Nealis, A.S., Dudhia, J., and Hardingham, T.E. (1989). Immunoglobulin fold and tandem repeat structures in proteoglycan N-terminal domains and link protein. Journal of Molecular Biology *206*, 737-748.

Pessin, J.E., and Bell, G.I. (1992). Mammalian Facilitative Glucose Transporter Family: Structure and Molecular Regulation. Annual Review of Physiology *54*, 911-930.

Plaisier, S.B., Taschereau, R., Wong, J.A., and Graeber, T.G. (2010). Rank–rank hypergeometric overlap: identification of statistically significant overlap between gene-expression signatures. Nucleic Acids Research *38*, e169.

Prince, M.E., Sivanandan, R., Kaczorowski, A., Wolf, G.T., Kaplan, M.J., Dalerba, P., Weissman, I.L., Clarke, M.F., and Ailles, L.E. (2007). Identification of a subpopulation of cells with cancer stem cell properties in head and neck squamous cell carcinoma. Proceedings of the National Academy of Sciences *104*, 973-978.

Purcell, S.H., and Moley, K.H. (2009). Glucose transporters in gametes and preimplantation embryos. Trends in Endocrinology & Metabolism *20*, 483-489.

Radisky, D.C., Levy, D.D., Littlepage, L.E., Liu, H., Nelson, C.M., Fata, J.E., Leake, D., Godden, E.L., Albertson, D.G., Angela Nieto, M.*, et al.* (2005). Rac1b and reactive oxygen species mediate MMP-3-induced EMT and genomic instability. Nature *436*, 123-127.

Raghow, R. (1994). The role of extracellular matrix in postinflammatory wound healing and fibrosis. The FASEB Journal *8*, 823-831.

Rillahan, C.D., Antonopoulos, A., Lefort, C.T., Sonon, R., Azadi, P., Ley, K., Dell, A., Haslam, S.M., and Paulson, J.C. (2012). Global metabolic inhibitors of sialyl- and fucosyltransferases remodel the glycome. Nat Chem Biol *8*, 661-668.

Rozario, T., and DeSimone, D.W. (2010). The extracellular matrix in development and morphogenesis: A dynamic view. Developmental Biology *341*, 126-140.

Sakuma, K., Aoki, M., and Kannagi, R. (2012). Transcription factors c-Myc and CDX2 mediate E-selectin ligand expression in colon cancer cells undergoing EGF/bFGF-induced epithelial–mesenchymal transition. Proceedings of the National Academy of Sciences *109*, 7776-7781.

Samih, N., Hovsepian, S., Aouani, A., Lombardo, D., and Fayet, G. (2000). Glut-1 Translocation in FRTL-5 Thyroid Cells: Role of Phosphatidylinositol 3-Kinase and N-Glycosylation. Endocrinology *141*, 4146-4155.

Sandler, H., Kreth, J., Timmers, H.T.M., and Stoecklin, G. (2011). Not1 mediates recruitment of the deadenylase Caf1 to mRNAs targeted for degradation by tristetraprolin. Nucleic Acids Research *39*, 4373-4386.

Sartor, M.A., Mahavisno, V., Keshamouni, V.G., Cavalcoli, J., Wright, Z., Karnovsky, A., Kuick, R., Jagadish, H.V., Mirel, B., Weymouth, T.*, et al.* (2010). ConceptGen: a gene set enrichment and gene set relation mapping tool. Bioinformatics *26*, 456-463.

Schuhmacher, M., Kohlhuber, F., Hölzel, M., Kaiser, C., Burtscher, H., Jarsch, M., Bornkamm, G.W., Laux, G., Polack, A., Weidle, U.H.*, et al.* (2001). The transcriptional program of a human B cell line in response to Myc. Nucleic Acids Research *29*, 397-406.

Schwartzenberg-Bar-Yoseph, F., Armoni, M., and Karnieli, E. (2004). The Tumor Suppressor p53 Down-Regulates Glucose Transporters GLUT1 and GLUT4 Gene Expression. Cancer Research *64*, 2627-2633.

Seales, E.C., Jurado, G.A., Singhal, A., and Bellis, S.L. (2003). Ras oncogene directs expression of a differentially sialylated, functionally altered β1 integrin. Oncogene *22*, 7137-7145.

Sedlyarov, V., Fallmann, J., Ebner, F., Huemer, J., Sneezum, L., Ivin, M., Kreiner, K., Tanzer, A., Vogl, C., Hofacker, I.*, et al.* (2016). Tristetraprolin binding site atlas in the macrophage transcriptome reveals a switch for inflammation resolution. Molecular Systems Biology *12*, 868.

Semenza, G.L. (2010). HIF-1: upstream and downstream of cancer metabolism. Current Opinion in Genetics & Development *20*, 51-56.

Shen, L., O'Shea, J.M., Kaadige, M.R., Cunha, S., Wilde, B.R., Cohen, A.L., Welm, A.L., and Ayer, D.E. (2015). Metabolic reprogramming in triple-negative breast cancer through Myc suppression of TXNIP. Proceedings of the National Academy of Sciences *112*, 5425-5430.

Simpson, M.A., Wilson, C.M., Furcht, L.T., Spicer, A.P., Oegema, T.R., and McCarthy, J.B. (2002). Manipulation of Hyaluronan Synthase Expression in Prostate Adenocarcinoma Cells Alters Pericellular Matrix Retention and Adhesion to Bone Marrow Endothelial Cells. Journal of Biological Chemistry *277*, 10050-10057.

Singer, A.J., and Clark, R.A.F. (1999). Cutaneous Wound Healing. New England Journal of Medicine *341*, 738-746.

Slomiany, M.G., Grass, G.D., Robertson, A.D., Yang, X.Y., Maria, B.L., Beeson, C., and Toole, B.P. (2009). Hyaluronan, CD44, and Emmprin Regulate Lactate Efflux and Membrane Localization of Monocarboxylate Transporters in Human Breast Carcinoma Cells. Cancer Research *69*, 1293-1301.

Smith, K.B., Tran, L.M., Tam, B.M., Shurell, E.M., Li, Y., Braas, D., Tap, W.D., Christofk, H.R., Dry, S.M., Eilber, F.C.*, et al.* (2013). Novel Dedifferentiated Liposarcoma Xenograft Models Reveal PTEN Down-Regulation as a Malignant Signature and Response to PI3K Pathway Inhibition. The American Journal of Pathology *182*, 1400-1411.

Stender, J.D., Pascual, G., Liu, W., Kaikkonen, M.U., Do, K., Spann, N.J., Boutros, M., Perrimon, N., Rosenfeld, M.G., and Glass, C.K. (2012). Control of proinflammatory gene programs by regulated trimethylation and demethylation of histone H4K20. Mol Cell *48*, 28-38.

Stern, R., Asari, A.A., and Sugahara, K.N. (2006). Hyaluronan fragments: An information-rich system. European Journal of Cell Biology *85*, 699-715.

Stoltzman, C.A., Peterson, C.W., Breen, K.T., Muoio, D.M., Billin, A.N., and Ayer, D.E. (2008). Glucose sensing by MondoA:Mlx complexes: A role for hexokinases and direct regulation of thioredoxin-interacting protein expression. Proceedings of the National Academy of Sciences *105*, 6912-6917.

Storchova, Z., and Pellman, D. (2004). From polyploidy to aneuploidy, genome instability and cancer. Nat Rev Mol Cell Biol *5*, 45-54.

Subramanian, A., Tamayo, P., Mootha, V.K., Mukherjee, S., Ebert, B.L., Gillette, M.A., Paulovich, A., Pomeroy, S.L., Golub, T.R., Lander, E.S.*, et al.* (2005). Gene set enrichment analysis: A

knowledge-based approach for interpreting genome-wide expression profiles. Proceedings of the National Academy of Sciences *102*, 15545-15550.

Tamada, M., Nagano, O., Tateyama, S., Ohmura, M., Yae, T., Ishimoto, T., Sugihara, E., Onishi, N., Yamamoto, T., Yanagawa, H.*, et al.* (2012). Modulation of Glucose Metabolism by CD44 Contributes to Antioxidant Status and Drug Resistance in Cancer Cells. Cancer Research *72*, 1438-1448.

Taube, J.H., Herschkowitz, J.I., Komurov, K., Zhou, A.Y., Gupta, S., Yang, J., Hartwell, K., Onder, T.T., Gupta, P.B., Evans, K.W.*, et al.* (2010). Core epithelial-to-mesenchymal transition interactome gene-expression signature is associated with claudin-low and metaplastic breast cancer subtypes. Proceedings of the National Academy of Sciences *107*, 15449-15454.

Toole, B.P. (1990). Hyaluronan and its binding proteins, the hyaladherins. Current Opinion in Cell Biology *2*, 839-844.

Toole, B.P. (2001). Hyaluronan in morphogenesis. Seminars in Cell & Developmental Biology *12*, 79-87.

Toole, B.P. (2004). Hyaluronan: from extracellular glue to pericellular cue. Nat Rev Cancer *4*, 528-539.

Toole, B.P., Wight, T.N., and Tammi, M.I. (2002). Hyaluronan-Cell Interactions in Cancer and Vascular Disease. Journal of Biological Chemistry *277*, 4593-4596.

Turley, E.A., Noble, P.W., and Bourguignon, L.Y.W. (2002). Signaling Properties of Hyaluronan Receptors. Journal of Biological Chemistry *277*, 4589-4592.

Van Den Broeck, A., Brambilla, E., Moro-Sibilot, D., Lantuejoul, S., Brambilla, C., Eymin, B., Khochbin, S., and Gazzeri, S. (2008). Loss of Histone H4K20 Trimethylation Occurs in Preneoplasia and Influences Prognosis of Non–Small Cell Lung Cancer. Clinical Cancer Research *14*, 7237-7245.

Vander Heiden, M.G., Cantley, L.C., and Thompson, C.B. (2009). Understanding the Warburg Effect: The Metabolic Requirements of Cell Proliferation. Science *324*, 1029-1033.

Wabitsch, M., Brüderlein, S., Melzner, I., Braun, M., Mechtersheimer, G., and Möller, P. (2000). LiSa-2, a novel human liposarcoma cell line with a high capacity for terminal adipose differentiation. International Journal of Cancer *88*, 889-894.

Wieman, H.L., Wofford, J.A., and Rathmell, J.C. (2007). Cytokine Stimulation Promotes Glucose Uptake via Phosphatidylinositol-3 Kinase/Akt Regulation of Glut1 Activity and Trafficking. Molecular Biology of the Cell *18*, 1437-1446.

Wu, N., Zheng, B., Shaywitz, A., Dagon, Y., Tower, C., Bellinger, G., Shen, C.-H., Wen, J., Asara, J., McGraw, Timothy E.*, et al.* (2013). AMPK-Dependent Degradation of TXNIP upon Energy Stress Leads to Enhanced Glucose Uptake via GLUT1. Molecular Cell *49*, 1167-1175.

Yang, J., and Weinberg, R.A. (2008). Epithelial-Mesenchymal Transition: At the Crossroads of Development and Tumor Metastasis. Developmental Cell *14*, 818-829.

Yokoyama, Y., Matsumoto, A., Hieda, M., Shinchi, Y., Ogihara, E., Hamada, M., Nishioka, Y., Kimura, H., Yoshidome, K., Tsujimoto, M.*, et al.* (2014). Loss of histone H4K20 trimethylation predicts poor prognosis in breast cancer and is associated with invasive activity. Breast Cancer Research *16*, R66.

Younes, M., Brown, R.W., Mody, D.R., Fernandez, L., and Laucirica, R. (1995). GLUT1 expression in human breast carcinoma: correlation with known prognostic markers. Anticancer Res *15*, 2895-2898.

Younes, M., Brown, R.W., Stephenson, M., Gondo, M., and Cagle, P.T. (1997). Overexpression of Glut1 and Glut3 in Stage I Nonsmall Cell Cung Carcinoma is Associated with Poor Survival. Cancer *80*, 1046-1051.

Younes, M., Lechago, L.V., Somoano, J.R., Mosharaf, M., and Lechago, J. (1996). Wide Expression of the Human Erythrocyte Glucose Transporter Glut1 in Human Cancers. Cancer Research *56*, 1164-1167.

Zeller, K.I., Jegga, A.G., Aronow, B.J., O'Donnell, K.A., and Dang, C.V. (2003). An integrated database of genes responsive to the Myc oncogenic transcription factor: identification of direct genomic targets. Genome Biology *4*, R69.

Zhang, L., Underhill, C.B., and Chen, L. (1995). Hyaluronan on the Surface of Tumor Cells Is Correlated with Metastatic Behavior. Cancer Research *55*, 428-433.

Zhang, P., Wang, C., Gao, K., Wang, D., Mao, J., An, J., Xu, C., Wu, D., Yu, H., Liu, J.O.*, et al.* (2010). The Ubiquitin Ligase Itch Regulates Apoptosis by Targeting Thioredoxin-interacting Protein for Ubiquitin-dependent Degradation. Journal of Biological Chemistry *285*, 8869-8879.